The role of the actin binding protein Calponin2 during embryonic development of Xenopus laevis

Dissertation to obtain the doctoral degree of Natural Sciences (Dr. rer. nat.)

Faculty of Natural Sciences

University of Hohenheim

Institute of Biology

Department of Zoology

submitted by

Sabrina Maria Mantino

from *Heilbronn*

2021

Date of submission: 10.08.2021

Date of oral doctoral examination: 29.11.2021

Faculty director: Prof. Dr. Uwe Beifuss

1st Reviewer: PD Dr. Kerstin Feistel (Universität Hohenheim)

2nd Reviewer: Prof. Dalit Sela-Donenfeld (Hebrew University)

Declaration in lieu of an oath on independent work

according to Sec. 18(3) sentence 5 of the University of Hohenheim's Doctoral Regulations for the Faculties of Agricultural Sciences, Natural Sciences, and Business, Economics and Social Sciences

1. The dissertation submitted on the topic

The role of the actin binding protein Calponin2 during embryonic development of Xenopus laevis

is work done independently by me.

2. I only used the sources and aids listed and did not make use of any impermissible assistance from third parties. In particular, I marked all content taken word-for-word or paraphrased from other works.

3. I did not use the assistance of a commercial doctoral placement or advising agency.

4. I am aware of the importance of the declaration in lieu of oath and the criminal consequences of false or incomplete declarations in lieu of oath.

I confirm that the declaration above is correct. I declare in lieu of oath that I have declared only the truth to the best of my knowledge and have not omitted anything.

Stuttgart, 23.07.2021

Zusammenfassung

Trotz der großen Variabilität innerhalb der verschiedenen Körperbaupläne adulter Wirbeltiere sind die embryonalen Entwicklungsschritte, welche die einzelne Eizelle in einen multizellulären Organismus von bemerkenswerter Komplexität verwandeln, evolutionär hoch konserviert. Morphogenetische Prozesse wie Gastrulation, Neuralrohschluss, Körperachsenverlängerung, Neuralleistenzellmigration und Organogenese sind dabei essentiell, um komplexe Formen während der Embryogenese entstehen zu lassen.

Ein bedeutender Schritt hierbei ist die Generierung eines geschlossenen Neuralrohrs, aus dem das zentrale Nervensystem entsteht. Der Neuralrohrschluss wird unter anderem durch konvergente Extension und apikale Konstriktion neuroepithelialer Zellen ermöglicht.

Einhergehend mit dem Fortschreiten der Neuralulationsbewegungen lösen sich auch die kranialen Neuralleistenzellen aus dem Randbereich des Neuroepithels. Um ihre gerichtete Wanderung in den Kiemenbögen zu initiieren, müssen sie polarisierte Zellfortsätze bilden und die für Migrationsbewegungen essentiellen mechanischen Kräfte übertragen können.

Die Veränderung von Zellform und Beweglichkeit, welche Neuralrohrschluss und Neuralleistenzellmigration zugrunde liegen, werden u.a. durch die gezielte Regulation des Aktin-Zytoskeletts gesteuert. Wie genau die Aktinfilament-Dynamik und die, durch Myosin vermittelte Kontraktion des Aktin-Netzwerks koordiniert wird, ist nicht vollständig geklärt.

Aktinfilament-assoziierte Proteine spielen dabei eine wichtige Rolle für die strukturelle Organisation verschieden gestalteter Aktin-Netzwerke.

Die Calponin-Familie ist eine Gruppe hochkonservierter Proteine, die mit Aktinfilamenten assoziieren. Die Bindung von Calponinen an F-Aktin beeinflusst die die Aktin-Myosin-Dynamik und stabilisiert Aktin-Fasern. Vorhergehende Studien haben bereits eine Funktion von Calponin-Proteinen bei der Kontraktion glatter Muskelzellen sowie für die Zellmotilität und Phagozytose aufgezeigt.

Wirbeltiere besitzen drei Calponin-Isoformen mit individuellen Expressionsmustern und spezifischen Eigenschaften. Calponin2 ist in unterschiedlichsten Zelltypen exprimiert und zahlreiche In-vitro-Studien deuten darauf hin, dass Calponin2 für die Vermittlung mechanischer Kräfte bei der Zellmigration wichtig ist.

Während der frühen Embryogenese des Afrikanischen Krallenfroschs *Xenopus laevis* ist *calponin2* in Geweben exprimiert, die extensive morphogenetische Bewegungen und Zellmigration durchlaufen. Dies deutet auf eine Rolle von Calponin2 bei entsprechenden morphogenetischen Entwicklungsschritten dieses etablierten Modelorganismus hin.

Im Rahmen der vorliegenden Arbeit sollte die genaue Funktion von Calponin2 bei der dynamischen Regulation des Aktin-Zytoskeletts näher untersucht werden.

Unter Verwendung einer markierten Proteinversion konnte dessen Lokalisierung in Zellen der Neuralplatte sowie in wandernden Neuralleistenzellen gezeigt werden. In beiden Zelltypen trat ein regulierter Abbau des Proteins auf, welcher zu einer spezifischen Regionalisierung des Selben am Apex konstringierender Zellen oder am äußeren Saum von Lamellipodien führte. Demnach war das markierte Calponin2 in der Region des Aktin Kortex zu finden. Der Calponin2-Funktionsverlust führte zu Defekten bei der Induktion und Wanderung von Neuralleistenzellen, sowie zur Fehlregulation der konvergenten Extension und apikalen Konstriktion innerhalb der Neuralplatte. Sämtliche dabei erzeugte Phänotypen konnten durch zusätzlich injizierte *calponin2* mRNA gerettet werden. Insgesamt zeigten diese Daten eine spezifische Funktion von Calponin2 für die korrekte Ausbildung der Neuralleiste sowie den erfolgreichen Neuralrohrschluss.

Des Weiteren war die genaue Regulation der Proteinlevel, welche in direktem Zusammenhang mit dessen korrekter Funktionsweise stand, von bestimmten Domänen abhängig. Diese könnten für die gezielte die Binding an Aktin verantwortlich sein. Clik1, Clik2 und der C-terminus wurden hierbei sowohl in Neuralleistenzellen als auch in Zellen der Neuralplatte als entscheidende, den Abbau regulierende, Einheit identifiziert. Zudem wurde gezeigt, dass die Funktion des Proteins im Rahmen der neuralen apikalen Konstriktion ebenfalls auf jeder dieser Domänen beruht.

Insgesamt deutet der Abbau von Calponin2, reguliert über dessen Binding an F-Aktin, auf eine stabilisierende Funktion des Proteins hin. Demnach wäre seine räumlich und zeitlich koordinierte Degradation elementar um Aktinfilamente gezielt zugänglich zu machen für andere regulierende Effektoren und so dynamische Umstrukturierungen des Aktin-Zytoskeletts im Rahmen morphogenetischer Prozesse, während der embryonalen Entwicklung von Wirbeltieren zu ermöglichen.

Abstract

Despite the abundant variability among adult vertebrate body plans, the developmental steps transforming the single zygote into a multicellular organism of remarkable complexity, are evolutionary highly conserved. Morphogenetic processes such as gastrulation, neural tube closure, body axis extension, neural crest cell migration and organogenesis are thereby at the heart of embryogenesis.
Especially the formation of a closed neural tube, which gives rise to the central nervous system, constitutes a fundamental event. Neural tube closure is achieved by convergent extension movements and by apical constriction of neuroepithelial cells.
Along with proceeding neurulation, cranial neural cells start to delaminate from the neuroepithelial border. In order to initiate directed migration movements, neural crest cells require polarised cell protrusions and mediate mechanical forces.
Changes in cell shape and motility underlying neural tube closure and neural crest cell migration are controlled by specific regulation of the actin cytoskeleton. How these actin dynamics and the myosin-mediated contraction of actin networks are precisely coordinated is not fully understood.
In this context, actin filament-associated proteins play an important role for the structural organisation of different actin network types.
Calponins constitute an evolutionary highly conserved family of F-actin binding proteins, which are able to influence actin-myosin dynamics and to stabilise actin filaments. Previous studies already demonstrated a role of Calponin proteins in smooth muscle contraction, cell motility and phagocytosis.
Vertebrates possess three Calponin isoforms, each displaying specific expression patterns and functions. Calponin2 is expressed in a variety of cell types and several studies performed *in vitro* indicated that Calponin2 is important for mechanical tension mediation during the course of cell migration.
In the early embryo of *Xenopus laevis*, *calponin2* is expressed in tissues that undergo extensive morphogenetic movements and cell migration. This implies an elemental role of Calponin2 for respective morphogenetic steps during embryonic development of this well-established model organism.

Within the scope of the present work, the specific function of Calponin2 for dynamic regulation of the actin cytoskeleton was analysed more closely.

Localisation of the protein, by utilising a tagged construct, was shown in neural plate cells as well as in migrating neural crest cells. In both cell types, regulated protein degradation occurred, which led to specific expression restricted to the apex of constricting neural plate cells or to forming lamellipodia. Thus, tagged Calponin2 localised to regions of the actin cortex. Loss of Calponin2 function led to defects in neural crest cell specification and migration as well as in convergent extension and apical constriction within the neural plate. All induced phenotypes were rescued by additional *calponin2* mRNA injection. In summary, these data demonstrated a specific function of Calponin2 for correct formation of the neural crest as well as for neural tube closure.

Furthermore, the precise regulation of protein expression levels, which directly correlated with correct Calponin2 function, was dependent on specific domains that potentially mediate actin-binding. Clik1, Clik2 and the C-terminus were identified as a critical unit regulating protein degradation, both in neural crest cells and neural plate cells. Additionally, it was shown that Calponin2 function for neural apical constriction depends on each of these domains as well.

Overall, the degradation of Calponin2, regulated via its F-actin binding, implies a filament stabilising function. Thus, a temporospatial coordination of protein degradation would be necessary to enable dynamic changes of the actin cytoskeleton by a regulated release of actin filaments and to allow the association of other structural effectors during morphogenetic processes of early vertebrate development.

Table of contents

Table of figures

Index of abbreviations

AC	apical constriction
AJ(s)	adherens junction(s)
BA	branchial arch
BPD(s)	blastopore closure defect(s)
CE	convergent extension
cf.	check for
Cnn(s)	Calponin(s)
co	control embryo, untreated / uninjected specimen
CRNP	Cas9 ribonucleoprotein
DNA	deoxyribonucleic acid
DLHP(s)	dorsolateral hinge point(s)
EC	eye cup
F-actin	filamentous actin
FD(s)	craniofacial defect(s)
HA	hyoid arch
IF	immunofluorescence staining
LSM	confocal Laser scanning microscope
LT	lineage tracer
MA	mandibular arch
MB	mid brain
MO	morpholino
mRNA	messenger ribonucleic acid
NB	neural plate border
NC	neural crest
NCC(s)	neural crest cell(s)
Nd	notochord
NP	neural plate
NT	neural tube
NTC	neural tube closure
NTD(s)	neural tube closure defect(s)
OV	otic vesicle
PBS	phosphate buffered saline
PFA	paraformaldehyde
RT	room temperature
splMO	splice blocking morpholino
st.	embryonic developmental stage
wt	wildtypic; wild type

In the following all gene names will be written uncapitalised and in italic letters (e.g. *cnn2*), proteins on the contrary will be characterized by capitalisation (e.g. Cnn2).

1. Introduction

1.1. *Xenopus laevis* – A convenient amphibian model organism

Early embryonic development is the basis of all biological studies as it marks the start of life itself. The entirety of living animals and higher plants as well, undergo this fundamental process to transform from a single cell into a multicellular and highly specialised organism. Despite the abundant variabilities of adult morphology among the different species, the underlying developmental processes were conserved in the course of evolution (Gilbert, 2014). Similar basic regulatory steps and signalling pathways can be observed in embryos of various animal groups. This enables comparative analyses and makes experimentally gained knowledge applicable to other species based on homologies. Therefore, different model organisms were established over the last decades to facilitate a more simplified analysis of basic developmental processes.

One popular vertebrate model organism is the African clawed frog *Xenopus laevis*, which was also chosen as object of study in the present work.

It provides numerous advantages for embryological analysis such as inducible egg deposition and season-independent availability of eggs. Moreover, one frog provides up to 1000 eggs per clutch, which can be fertilised *in vitro* (Gradl, 2019). The oocytes display an extraordinary size with a diameter of 1.2 mm and a volume 10^5 to 10^6 times compared to typical somatic cells. This allows directed manipulations of the early embryo and its relatively fast extrauterine development facilitates subsequent observations (Kloc & Kubiak, 2014). The first cleavage of the zygote takes place at about one and a half hour after fertilisation. Already in 4-cell embryos, the dorsal-ventral axis is visible from the outside and, together with established fate map data, makes targeted manipulation of cell lineages possible until 64-cell stages. Region-specific manipulations are achieved by injection of defined blastomeres. Hereby, applicable methods are classical gain-of-function (GOF) and loss-of-function (LOF) approaches to alter gene function. Injection of cDNA or RNA molecules as well as mutagenesis, CRISPR-based genome editing, RNA interference, morpholino-mediated knockdown or pharmacological inhibition are possible (Gradl, 2019; Housden et al., 2017). In addition to that, detailed morphological studies are available, to complement the basis for further analysis by

providing deep insights into the characteristics of morphogenetic events like gastrulation and neurulation (Keller & Sutherland, 2020). The overall robustness of early frog embryos allows the conduction of transplantation and explantation experiments as well as the cultivation of whole mount embryos or even just specific tissues and cell types for detailed analysis.
Taken together, *Xenopus laevis* represents a convenient vertebrate model organism and hence was chosen for the experimental analysis performed in the course of this study.

1.1.1. From oocyte to frog

For a better understanding of the conducted experiments and analysis performed in *Xenopus* embryos, this section should provide a short overview of their development.
The mature amphibian oocyte already displays polarity, as the lower vegetal half is filled with yolk and the upper animal half contains only little. Also, proteins and mRNAs provided by the mother are pre-localised in specific regions of the cell (Gilbert & Barresi, 2016).
In the course of fertilisation, the sperm is able to enter the egg anywhere within the animal hemisphere, thereby marking the future ventral side of the embryo. The exact opposite of the point of sperm entry will become the dorsal side (Gilbert, 2014). The paternal centriole, delivered by the sperm, then recruits maternal proteins and organises the microtubules of the cell anew. On the one hand, to enable meeting of the two pronuclei within the animal hemisphere where they enter first mitosis. On the other hand, it structures the microtubules of the vegetal cytoplasm into parallel tracks for associated motor proteins, thereby separating the cortical cytoplasm from the inner yolky part. This reorganisation enables a rotation movement of both cytoplasmic regions with respect to each other at about 30° (Cha & Gard, 1999; Gilbert & Barresi, 2016). Overall, this leads to a rearrangement of several maternally deposited proteins towards the future dorsal side, where they finally enable

accumulation of ß-catenin (Schneider et al., 1996; Weaver & Kimelman, 2004; Tao et al., 2005;). Thus, the molecular definition of the dorsal-ventral axis takes place at and is orientated towards the point of sperm entry.

Following this, the zygote undergoes a sequence of radially symmetric and holoblastic cleavages. The first cleavage, along the animal-vegetal axis, defines left and right side of the presumptive body. Second cleavage occurs about 30 minutes later perpendicular to the first divisional plane and separates dorsal from ventral blastomeres. Within the same time frame, the third cleavage follows around the equator to separate vegetal and animal hemisphere, whereas the furrow is slightly displaced towards the less yolk containing animal pole (Valles et al., 2002). Further synchronous cleavages are completed in the same frequency until the early blastula stage is reached, consisting of about two thousand cells with a fluid-filled cavity within the animal hemisphere, the blastocoel (Gradl, 2019). In the course of the next two rounds of cell division, synchrony gets lost and mid-blastula transition (MBT), precisely the activation of zygotic transcription takes place. This leads to an extension of the cell cycle by installing checkpoints and reintroducing the G2 phase (Maller et al., 2001; Yang et al., 2002).

Already at this stage, the different regions of the blastula are specified to subsequently contribute to one of the three germ layers. The cells of the animal hemisphere will give rise to the ectoderm (skin and nerves), the mesoderm (muscle, bone, heart) arises from the cells just beneath the blastocoel cavity and the vegetal half of the embryo becomes endoderm (gastro-intestinal tract). Thereby, the mesoderm gets induced by the more vegetally located endodermal cells (Gilbert & Barresi, 2016). The presumptive neuroectoderm is specified just opposite the point of sperm entry (Keller, 1975, 1976). In this set-up the blastocoel serves as spacer between pluripotent epithelial cells of the animal cap and endodermal cells of the vegetal hemisphere in order to inhibit early induction. Furthermore, the cavity provides space for inward-migrating cells during gastrulation.

Over the course of gastrulation, the bi-layered blastula is transformed by morphogenetic movements into a gastrula consisting of the three described germ layers in their designated positions. In *Xenopus*, gastrulation is initiated at stage 10, about 9 hours after fertilisation, by the formation of bottle cells in the dorsal marginal zone (DMZ) just below the equator (J. Y. Lee & Harland, 2007). Here, the crescent-

shaped dorsal blastopore lip is formed through which the gastrulating cells start to involute into the cavity (Keller, 1981). Before the onset of involution movements, the endodermal cells of the blastocoel floor plate undergo rearrangements. The so-called vegetal rotation positions the prospective pharyngeal endoderm right above the involuting mesoderm and next to the blastocoel, where its cells start to migrate along the blastocoel roof into anterior direction (Ibrahim & Winklbauer, 2001; Winklbauer & Damm, 2012). The overall involution movement is achieved by actively migrating deep cells and attached cells of the superficial marginal layer that are pulled along. In parallel, the dorsal mesoderm undergoes convergent extension (CE) to enable continuous cell movements into the embryo. Meanwhile, the ectoderm expands by epiboly and supplants the involuting mesoderm to finally cover the embryo from the outside (Keller & Schoenwolf, 1977; Saka & Smith, 2001).

The mesodermal cells that compose the dorsal lip over time, as well as the attached pharyngeal endoderm, instruct the embryonic axis formation. Hence, the first entering endomesodermal cells subsequently induce the ectoderm above to form anterior head structures, while the following trunk mesoderm induces posterior structure formation. Due to its inductive properties, the dorsal blastopore lip is referred to as “the organizer” (Bouwmeester, 2001). With proceeding gastrulation, the lip expands laterally and ventrally as a result of further bottle cell formation and extensive involution movements (R. Keller, Shook, & Skoglund, 2008). At the end of gastrulation, the blastopore ring contracts until a small patch of endoderm is left and eventually gets internalised at the site of the future anus. At stage 13, all three germ layers have reached their final destination. The mesoderm is situated right beneath the ectoderm and the blastocoel is completely displaced by the endoderm-lined archenteron.

As already mentioned above, the organizer tissue induces the neural ectoderm in the next developmental step by sending instructive signals to the overlying ectoderm. These signals are sequestered inhibitors of bone morphogenetic protein (BMP) signalling like Chordin, Noggin and Follistatin, thereby inducing a fate change from epidermal to neural (Harland, 1994; Piccolo et al., 1996; Iemura et al., 1998). The region-specific patterning of the neural ectoderm along the anterior-posterior axis is based on respectively induced gradients of wingless int-1 (Wnt), fibroblast growth factor (FGF) signalling and retinoic acid (RA). Secreted Wnt inhibitors in the

most anterior part of the organizer allow the subsequent induction of head structures (De Souza & Niehrs, 2000). Corresponding patterning of the trunk region is influenced by increasing levels of posteriorising factors like Wnt8, FGF and RA towards the future tail. These gradients in turn regulate the succession of Hox gene boundaries along the anterior-posterior axis and influence the tailbud formation as well as the tail outgrowth (Durston et al., 2010; Janesick et al., 2014).

After gastrulation is completed, the neurulation follows at stage 14 and about 16 hours after fertilisation, representing the next fundamental morphogenetic step in development.

During this process the closed neural tube (NT) forms situated between mesoderm and epidermis, where it will give rise to the central nervous system (CNS). The specific position of the NT is critical for its further specification as the dorsal epidermis sequesters BMP signals, while the ventrally located chorda dorsalis releases the growth factor sonic hedgehog (Shh). These two signalling centres are finally shifted to the floor and roof plate of the NT respectively. Thus, the NT is influenced by two opponent signalling gradients along the dorsal-ventral axis. Both are responsible for the patterning of the CNS including the spatial organisation and specification of different neuron types within the spinal cord (Briscoe & Ericson, 1999; Gilbert & Barresi, 2016).

The patterning along the anterior-posterior axis is more complex. Within the most anterior region, three signalling centres subdivide the future brain into five distinct parts. These are, from anterior to posterior, the telencephalon, diencephalon, mesencephalon, metencephalon and the myelencephalon (Gradl, 2019). The first signalling centre is characterised by secreted FGF8 and antagonists of Wnt at the anterior neural ridge (Eagleson & Dempewolf, 2002). At the following border between telen- and diencephalon, the so called “zona limitans intrathalamica” (ZLI), Shh gets secreted (Martinez-Ferre & Martinez, 2012; Sena et al., 2016). In the border region between mesen- and metencephalon or the “isthmus”, members of the Wnt-family as well as FGF8 are secreted (Harada et al., 2016). The remaining posterior part of the CNS is patterned by segmented Hox gene expression along the anterior-posterior axis, which is mainly regulated by specific levels of RA as described above.

Already in the early gastrula, the neural crest (NC) gets induced at the border between presumptive neuroectoderm and epidermis (Pla & Monsoro-burq, 2018). During the course of neurulation neural crest cells (NCCs) start to delaminate and eventually emigrate from the dorsal apex of the forming NT. They proceed along defined routes to numerous destinations within the embryonic body, where they will contribute to different cell types and tissues of the adult organism.

Another fundamental step in early vertebrate development is the establishment of the left-right axis, as several internal organs display distinct asymmetries. The molecular symmetry breakage is marked by the expression of *nodal* in the left lateral plate mesoderm. In *Xenopus*, the corresponding homologue *Xenopus nodal-related 1* (*xnr1*) is unilaterally expressed at stage 19 and induces a side-specific signalling pathway, which ultimately results in the rightward heart looping and the counter clockwise gut coiling visible in the tadpole (Ryan et al., 1998). Already during the first cleavage of the frog embryo, maternally deposited components seem to be distributed differentially between the left and right blastomeres in a tubulin-dependent manner (Lobikin et al., 2012). Nonetheless, the lateral induction of the Nodal cascade occurs in the *Xenopus* neurula, starting at about stage 15 by a developing cilia-driven leftward fluid flow within the archenteron (Schweickert et al., 2007).

Finally, after all tissues are properly induced and morphogenetic movements as well as organogenesis are completed, a fully developed and already hatched tadpole is present. It starts feeding around stage 45, after about 4 days of embryonic development, to prepare for its metamorphosis and become an adult African clawed frog.

1.2. Morphogenesis – Cell shape changes during embryonic development

As it was illustrated in the previous chapter, the early development of *Xenopus laevis* represents a highly regulated transformation from one single cell to the remarkable complexity of the animal body.

Four fundamental processes underlie this precise patterning and cell rearrangement, namely proliferation, cell-cell interaction, differentiation and cell movement (Alberts et al., 2015). These are precisely coordinated to orchestrate each cell according to its individual and genetically encoded fate, to grow, proliferate or reach its final destination within the developing organism. The entirety of all cell movements resulting in the formation of specific body parts can be summarised under the term of “morphogenesis”. Derived from the Greek term “morpho genésis” which literally means “the generation of form” (Brechner et al., 2001).

In summary, the stepwise assembly of the embryonic body is driven by several morphogenetic processes. Among those, neurulation as well as induction and migration of NCCs play a central role.

As the present work focused on the analysis of those two fundamental events, both are introduced in more detail in the following sections.

1.2.1. Neurulation

The vertebrate CNS arises from a flat plate of neuroectodermal cells by folding up along the body axis, thereby forming the NT. This process is referred to as “neurulation”, a conserved mechanism among all vertebrates that constitutes a paradigm of embryonic morphogenesis (Harrington et al., 2009; Gilbert & Barresi, 2016). If neurulation in humans is not completed correctly, the NT stays open resulting in severe congenital malformations like anencephaly, spina bifida or even craniorachischisis (Greene & Copp, 2014).

In general, the non-neural and neural ectoderm (neural plate), as well as cells of the mesoderm and the notochord, are involved in this process. The neural plate (NP) in *Xenopus* consists of superficial epithelial cell layers and a deep mesenchyme-like cell layers (Elul et al., 1997). Like in all amphibia, it undergoes bending, fold elevation and fusion at all axial levels within a short time frame. As described in the preceding section, the specification and patterning of the ectoderm as well as the presumptive neural tissue is accomplished by the regulation of BMP levels during gastrulation. Very low levels of BMP induce the ectodermal cells to become NP, intermediate levels specify the bordering NC and high levels of BMP manifest the epidermal fate. With the onset of neurulation, the cells of the NP start to express transcription factors of the SRY-related HMG-box (Sox) gene family, more precisely *sox1*, *sox2* and *sox3*. These transcription factors in turn activate the expression of NP specific genes and inhibit BMP signalling further (Archer et al., 2011; Wilson & Edlund, 2001). Upon induced differentiation of the neural cells, the superficially located NP is transformed into an internal NT. This transformation is realised by primary and secondary neurulation.

Primary neurulation involves bending of the NP to create neural folds at its periphery, which progressively elevate towards the dorsal midline where they finally fuse. Secondary neurulation, on the other hand, is achieved by an internal process of aggregation and epithelialisation of mesenchymal cells (MET). Thereby, a solid cord is formed that subsequently turns into a hollow tube without preceding neural fold formation (Nikolopoulou et al., 2017).

In *Xenopus* embryos the main part of the NT is derived from primary neurulation, whereas only the tail region undergoes secondary neurulation (Lowery & Sive, 2004).

Neurulation is completed when both differently assembled anterior and posterior NT regions fuse in the so-called transition zone via junctional neurulation (Harrington et al., 2009; Dady et al., 2014).

Considering that primary neurulation represents the main part of amphibian neurulation, this should be elucidated more closely. Primary neurulation consists of four specific and highly coordinated steps, which overlap each other in a spatiotemporal manner (cf. **Fig. 1**). At first, elongation along the anterior-posterior axis and bending of the NP is initiated. To enable proper shaping of the tissue, neural cells mainly proliferate in anterior-posterior direction fuelled by one elemental morphogenetic process, i.e. convergent extension (CE). Hereby, cells at the dorsal midline intercalate mediolaterally (R. Keller, Shih, & Sater, 1992). This axial elongation movement is associated with gastrulation. The driving force of NP bending and elevation of neural folds is the reduction of apical surface area within the NT accomplished by apical constriction (AC), which represents a second essential morphogenetic mechanism (J. Y. Lee & Harland, 2007). As a result, the NP invaginates at the midline creating neural groove as well as laterally located neural folds along the body axis. Distinct patches of apically constricting cells become prominent in the anterior NP region and build paired dorsolateral hinge points (DLHPs) (Haigo et al., 2003; Lee et al., 2007). The correct spatial formation of these hinge points seems to be regulated by Shh signalling radiating from notochord and floor plate as well as through BMP signals sequestered non-neural ectoderm. The latter is partially inhibited by Noggin expressed in the neural folds (Gilbert & Barresi, 2016). At the same time, deep cells elongate basolaterally to promote neural fold elevation further (Edlund et al., 2013). Radial intercalation of superficial and deep cells finally transform the multi-layered NP into a single-layered pseudo-stratified NT (Sokol, 2016). Meanwhile, the non-neural ectoderm continuously pushes towards the midline, the plate bends further around the DLHP regions and neural folds converge (Schroeder, 1971; Sokol, 2016). This way, the neural folds are brought into apposition at the dorsal midline, where they adhere and neural as well as surface ectoderm can fuse respectively.

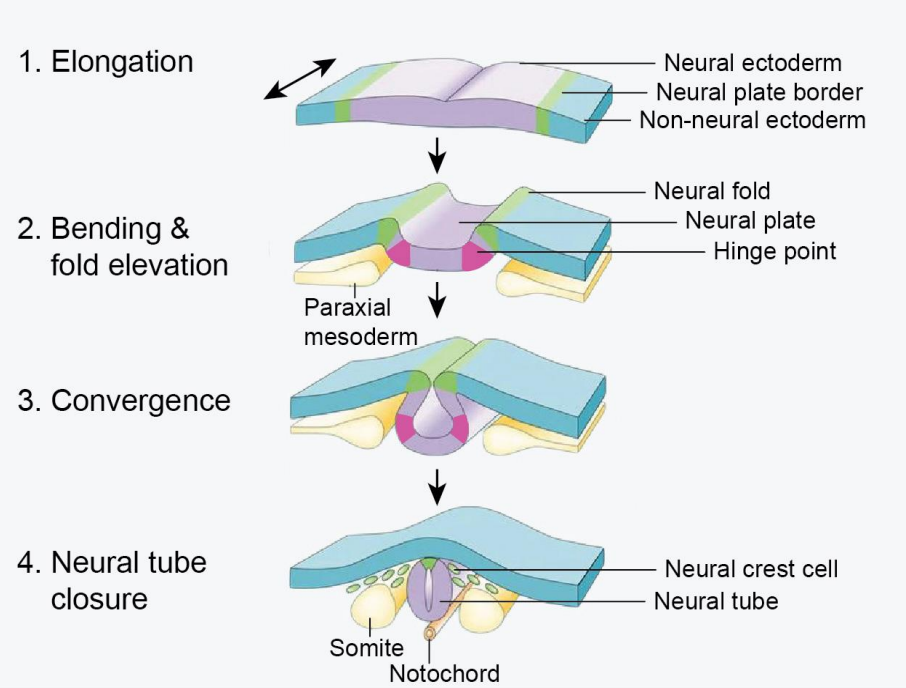

Figure 1: Steps in primary neurulation
Schematic illustration displays section of tissues involved in neurulation at different stages. Neural plate (=lavender) gives ultimately rise to the closed NT, representing the precursor of the CNS. The dorsolateral hinge points (=pink; DLHPs) are critical for elevation and apposition of the neural folds (=green), which will release the migratory NCCs during fusion of the neural folds and overlying epidermis (=light blue). (Based on Gammill & Bronner-Fraser, 2003)

1.2.1.1. Neural convergent extension in *Xenopus*

In the course of neural CE in the frog, mediolateral intercalation of deep cells occurs to form a longer and narrower NP without significant changes in cell shape or division rates (cf. **Fig. 2A**). The corresponding cell movements appear to be autonomous and are accomplished by monopolar medially oriented protrusions, which exert traction forces between intercalating cells. This directed behaviour of NP cells moving towards the midline, is governed by signals from underlying mesoderm as well as from midline structures themselves. Absence of the midline structures, also referred to as `notoplate´ or floor plate at later stages, leads to formation of bipolar and mediolaterally oriented protrusions (Elul et al., 1997; Ezin

et al., 2003, 2006). In parallel, the mesoderm experiences CE separately driven by formation of mediolaterally oriented bipolar cell protrusions (Shih & Keller, 1992).
Both, CE within the NP as well as of mesodermal cells, are regulated by non-canonical Wnt/planar cell polarity (PCP) signalling pathway and defective regulation of PCP-mediated CE results in severe neural tube closure defects (NTDs; Wallingford & Harland, 2002).
Wnt/PCP signalling plays a central role in the molecular regulation of CE. In general, it acts as an upstream regulator of cytoskeletal actin dynamics via modulation of small GTPases of the Rho family, thereby controlling cell polarity, AC, CE and cell motility (J. B. Wallingford, 2012). An essential feature of PCP is the polarised distribution of core PCP proteins like Frizzled (Fzd), Dishevelled (Dsh), Vang-like protein 2 (Vangl2), Prickle (Pk) and Diversin (Yang & Mlodzik, 2015). Within NP cells of *Xenopus*, polarised Vangl2 can be found at the anterior side. Its polarisation depends on complex formation with Pk as well as its phosphorylation by Wnt, which is critical for correct neural tube closure (NTC). Additionally, it has been shown that the polarisation of Vangl2 relies on Rho-kinase (ROCK) induced phosphorylation of myosin light chain (pMLC), representing a component of actomyosin dynamics (Ossipova et al., 2015). Depletion of Vangl2 reduces the amount of pMLC within NP cells indicating a feedback loop between Wnt/PCP signalling and cytoskeletal dynamics (Ossipova et al., 2014). Another core PCP component, which is polarised along the medial-lateral axis of NP cells is Diversin. It regulates spatial distribution of the endosome recycling marker Rab11 with pMLC as downstream effector during NTC (Ossipova et al., 2014). To summarise this, PCP-dependent protein polarisation along the anterior-posterior as well as the mediolateral axis seems to play an important role for neural CE and the entire neurulation process. This regulation, with pMLC acting as downstream regulator, is conserved among vertebrates (Nikolopoulou et al., 2017).
Although PCP-mediated CE is essential for correct NTC, anterior NP cells of the presumptive forebrain region do not converge mediolaterally (Darken et al., 2002; Goto & Keller, 2002; Wallingford & Harland, 2002; Lindqvist et al., 2010). This leads to a visible delay in anterior neural fold apposition of *Xenopus* embryos. Still, PCP components are crucial for anterior NP bending and NTC by mediating radial intercalation (Prager et al., 2017).

1.2.1.2. Apical constriction and hinge point formation

As already described, bending of the NP results from reduction of apical surface caused by AC in cells of the superficial NP layer, which also leads to the formation of DLHPs (cf. **Fig. 2A**).

In general, AC is defined as shrinkage of the apical side in epithelial cells changing the overall shape from columnar or cuboidal to a trapezoidal, wedge-shaped or bottle-shaped form (Martin & Goldstein, 2014). Coordinated AC of adhered cells, as it is the case within the NP, is able to bend and fold epithelial tissues and to transform initially flat cell sheets into three-dimensional tubes (Wallingford et al., 2013). Underlying biological processes that drive AC are the contraction of apical actin-myosin networks to generate force and the attachment of these networks to cell-cell-junctions in order to transmit developing mechanical strains between neighbouring cells (cf. **Fig. 2B**). Thereby, individual changes in cell geometry are able to affect global tissue remodelling (Martin & Goldstein, 2014).

A conserved core set of cytoskeletal and adhesion proteins is responsible for regulation of AC and other cell shape changes (Sawyer et al., 2010; Mason & Martin, 2011). Actin-myosin contraction mainly results from interactions between the non-muscle myosin II motor proteins (myosin) and actin filaments (F-actin; Lecuit et al., 2011; Salbreux et al., 2012). Generated contractile forces are exerted on the apical circumference as well as between neighbouring cells through their linkage to the actin cortex via adherens junctions (AJs; Martin & Goldstein, 2014).

One regulator of AC and DLHP formation is the F-actin binding protein Shroom3 (Haigo et al., 2003). Studies in mice and chick embryos revealed that Shroom3 localises to the apical tip of AJs, where it recruits Rho-associated protein kinase (ROCK), thus initiating actin-myosin cable formation. The circumferential tension seems to be increased by Shroom3-mediated myosin assembly (Hildebrand, 2005; Nishimura & Takeichi, 2008). How these components interact with each other precisely is unknown so far.

A second step for proper hinge point formation, besides AC, is the apicobasal elongation of constricting cells (cf. **Fig. 2B**). In *Xenopus*, it has been shown that Shroom3 is also required for assembly of parallel microtubule (MT) arrays in the apical region of superficial NP cells to enable respective elongation (Lee et al., 2007).

Overall, dynamic cell shape changes underlying AC as well as apicobasal elongation, are essential for DLHP formation and based on the spatial regulation of cytoskeletal components.

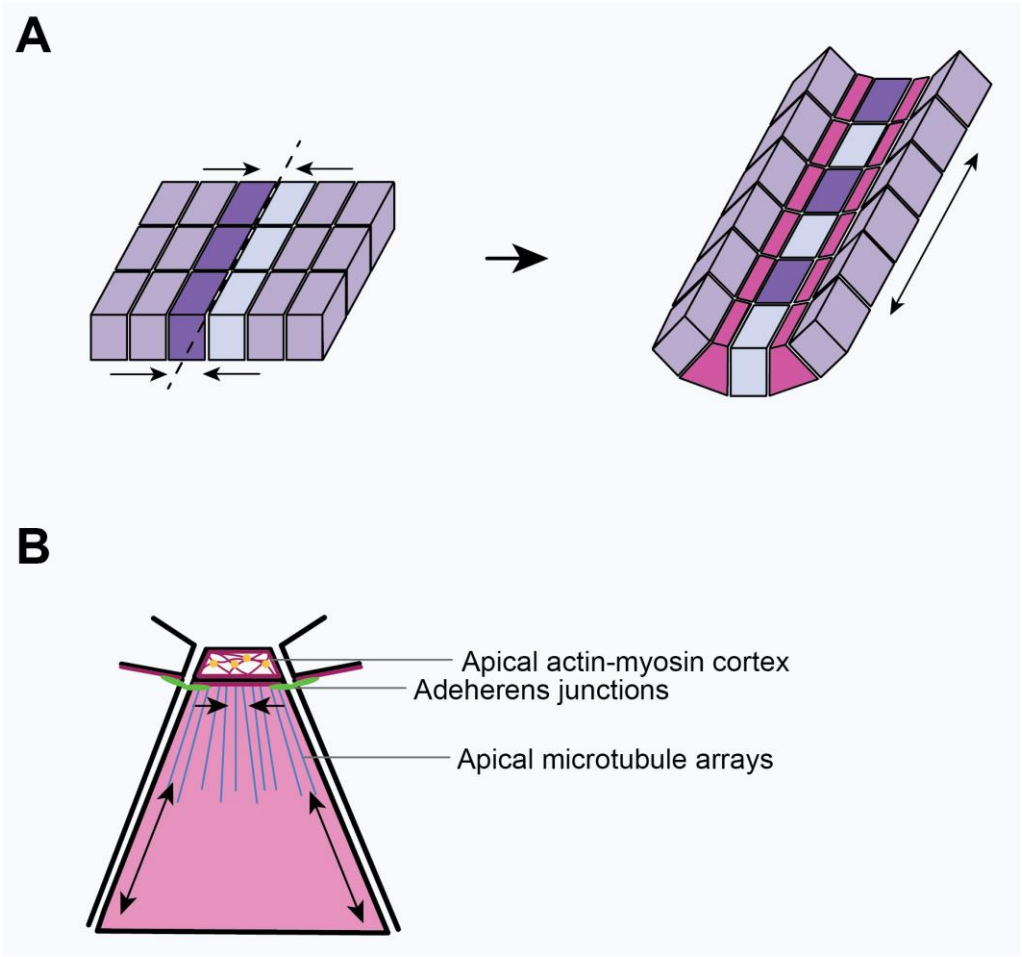

Figure 2: Morphogenetic events within the neural plate
(**A**) Simplified schematic representation of cell behaviour during CE (movement indicated by arrows, imaginary midline marked by dashed line) and DLHP formation (pink cells), leading to elongation and narrowing of the tissue. (**B**) Apically constricting cell with critical components indicated. F-actin (dark pink) and associated myosin (yellow dots) form a contractile apical network (cortex), which is linked to the cortex of neighbouring cells via apical adherens junctions (AJs; green). Apical microtubule arrays (blue lines) drive elongation of the constricting cell. Shape changes indicated by arrows (inspired by Wallingford et al., 2013; Martin & Goldstein, 2014).

1.2.2. The neural crest

The NC represents a fundamental, vertebrate-specific cell population. It is induced at the neural plate border (NB) by a multistep signalling process involving BMP, Wnt, FGF as well as Notch and RA signals emerging from the NP, epidermis and lateral mesoderm (Basch et al., 2004; Steventon et al., 2005; Sauka-Spengler & Bronner-Fraser, 2008). NCCs contribute to various cell types and tissues in the adult organism and are therefore often referred to as the fourth germ layer (Hall, 2000).
In the course of neurulation, NCCs start to delaminate from elevating neural folds along the body axis, except for the anterior neural ridge, to finally emigrate from the ectodermal tissue. These cells move in an amoeboid, monopolar protrusive manner and in distinct streams to reach their predetermined destination in the animal body. NCCs are multipotent cells, to a certain degree, before the onset of migration. They become specified while moving through the embryo and finally differentiate due to signals from their individual environment (Trainor et al., 2014).
In general, four NC regions can be distinguished depending on their axial origin, each giving rise to specific anatomical derivatives. The most anterior region represents the cranial or cephalic NC, which contributes to craniofacial mesenchyme. More posteriorly follows cardiac, trunk and finally vagal as well as sacral NC (Gilbert & Barresi, 2016). In total, NCCs contribute to more than thirty different cell types or tissues of higher vertebrates, including parts of the nervous system, gland tissue, pigment cells or skeletal and connective tissue components (Trainor, 2014).
To enable this contribution through directed migration, NCCs separate from neighbouring neuoectoderm by delamination and eventually experience epithelial-to-mesenchymal transition (EMT; Theveneau & Mayor, 2012). A, in *Xenopus* well-studied NCC population, is the cranial NC. It arises from the region of between presumptive diencephalon and caudal hindbrain. Here, NCCs start to delaminate between stage 16 and 18, while the NT is still wide open (Sadaghiani & Thiébaud, 1987; Theveneau & Mayor, 2010). Following this, migration starts around stage 19 in a continuous wave-like manner. Although all cells move together, most anterior NCCs are slightly further advanced and eventually separate as mandibular stream. At stage 22 three distinct bulges of NCCs become visible, until at stage 25 all cells

are divided into mandibular, hyoid and branchial stream. The latter finally splits into three individual streams (Theveneau & Mayor, 2012; cf. stream pattern **Fig. 3A**).

With proceeding migration, NCCs progressively develop their mesenchymal organisation (T. Schroeder, 1970). In general, EMT is achieved by the degradation of basement-membrane, loss of cell-cell adhesion, acquirement of motility and final invasion of the extracellular matrix (ECM; Trainor, 2014). On cellular level, this requires changes in cell polarity as well as reorganisation of the cytoskeleton to enable active formation of polarised cell protrusions. Migrating cranial NCCs display such a functional front-to-rear organisation, marked by localised actin polarisation and spreading of lamellipodia at the front end as well as a corresponding retraction area at the back.

Molecular actin regulation is thereby based on spatial organisation of Wnt/PCP-signalling and downstream localisation of small GTPases, comparable to its function in CE. At the front, regionalised expression of CDC42 and Rac1 induces cytoskeletal rearrangements and rapid actin polymerisation resulting in directed protrusion formation and attachment to the ECM. Whereas RhoA and ROCK promote collapse of protrusions, mediated by actin-myosin contractions, at the rear end of the cell (Mayor & Etienne-Manneville, 2016; cf. localised expression **Fig. 3B**). Overall, this essential step in embryonic development is also based on the precise control of actin dynamics as well as of cytoskeletal organisation within individual cells.

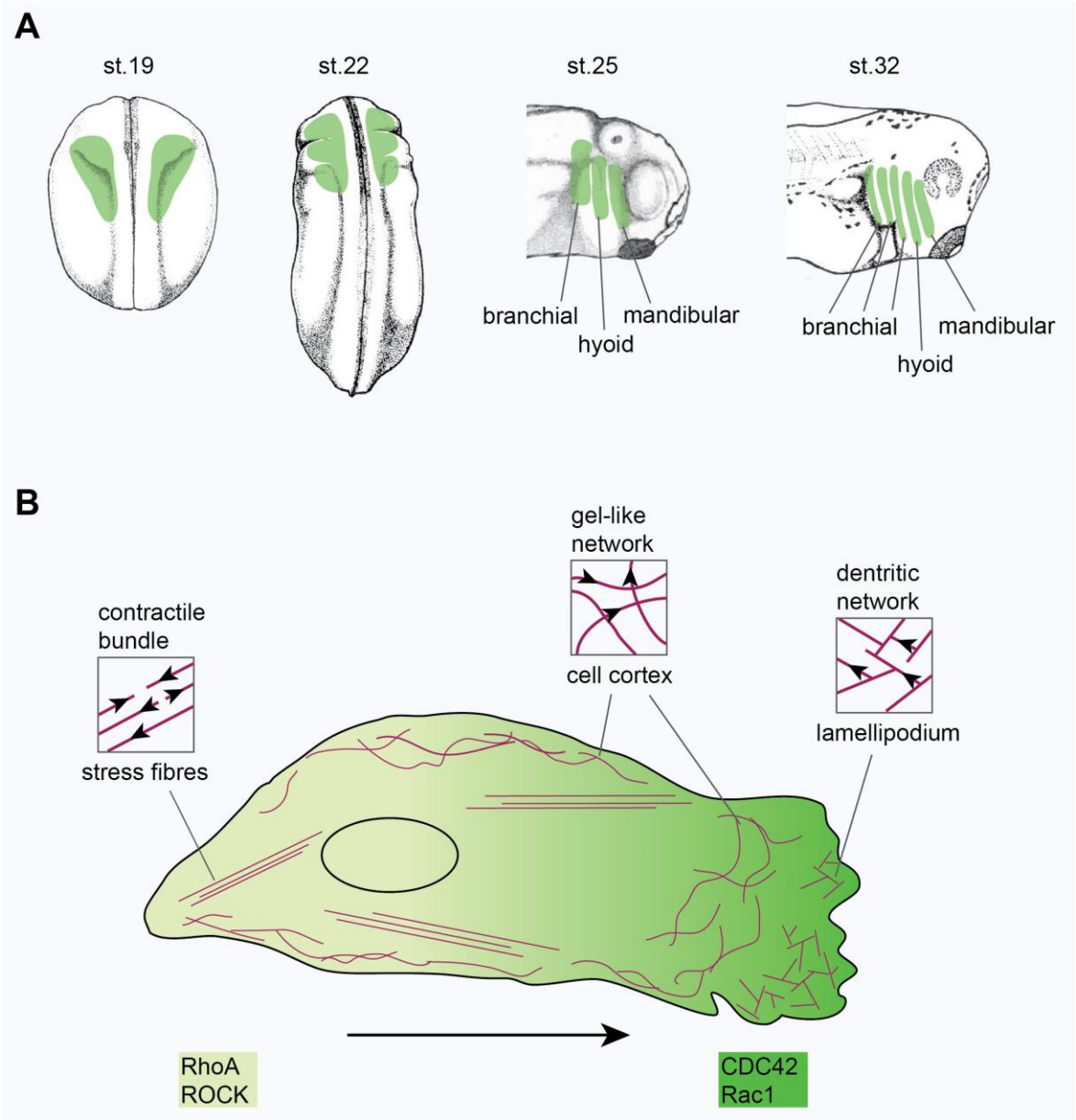

Figure 3: Cranial neural crest cell migration

(**A**) Schematic representation of sequential progress in cranial NCC migration at different embryonic stages. Advancing NCC streams indicated in light green.

(**B**) Simplified sketch of migrating NCC. Direction of migration indicated by black arrow (bottom), regionalised localisation of critical small GTPases and kinase implied by respective colouring in different shades of green. Distribution and organisation of underlying actin filaments (pink lines) displayed for stress fibres, cell cortex and in lamellipodia. Please note corresponding boxes on top for higher magnification (inspired by Theveneau & Mayor, 2012 and Alberts et al., 2015).

1.3. The Cytoskeleton

As already indicated, the very core of all morphogenetic processes is the spatial and mechanical organisation of single cells. In order to establish large-scale polarity and enable dynamic shape changes, each cell contains a complex system of thin filaments representing the cytoskeleton. It consists of actin filaments, microtubules and intermediate filaments, all displaying distinct mechanical properties and function collectively in a highly organised manner (Alberts et al., 2015).

Intermediate filaments are rope-like fibres with a diameter around 10 nm. They either line the nuclear envelope, in order to form a protective meshwork for DNA, or span the cytoplasm as robust cables transducing mechanical strength between epithelial cells (Quinlan et al., 2017).

Microtubules on the other hand, are long and hollow tubes built by tubulin with an outer diameter of 25nm. They are highly dynamic and constitute for example the mitotic spindle, form different types of cilia or serve as tracks for intracellular transport of motor protein associated components (Goodson & Jonasson, 2018).

Cell shape changing dynamics mainly are actin filament-dependent. Those flexible filaments display a diameter of about 8nm and are assembled by globular actin monomers (G-actin) in a helical manner. Each G-actin molecule carries an associated ATP/ADP molecule that serves as substrate for interacting myosin motor proteins to enable contractility. Filamentous actin (F-actin) displays the highest concentration just beneath the plasma membrane within the cellular cortex, where it provides stability for the overlying lipid bilayer (Alberts et al., 2015).

In general, actin filaments are organised into differently structured arrays forming tight bundles, stress fibres as well as dendritic or gel-like networks (cf. **Fig. 3B**). Each type of organisation is regulated by specific nucleating and accessory proteins (Alberts et al., 2015). Stress fibres traverse the cell as straight, contractile bundles, which are linked to the ECM via focal adhesions. Consequently, they contribute to stabilisation as well as tension transduction and are degraded in migrating cells (Burridge & Guilluy, 2016). The cell cortex contains a looser meshwork of filaments, which are attached in large angles with respect to each other. In order to form sheet-like lamellipodia, cortical F-actin gets organised into dendritic structures by attaching minus ends of single filaments to the side of others (Winder & Ayscough, 2005).

Overall, these different possibilities in organising actin structures facilitate highly regulated dynamics of the cytoskeleton. In the course of intercalation and migration, respective F-actin organisation is crucial for the cooperation between forming protrusions at the frontal plasma edge and back sided contraction of the cell body (Small & Resch, 2005).

The precise regulation of actin dynamics is thereby achieved by numerous accessory proteins like F-actin binding proteins, which possess at least one actin binding domain. Members with two binding sides are able to either bind and stabilise one filament or they cross-link two different filaments in contractile bundles and viscous networks (Winder & Ayscough, 2005). Thus, F-actin binding proteins embody essential molecular switches for spatial organisation of cell shape changes.

1.4. The Calponin protein family

Calponins (Cnns) represent an evolutionary highly conserved family of F-actin binding proteins, also referred to as “calcium and calmodulin-binding troponin T-like protein(s)” (Winder & Walsh, 1990).

The first Calponin, with a size of 34-kDa, was isolated from chicken gizzard smooth muscle tissue 35 years ago (Takahashi et al., 1986). In general, all vertebrates possess three isoforms named Calponin (Cnn) 1-3, formerly known as h1-3 Calponin. They are encoded by homologues genes whose expression is detectable during vertebrate development in various tissues and in an isoform-specific pattern (Miano & Olson, 1996; Samaha et al., 1996).

As the name already indicates, Cnn is capable of binding Calcium or different proteins like F-actin, Calmodulin and Tropomyosin. *In vitro* analysis of Cnn1 revealed additional interactions with Myosin, Caldesmon, Tubulin, Desmin, kinases and phospholipids (Gimona & Mital, 1998). Cnn1 and Cnn3 also display functional ROCK target sides (Kaneko et al., 2000; Shibukawa et al., 2013). Therefore, it associates with key components of cytoskeletal organisation and seems to be involved in corresponding regulative as well as signal transduction events.

About two thirds of the N-terminal Cnn amino acid sequences are highly conserved, not only between different species but also among the three isoforms. Every isoform has a N-terminal Calponin homology (CH) domain, followed by two actin binding domains and an individual C-terminus that gives each protein its specific characteristics (Rozenblum & Gimona, 2008; cf. protein structure **Fig. 4**).

The CH domain comprises about 100 residues, which form predominantly a helical globular structure. It mediates the binding of Calcium, Calmodulin and Tropomyosin but does not influence F-actin binding (Gimona & Mital, 1998; Winder & Walsh, 1993).

Close beside it, the first actin binding domain (ABD1) lies as part of the surface-exposed protein region. ABD1 mediates actin binding and constitutes phosphorylation sites for different kinases like protein kinase C, Cam kinase II and ROCK (Naka et al., 1990; Winder & Walsh, 1993; Kaneko et al., 2000). It also possesses an ATPase inhibitory peptide that is involved in the inhibition of actin-myosin ATPase activity (Kolakowski et al., 1995; El-Mezgueldi, 1996).

Next to this, ABD2 follows which is thought to be essential for actin binding functions of Cnn and contains a succession of three sequence repeats copies with 23-29 amino acids each, designated as Calponin-like (Clik) repeats (Burgstaller et al., 2002; Rozenblum & Gimona, 2008). They are able to influence actin filament stability as well as bundle formation in smooth muscle cells (Gimona, Kaverina, Resch, Vignal, & Burgstaller, 2003). Altogether, both ABDs display different activities within the single isoforms, therefore Cnns are enable to bind at least one filament subunit per protein.

Finally, the C-terminal region gives each isoform its specific isoelectric characteristics, based on intermolecular differences regarding total length and number of negatively charged amino acid residues present. It was shown that this unique tail sequence has a regulatory effect on Cnn function in the course of F-actin binding and consequently on its intercellular localisation (Bartegi et al., 1999; Danninger & Gimona, 2000). Due to their specific C-termini, Cnn1 is considered as basic, Cnn2 as neutral and Cnn3 displays acidic properties.

Cnn1 is predominantly expressed in smooth muscle cells of mammals, where it modulates contractility by association with stress fibres and inhibition of myosin ATPase activity. Most experimental and biochemical studies regarding general Cnn function are based on analyses of this isoform (Szymanski, 2004).

Although it is also present in smooth muscle cells, Cnn2 can be found in a variety of non-muscle cells like keratinocytes, fibroblasts, endothelial and lung alveolar cells (Fukui et al., 1996; Masuda et al., 1996; Hossain et al., 2003, 2006). Moreover, it seems to be differentially regulated in breast and prostate cancer cells (Hossain et al., 2014; Ji et al., 2015). Cnn2 localises to the periphery of migrating cells as well as to the end of stress fibres in regions of membrane anchorage and has been indicated to stabilise stress fibres (Danninger & Gimona, 2000).

Cnn3 is expressed in smooth muscle cells and numerous other cell types, including different neural cell types, myoblasts, trophoblasts or lymphocytes (Represa et al., 1995; C. Agassandian et al., 2000; Ferhat et al., 1996; Flemming et al., 2015). It plays a role for cytoskeleton organisation in the course of neurite process formation, NTC as well as during cell fusion events of myogenesis (Ferhat et al., 2001, 2003; Shibukawa et al., 2013, 2010; Junghans & Herzog, 2018).

Despite the fact that the Cnn protein family has been discovered for several decades and its members are evidently associated with elemental actin dynamics in different cell types, their specific regulation and mechanics are poorly understood.

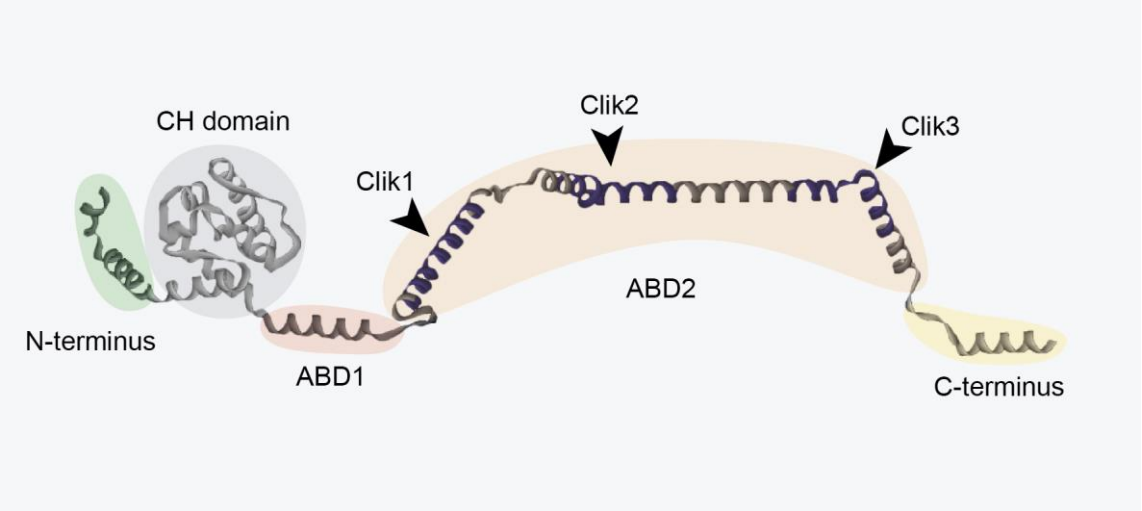

Figure 4: Calponin protein structure
Schematic representation of conserved secondary protein structure. Cnn domains are highlighted in different colours. N-terminus (green) on the left, followed by helical globular structure of CH domain (grey). Neighbouring ABD1 (red) constitutes surface-exposed region containing actin binding motif and myosin ATPase inhibiting peptide. Followed by intrinsically unstructured ABD2 (orange) including the Clik domains 1-3 (indicated by black arrowheads and marked in blue). Isoform-specific C-terminus (yellow) on the right side (protein structure retrieved from Rozenblum & Gimona, 2008).

1.4.1. Calponin in *Xenopus laevis*

The analysis of the potential role of Cnns during the early development of *Xenopus* has been started in different projects.

It has been shown that *cnn2* and *cnn3* mRNA is expressed in early frog embryos. First *cnn2* expression can be found in the presumptive neural and non-neural ectoderm as well as in pre-migratory mesoderm and endoderm of gastrulas at stage 12 (Schmalholz, 2008). It is also expressed in notochord, floor plate and in migratory NCCs (Ulmer et al., 2013). Additionally, artificial *cnn2* expression can be observed in mesodermal-induced animal caps (Hagenlocher, 2010).

Cnn3 mRNA is already detectable in 4-cell embryos within the animal blastomere regions. It resembles the expression pattern of *cnn2* during gastrulation and is also expressed in neural folds, dorsal endoderm, NT and neuroectodermal head region of older stages (Schmalholz, 2008; Ulmer, 2012).

Functional analysis, as part of GOF experiments, indicated a role of Cnn2 during early NCC migration within the branchial arch (Schmalholz, 2008). Additionally, overexpression of a tagged Cnn2 protein version led to a detectable and localised expression of the protein in NCC explants (Ulmer, 2012). First *cnn2* LOF experiments indicated gastrulation defects, which eventually led to malformations in neurulation (Loges, 2008). In mesodermal-induced animal caps, the *cnn2*-knockdown caused a reduction in elongation (Hagenlocher, 2010). Comparable experiments analysing *cnn3* function, induced NTDs as well as craniofacial malformations of the cartilage tissue in tadpole stages (Loges, 2008; Fürst, 2016).

In summary, all analyses conducted so far demonstrated an expression of both genes in tissues undergoing CE or dynamic shape changes in the course of cell migration. Further experimental data underlined the potential role of Cnn2 and Cnn3 during these fundamental morphogenetic processes.

1.5. Aim of this study

Cnns constitute an elemental group of actin binding proteins that are critical for the precise cytoskeletal organisation within the cells. It has been shown that all Cnn isoforms are expressed in *Xenopus* embryos at different developmental stages and that experimental data is obtainable. Especially, expression of *cnn2* during gastrulation, neurulation and its potential role in cranial NCC migration is highly interesting, as it covers most basic steps in embryonic morphogenesis.

Preceding studies already implied a polarised localisation of Cnn2 and its function in NCC migration (Ulmer et al., 2013). As temporospatial recruitment of regulating proteins and Wnt/PCP components is a prerequisite for directed cell migration, a respective role of Cnn2 in this context is conceivable.

Therefore, the specific function of Cnn2 in migrating NCCs was analysed more closely within the scope of this work. In a first step of analysis, its precise localisation in NCCs was examined. Based on the assumption, that proper F-actin binding is necessary to enable Cnn2 function, deletion constructs were synthesised, each missing one potential actin-binding domain. Thus, the influence of individual actin binding domains was tested by overexpressing respective deletion constructs separately within NCC explants.

Additional LOF approaches were utilised to elucidate Cnn2 function during the course of elemental morphogenetic events, such as NC formation or NCC migration and neurulation.

Finally, experiments testing the rescue ability of individual deletion constructs were conducted to identify protein domains that are crucial for proper Cnn2 function.

Overall, the specific role of Cnn2 as regulator of actin dynamics was analysed in detail within the scope of this study. Regarding the high degree of Cnn2 sequence conservation among different species as well as the conserved morphogenetic processes during early vertebrate development, the experiments performed here should reveal general regulative mechanisms.

2. Results

As already described Calponin2 (Cnn2) belongs to a highly conserved actin-binding protein family. Detailed sequence comparison of the Cnn2 homologue in *Xenopus* to other species displayed a high degree of amino acid similarities and confirmed evolutionary conservation among vertebrate species. Especially the N-terminal Calponin homology domain as well as the two regions involved in actin-binding of the protein are highly conserved between chick, mouse and humans (cf. **Fig. 5**). The total sequence homology between *Xenopus laevis* and *Gallus gallus* Cnn2 adds up to 87 %, to 91 % compared with *Mus musculus* and to 90 % regarding the *Homo sapiens* protein version.

This high degree of homology is very interesting in terms of a possible transferability of experimental results to studies in these model organisms and among each other. Furthermore, the evolutionary conservation of Cnn2 underlines its potentially central role for early vertebrate development in general.

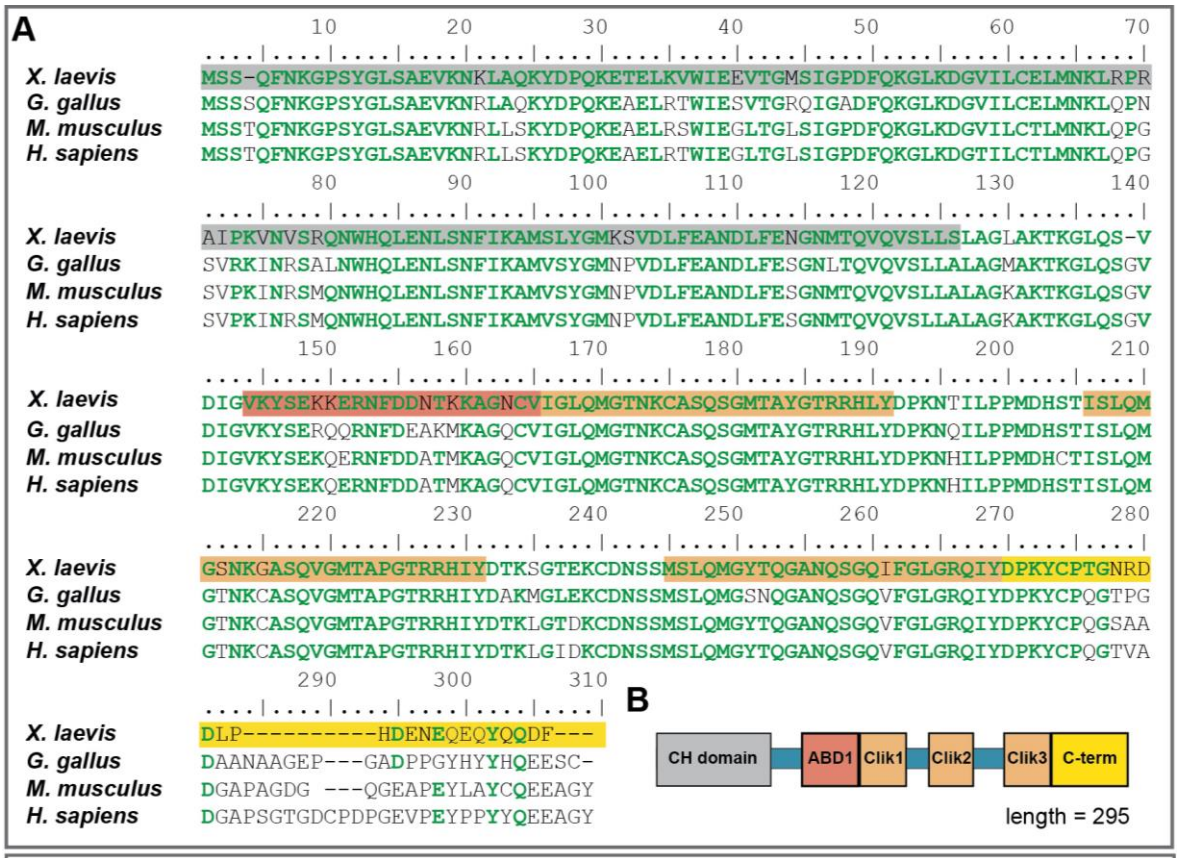

C

	length	identities	positives
Gallus gallus Cnn2	305	233/286(81%)	250/286(87%)
Mus musculus Cnn2	305	238/279(85%)	254/279(91%)
Homo sapiens Cnn2	309	238/279(85%)	253/279(90%)

Figure 5: Comparison of Cnn2 protein sequences between frog, chick, mouse and human.

(**A**) Multiple alignment of Cnn2 homologue amino acid sequences of frog (*X. laevis*), chick (*G. gallus*), mouse (*M. musculus*) and human (*H. sapiens*). Amino acids matching with the frog residues were marked in green bold letters. (**B**) Simplified draft of the protein domains composing *Xenopus* Cnn2 (cf. coloured boxes), corresponding amino acids were highlighted in same colour code within the alignment. (**C**) Table shows respective protein lengths and number/percentage of identical amino acids (=identities) or of amino acids with similar biochemical characteristics (=positives). Annotated sequences were retrieved from "https://www.ncbi.nlm.nih.gov/", with following source IDs; *Xenopus l.* (GenBank: AAH46257.1), *Gallus g.* (NCBI Ref. Seq.: NP_001135728.1), *Mus m.* (NCBI Ref. Seq.: NP_031751.1) and *Homo s.* (NCBI Ref. Seq.: NP_004359.1).

2.1. Calponin2 in the neural crest

2.1.1. *Calponin2* is expressed in cranial neural crest cells

In the first step of this project, the potential function of Cnn2 in migrating NCCs was analysed more closely. Therefore, its specific gene expression was examined using whole-mount *in situ* hybridisation (WMISH). An anti-sense probe against *cnn2* mRNA was synthesised and sequenced before usage.

To identify the tissues expressing *cnn2*, stage 32 embryos were fixed and stained. At this time point, NCC migration is well advanced and especially the cell streams within the pharyngeal arches, comprising the cranial NCCs, have reached their final lateral positions. Primary analysis of whole-mounts showed clear *cnn2* expression in the embryonic head around the eye cup, in the branchial arches, throughout the notochord and in the heart primordium (cf. **Fig. 6A** and **B**). Histological sections of these specimens revealed the exact expression localisation. Frontal sections through and beneath the developing eye displayed *cnn2* mRNA localisation in close vicinity of the eye cup, both anteriorly and posteriorly next to the otic vesicle. It was also detectable in the notochord and in the core of the branchial arches (cf. **Fig. 6A´-A´´**). Additional transversal sections confirmed the restricted *cnn2* expression within the lateral NCC streams and in the notochord. The prominent mRNA localization in the heart primordium was also visible in transversal sections (data not shown).

In summary, *cnn2* mRNA was clearly expressed in tissues derived from the cranial NC as well as in the heart primordium, which includes vagal NCCs. Together with the detected notochord expression, it can be stated that *cnn2* was expressed in embryonic tissues undergoing dramatic morphogenetic changes such as cell migration and convergent extension.

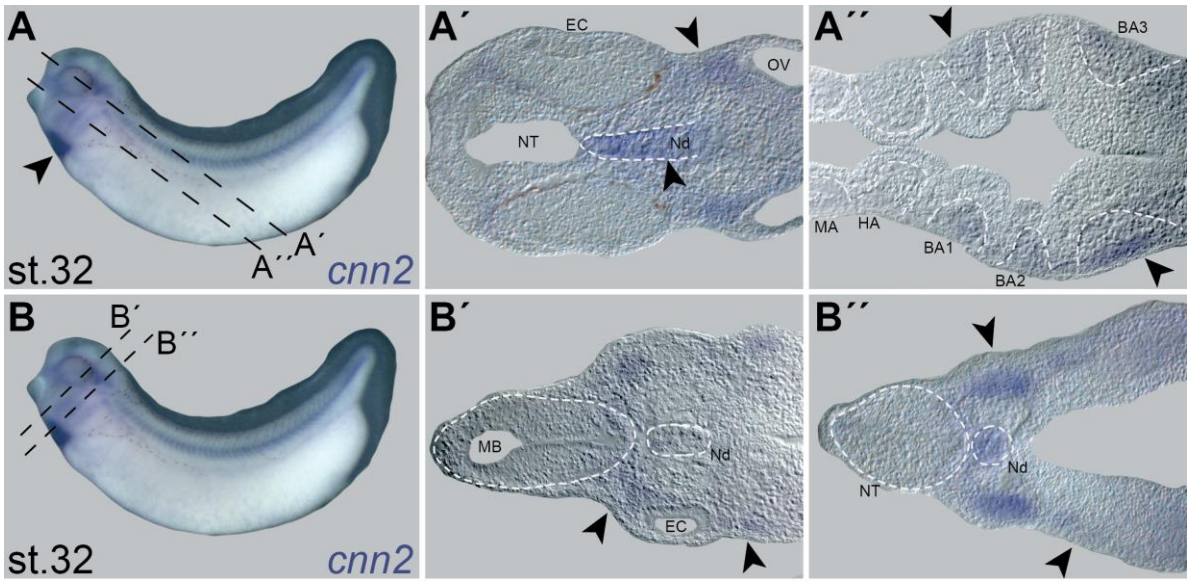

Figure 6: *Cnn2* expression pattern within cranial neural crest cells.
(**A** and **B**) Expression of *cnn2* mRNA visualised by WMISH at st. 32 (=purple staining). Expression was detectable in whole mount embryos around the eye, in front of the otic vesicle, within the branchial arches, in the notochord (Nd) and in the heart primordium (cf. **A**, black arrowhead). Shown embryos were cut as indicated by black dashed lines to analyse respective sections. (**A´**) Histological frontal section showed expression in notochord or in proximity to eye cup (EC) and otic vesicle (OV) in detail (cf. arrowheads). (**A´´**) More ventrally located sections displayed expression in the core of branchial arches (BA 1-3, cf. arrowheads; MA=mandibular arch, HA=hyoid arch). (**B´**) Transversal section displayed *cnn2*mRNA expression laterally between the developing brain (midbrain=MB) and the otic vesicle, as well as in the adjacent branchial arch. (**B´´**) Section of more posterior regions revealed clear expression in the notochord, next to the otic vesicle and in the branchial arches (cf. arrowhead; NT=neural tube).

2.1.2. *Cnn2* mRNA constructs

After *cnn2* mRNA expression was analysed in cranial NCCs, the role of the protein itself during NCC migration was examined. Unfortunately, of several anti-Cnn2 antibodies tested, none worked in *Xenopus* embryos. For this reason and to enable a detailed analysis of Cnn2 function *in vivo*, several mRNA constructs encoding different protein versions were synthesised. All constructs were generated using PCR technique, cloned into the CS2+ vector and mRNA synthesized from the vectors was injected into early embryos.

Besides a full-length construct encoding the whole Cnn2 sequence, various deletion constructs were designed additionally. As already described, Cnn2 has five protein domains, which were indicated to play a role in the regulation of actin binding, i.e. ABD1, Clik1-3 and the C-terminus. Each of these critical domains was deleted separately in the corresponding constructs. This resulted in a total of six mRNA constructs for experimental testing (cf. **Fig. 7**). To facilitate intracellular localization assays for the different protein versions, all constructs were tagged at their N-terminus with six repeats of a polypeptide protein tag derived from the c-myc gene, which comprises ten amino acids per repeat (EQKLISEEDL). All constructs were sequenced before experimental usage.

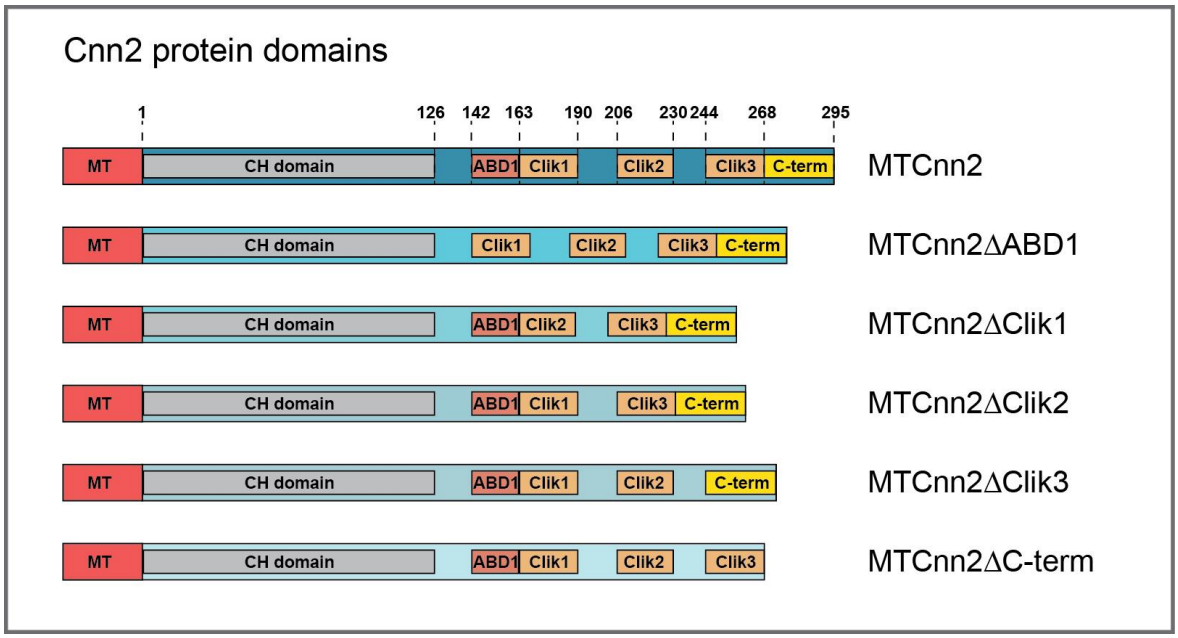

Figure 7: Cnn2 protein domains and deletion constructs.
Schematic illustration shows Cnn2 protein deletion constructs. Molecular c-myc tag (MT=red; 6 c-myc repeats) and protein domains are mapped for each construct. Calponin homology domain (CH domain=grey), actin binding domain1 (ABD1=rust), Calponin-like repeat domains 1-3 (Clik1-3=beige) and the C-terminus (C-term=yellow). On top, MTCnn2 full-length construct, comprising N-terminal MT and wild type Cnn2 sequence, position of amino acids indicated in scale above (cf. dashed lines and numbers). Below, maps of deletion constructs, each missing one protein domain marked by Δ and indicated in corresponding nomenclature (cf. MTCnn2ΔX, X=deleted domain). All deletions were implemented in frame and plasmids encoding respective mRNA constructs were sequenced before experimental usage.

2.1.3. Overexpression of MTCnn2 and MTCnn2ΔABD1 in NCC explants

In a first step of analysis, the exact localisation of Cnn2 within emigrating NCCs was examined. To achieve this, 0.32 ng of mRNA encoding the full-length MTCnn2 construct were injected unilaterally into 8-cell embryos, targeting the NC lineage of the left side. In the same experimental set-up, mRNA encoding MTCnn2ΔABD1 was injected in parallel to observe possible alterations regarding protein localisation upon deletion of the first intramolecular actin-binding domain. All embryos were co-injected with mRNA encoding enhanced green fluorescent protein (eGFP) serving as constitutively fluorescent lineage tracer (LT). After the injection, specimens were allowed to grow until stage 14, when neural fold formation becomes visible. At this time point, all embryos were controlled for correct targeting of the left NC. Following this, explants of the respective tissue were dissected at embryonic stage 16 and incubated on cover glasses coated with fibronectin to enable cell adhesion and migration. Explants excised from the contralateral non-treated NC served as positive control for successful cell attachment and migration in the culture medium. All samples were incubated for ~18 h at room temperature (RT) until NCCs had started to migrate out of the explanted tissue. Subsequently, they were fixed, subjected to immunofluorescence (IF) staining and by confocal laser scanning microscopy (LSM). The N-terminal MT was visualised by a primary anti-c-myc antibody in combination with red-fluorescing secondary antibody. Cytoskeletal F-actin was stained with fluorescently labelled green phalloidin and cell nuclei rendered visible with 4′,6-diamidino-2-phenylindole (DAPI) (cf. **Fig. 8**). In the course of detailed analysis, the MT signal was detectable in all explants derived from injected NC tissue.

The full-length MTCnn2 was strongly expressed in all cells migrating away from the explant. It was also detectable within the explant itself, although some patches were devoid of signal despite evenly distributed LT throughout the entirety of cells (cf. **Fig. 8A´**, **A´´**; white arrowhead). Scans in higher magnification of cells at the explant boundary revealed a polarised localisation of MTCnn2 towards the outer edges and in already formed lamellipodia of cells, which were about to emigrate from the explant (cf. **Fig. 8B´´**; white arrowheads). Contrary to this, the overall expression of MTCnn2ΔABD1 seemed to be more prominent within the whole NCC explant and displayed clearly detectable expression in all cells. Additionally, the intracellular

distribution of the protein construct was extensive and non-polarized (cf. **Fig. 8C´´**; white arrowheads). Close-ups of the respective explant edges confirmed the uniform distribution of MTCnn2ΔABD1 in the fringe cells (cf. **Fig. 8D´´**; white arrowheads).

In summary, this analysis displayed a differential localisation of MTCnn2 compared with MTCnn2ΔABD1. The distribution pattern of the full-length construct indicated that Cnn2 firstly is degraded in a subpopulation of cells within the explants secondly localises in polarised manner in emigrating NCCs, while the deletion of ABD1 impaired polarisation and degradation.

Nevertheless, the overall very strong signal of the artificially overexpressed constructs made it difficult to analyze potential differences in degradation and localization more precisely. Besides, former studies had already indicated a more prominently visible degradation as well as a polarised localisation of MTCnn2 in NCC explants (Ulmer et al., 2013). Conspicuously, compared to uninjected control explants, fewer injected explants attached properly, which implied a negative effect of the high amount of injected mRNA.

Therefore, the mRNA was titrated and reduced accordingly in the following experiments to enable a more detailed analysis.

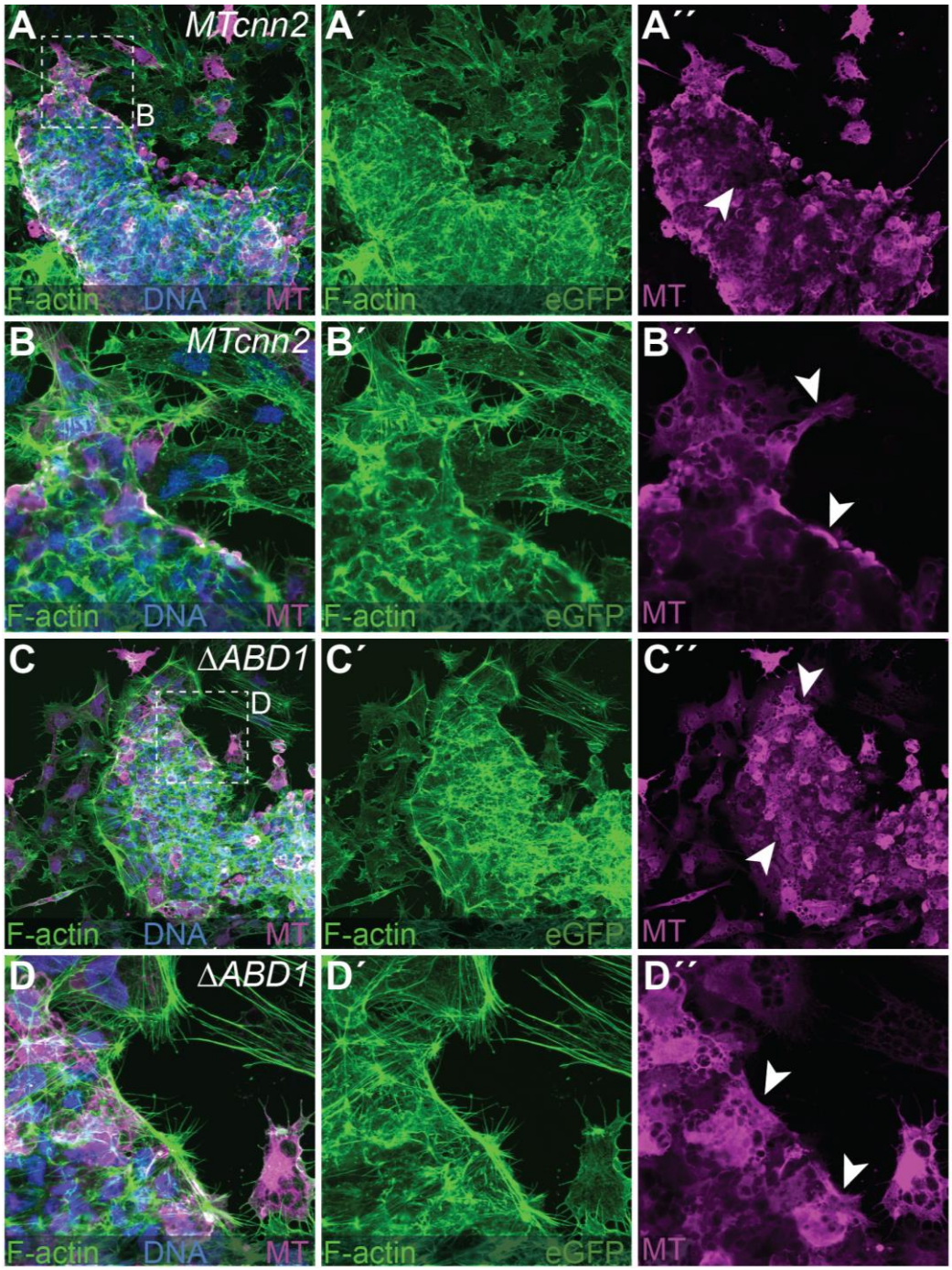

Figure 8: Localisation of MTCnn2 and MTCnn2ΔABD1 in neural crest cell explants. (**A**-**D**) Fixed NCC explants dissected from injected NCs and stained by indirect immunofluorescence (IF) technique. MT visualised by anti-c-myc 1st combined with red fluorescing 2nd antibody (=magenta signal), F-actin marked by fluorescently labelled phalloidin and detected together with eGFP serving as LT (=green signal) and nuclei were stained by DAPI (DNA=blue signal). (**A**-**B**) NCC explant injected with *MTcnn2* mRNA displayed MT signal in all cells leaving the explant on top and at the edges. Signal was reduced in the middle (cf. **A´´**, white arrowhead). MTCnn2 localisation was polarised to the outer edges and lamellipodia of cells at the explant boundary (cf. **B´´**, white arrowheads). (**C-D**) Upon *MTcnn2ΔABD1* mRNA injection, MT signal was comparably stronger throughout entire explant (cf. **C´´**, white arrowheads). Boundary cells displayed even MTCnn2ΔABD1 distribution (cf. **D´´**, white arrowheads).

2.1.4. Low-dose *MTcnn2* mRNA-injection enabled detailed analysis

In the course of establishing the optimal experimental dose for injection, *MTcnn2* mRNA was used in numerous experiments using different concentrations. Furthermore, NCC explants were dissected from slightly older embryos at stage 17 and incubated overnight at 15 °C for ~21 h. The individual amount of mRNA ranged from the initial concentration of 0.32 ng to finally 0.1 ng. In addition, different LTs were tested to optimize NCC explant analysis. With an injection of 0.1ng mRNA and the usage of blue fluorescently labelled dextran (Cascade Blue^{TM}) as LT, the expression was detectable specifically at the explant edges, reproducing the observation of Ulmer et al., 2013. The fixed explants displayed MTCnn2 localisation confined to the forming lamellipodia of NCCs which were about to emigrate. MTCnn2 was absent in the remaining explant although LT was detectable throughout. Within cell protrusions, MTCnn2 co-localised to the F-actin stress fibres (cf. **Fig. 9**).

To sum this up, by injecting a low-dose of *cnn2* mRNA and slight adjustments to the experimental set-up of explant dissection and culture, a specific and polarised localisation of the tagged protein towards the forming lamellipodia became detectable. Furthermore, the MTCnn2 expression was clearly restricted to cells at the explant boundary, strongly suggesting that the protein levels of Cnn2 within NCCs are tightly regulated by protein degradation.

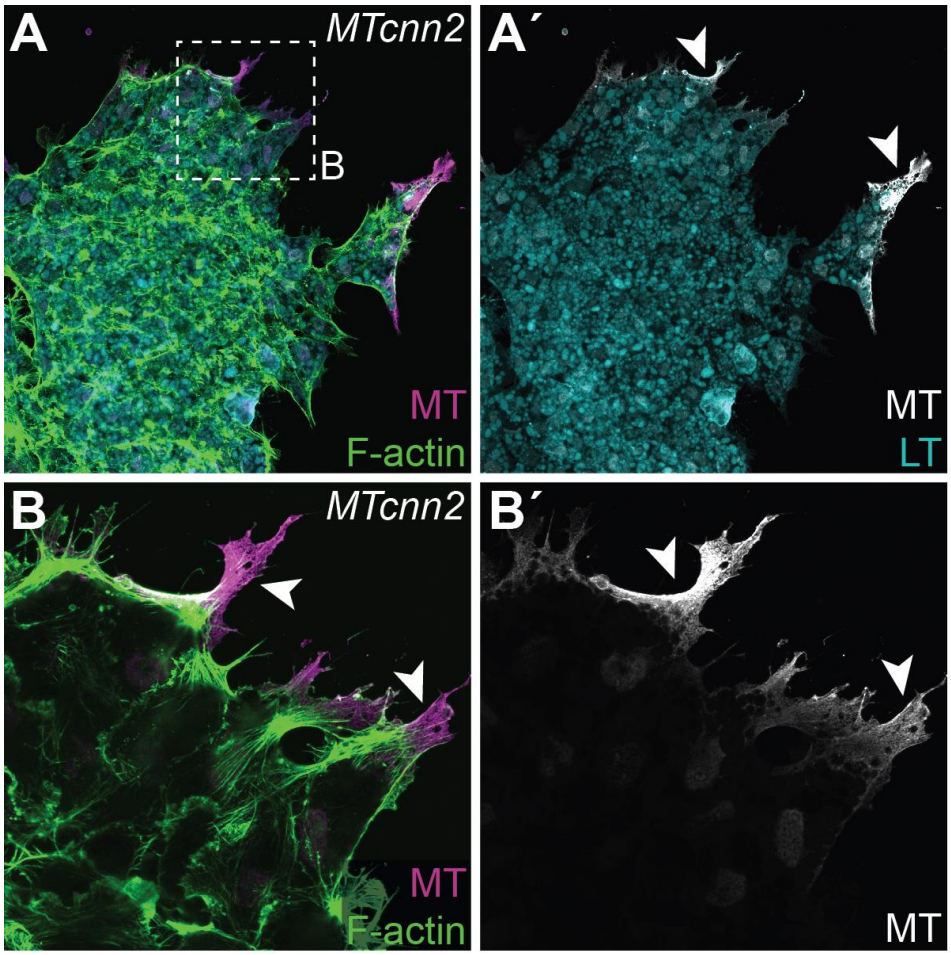

Figure 9: Reduced protein levels and polarised localisation of MTCnn2 in neural crest cell explants upon low-dose mRNA injection.

(**A**) mRNA encoding full-length construct was injected into 8-cell embryos targeting the NC lineage and visualised by IF staining in excised NCC explants. MTCnn2 MT was visualised by anti-c-myc 1st combined with red fluorescing 2nd antibody (=magenta signal) was localised at the edge of the explant, although Cascade Blue^{TM} (LT= cyan signal) was detectable in entire explant (cf. **A´**). F-actin was stained by fluorescently labelled phalloidin (=green signal) (**B**) Close-up of emigrating NCCs displayed MTCnn2 localisation in detail around actin filaments in lamellipodia (cf. white arrowheads, MT and F-actin staining shown). (**A´** and **B´**) MT signal elucidated by displaying respective channel in white.

2.1.5. Cnn2 is differentially expressed in neural crest cells upon the deletion of distinct domains that mediate actin binding

After the mRNA dose was titrated and the experimental setup was optimised, all six mRNA constructs, described in chapter 2.1.2., were analysed in NCC explants towards their individual expression level and intracellular localisation. To that end, all constructs were injected separately but into the same clutch in parallel to allow for comparative analysis. Again, 0.1 ng of mRNA was injected each together with blue fluorescing dextran. Explants were dissected at stage 17 and fixed for analysis after ~21 h of incubation at 17 °C. At this time point, the explanted NCCs had spread properly and started to migrate. Explants were stained as described above and analysed using confocal the LSM.

Closer examination of the specimens revealed a clear difference in expression of the constructs. All NCC explants attached properly and displayed similar cellular structure as well as migration behaviour compared to the co-cultured uninjected NCCs. However, the individual MT-constructs differed regarding their localisation in the whole explants and especially in cells which were just emigrating. Explants derived from NCs injected with the full-length *MTcnn2* mRNA construct displayed very weak protein expression despite evenly distributed LT signal. Notably in emigrating cells, the MTCnn2 signal was strongly reduced (cf. **Fig. 10C**-**D**). A similar expression pattern was observed in explant cells injected with *MTcnn2ΔClik3* mRNA (cf. **Fig. 10K**-**L**). Upon *MTcnn2ΔABD1* mRNA injection, the respective explant showed weak but detectable MTCnn2ΔABD1 signal and a strongly reduced expression in recently emigrated NCCs (cf. **Fig. 10E**-**F**).

In contrast to this, explants dissected after injection of *MTcnn2ΔClik1*, *-ΔClik2* or *-ΔC-term* mRNA displayed an overall strong expression of the respective construct. Especially NC explants which expressed MTCnn2ΔClik2 showed a strong signal in both, cells that were still attached to the explant as well as in already emigrated cells (cf. **Fig. 10I**-**J**). MTCnn2ΔClik1 and MTCnn2ΔC-term expressing explants displayed a signal reduction in some cells at the explant boundary but strong and extensively distributed protein localisation in emigrating NCCs (cf. **Fig. 10G**-**H** and **M**-**N**).

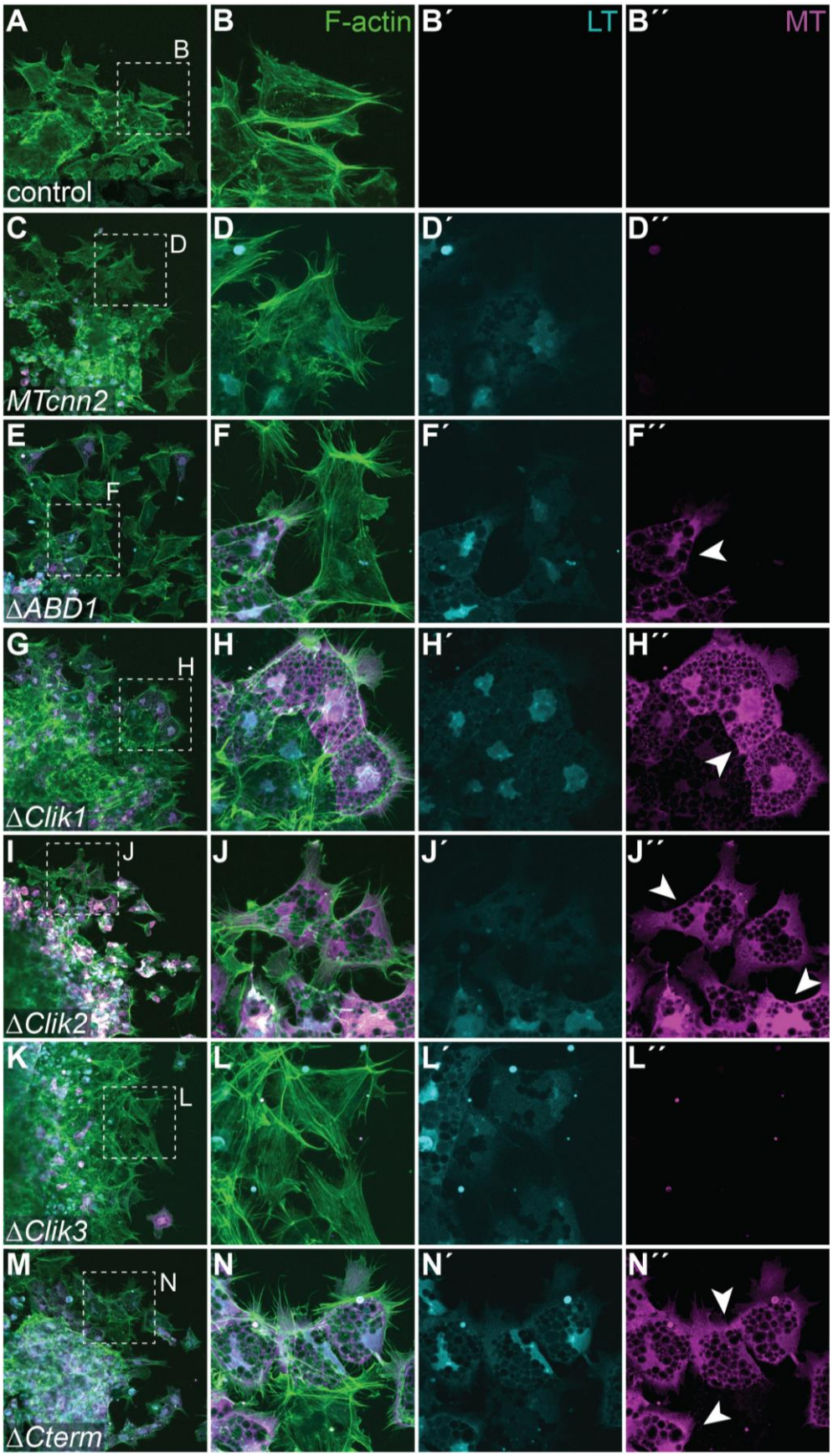

Figure 10: Deletion of distinct protein domains affects expression levels of Cnn2 in neural crest cell explants.

mRNA constructs were injected into 8-cell embryos targeting the NC lineage and visualised by IF staining in excised explants. MT was visualised by anti-c-myc 1st combined with red fluorescing 2nd antibody (=magenta signal) and F-actin structure with fluorescently labelled phalloidin (=green signal), Cascade Blue™ served as LT (=cyan signal). LT and MT signals were additionally separated (cf. 3rd and 4th column). (**A**-**B**) Uninjected NC explants served as control for wildtypic explant cell structure. (**C**-**M**) mRNA constructs encoding MTCnn2 and deletions were injected at 8-cell stage into NC to cut respective explants. (**C**) NCC explants excised after injection with *MTcnn2* mRNA showed overall very weak MTCnn2 signal. (**D**) Higher magnification images revealed LT signal in emigrating cells and reduced MTCnn2 expression (cf. **D´**; **D´´**). (**E**) Upon *MTCnn2ΔABD1* mRNA injection, MT signal was detectable in explants and partially degraded in emigrated cells (cf. **F´**; **F´´**, white arrowhead) (**G**) *MTcnn2ΔClik1* mRNA injection led to prominent protein signals, especially in outmost cells (c.f. **H´**; **H´´**, white arrowhead). (**I**) After *MTcnn2ΔClik2* mRNA injection construct signal was even more intense throughout the explants and in cells at the rim (cf. **J´**; **J´´**, white arrowheads). (**K**) MTCnn2ΔClik3 expression was detectable within explants, whereas delaminated NCCs showed nearly no expression (cf. **L´**; **L´´**). (**M**) Explants injected with *MTcnn2ΔCterm* mRNA displayed strong construct signals altogether, including emigrated cells (cf. **N´´**, white arrowheads).

To quantify the observed differences in protein expression and localisation, the entirety of experimentally tested NCC explants was analysed for their level of protein construct expression (cf. **Fig. 11**). Specimens were categorised according to their expression level in out-migrating explant cells by comparing the individual signal strength to full-length MTCnn2 expression. All expression levels similar to that of *MTcnn2* mRNA injected cells were scored as “reduced” (cf. **Fig. 10C** and **D**), while levels comparable to those upon *MTcnn2ΔClik2* mRNA injection were scored as “strong” (cf. **Fig. 10I** and **J**). Subsequent statistical analysis, utilizing chi^2-students test, attested no significant difference between *MTcnn2ΔClik3* mRNA-injected explants and those injected with the full-length *MTcnn2* mRNA construct. MTCnn2ΔABD1 expression slightly differed in signal strength, as about the expression was reduced in 63.2 % of explants. The signal strength in MTCnn2ΔClik1 and MTCnn2ΔC-term-expressing explants was comparably high with reduced signals only in 7.7 % and in 33.3 % of specimens. In MTCnn2ΔClik2-expressing explants no signal reduction was observed, which led to a statistically highly significant difference compared with MTCnn2 expression levels.

Overall, reduced construct expression levels were observed upon *MTcnn2*, *-ΔClik3* and *-ΔABD1* mRNA injection, whereas the introduction of *MTcnn2ΔClik1*, *-ΔClik2* or *-ΔC-term* mRNA led to a comparably strong expression. This differential construct expression indicates a tight regulation of Cnn2 protein levels which was impaired upon deletion of Clik1, Clik2 or the C-terminal domain. Each of these domains is potentially involved in the mediation of Cnn2 actin binding.

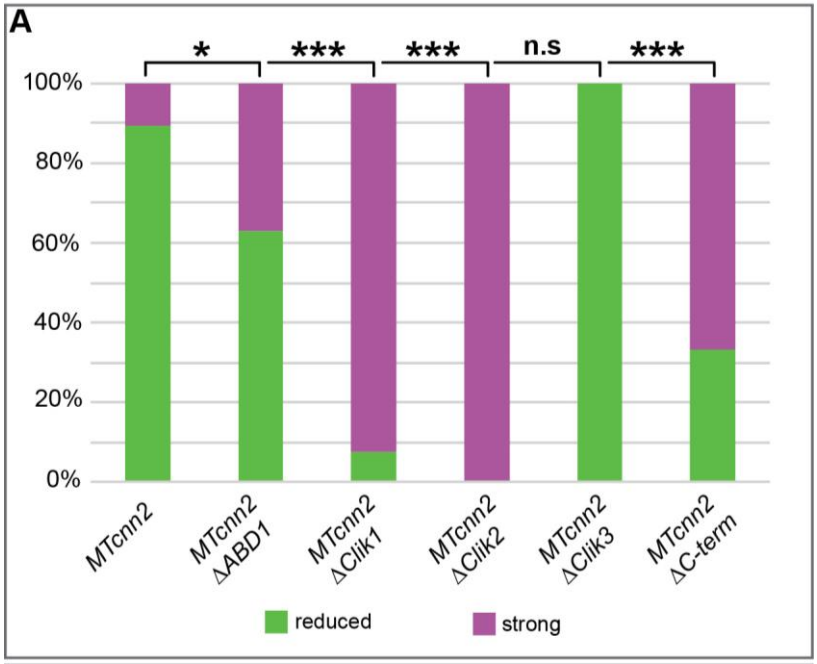

B

mRNA construct	*cnn2MT*	*MTcnn2 ΔABD1*	*MTcnn2 ΔClik1*	*MTcnn2 ΔClik2*	*MTcnn2 ΔClik3*	*MTcnn2 ΔC-term*
reduced MT signal	33	12	1	0	9	3
strong MT signal	4	7	12	10	0	6
	N=9	N=4	N=4	N=3	N=2	N=2

Figure 11: Statistical analysis confirmed domain-dependent regulation of Cnn2 expression levels.

(**A**) All injected NC explants were analysed towards their MT expression. Specimens were categorised depending on signal strength (cf. “reduced signal” vs “strong signal”) while respective co-injected LT was evenly distributed. Explants were scored as “reduced” when phenotype correlated with already described signal decrease in *MTcnn2* mRNA injected cells (cf. **Fig.6**, **C** and **D**) and categorised as “strong” if MT signal strength was comparable to *MTcnn2ΔClik2* mRNA injection phenotype (cf. **Fig.6**, **I** and **J**). (**B**) Table of absolute explant number and conducted injection experiments (N=X). Statistical analysis of phenotype distribution between different treatments was accomplished by chi²- students test (cf. **A**; n.s.=p>0.05; *=p≤0.05; ***=p≤0.001).

In summary, mRNA constructs encoding deletion variants of Cnn2, with an N-terminal c-myc tag, were successfully cloned. Furthermore, they were utilised and titrated for specific experimental testing in NCC explants.

In the course of performed analysis, the full-length Cnn2 construct displayed a polarised distribution within NCC explants and localisation towards actin stress fibres in lamellipodia of emigrating NCCs. The clearly reduced MTCnn2 expression after experimental adjustment of the injected mRNA concentration, indicated a highly regulated control of Cnn2 protein levels within NCCs. These characteristics were lost upon deletion of the domains Clik1, Clik2 and the C-terminus and resulted in an overall strong protein expression, i.e. in a dysregulation of protein homeostasis of the individual constructs.

The high degree of evolutionary sequence conservation within those three protein domains, among different vertebrate species and compared with *Xenopus*, suggests an elemental role of Clik1, Clik2 and the C-terminus in regulating the actin cytoskeleton of NCCs.

2.2. Loss-of-function (LOF) experiments

2.2.1. Design of molecular tools

To further elucidate the role of Cnn2 during embryonic development, its function was analysed using LOF approaches. Production of functional Cnn2 protein was inhibited utilising morpholino oligonucleotide (MO)-mediated gene knockdown and Clustered Regularly Interspaced Short Palindromic Repeats (CRISPR)-mediated genome editing, thus the wild type function of *cnn2* should be revealed by phenotypes caused upon the perturbation.

Before respective molecular tools were designed, it had to be taken into account that *Xenopus laevis* is a allotetraploid species. Its genome arose from two diploid progenitor species and consequently comprises two homoeologous subgenomes with respective chromosome sets (Session et al., 2016). These chromosomes differ in size and are present as long “L“- or short “S”-form, which results in two transcriptional active alloalleles for one portion of all genes. The *cnn2* locus is located to both versions of chromosome 1 (chr1L and chr1S) and transcriptome mining confirmed transcriptional activity of both alloalleles during early development. According to that, transcription starts at stage 8, with an expression peak of *cnn2.S* at stage 10 and highest expression levels of *cnn2.L* between stage 10 and 15 (cf. RNA-Seq. Data, xenbase.org; Session et al., 2016).
Therefore, all molecular tools for specific manipulation of *cnn2* gene function during embryonic development were designed in order to target both alloalleles.

In the first step, two specific MOs were designed for MO-mediated gene knockdown experiments. The “5´UTR-MO” targets the regulatory 5´ untranslated region (5´UTR) of *cnn2* mRNA to block the start of translation. As the 5´UTRs of the L- and S-allele display high sequence similarity, it was possible to identify a conserved region that was suitable for the design of one MO targeting both alloalleles. The second was a splice blocking MO (splMO), which binds the mRNA at the exon-intron border of exon3 and intron3 to inhibit splicing. Due to higher sequence differences within that region, two separate splMOs, namely “*cnn2.L*-splMO” and “*cnn2.S*-splMO”, were designed. In the following experiments both splMOs were injected together to impair function of both alloalleles at the same time.

To enable additional LOF experiments comparable with MO-mediated knockdown analysis, single guide RNAs (sgRNAs) were designed and synthesised for CRISPR/Cas9-mediated genome editing. Therefore, also "*cnn2.L*-sgRNA" and "*cnn2.S*-sgRNA" were designed to target the respective alloalleles. In the following injection experiments, both sgRNAs were pre-incubated with Cas9 protein and the built Cas9 ribonucleoprotein (CRNP) complex was used for injection.
The positions of all target sites were displayed in Figure 12 (cf. draft below).

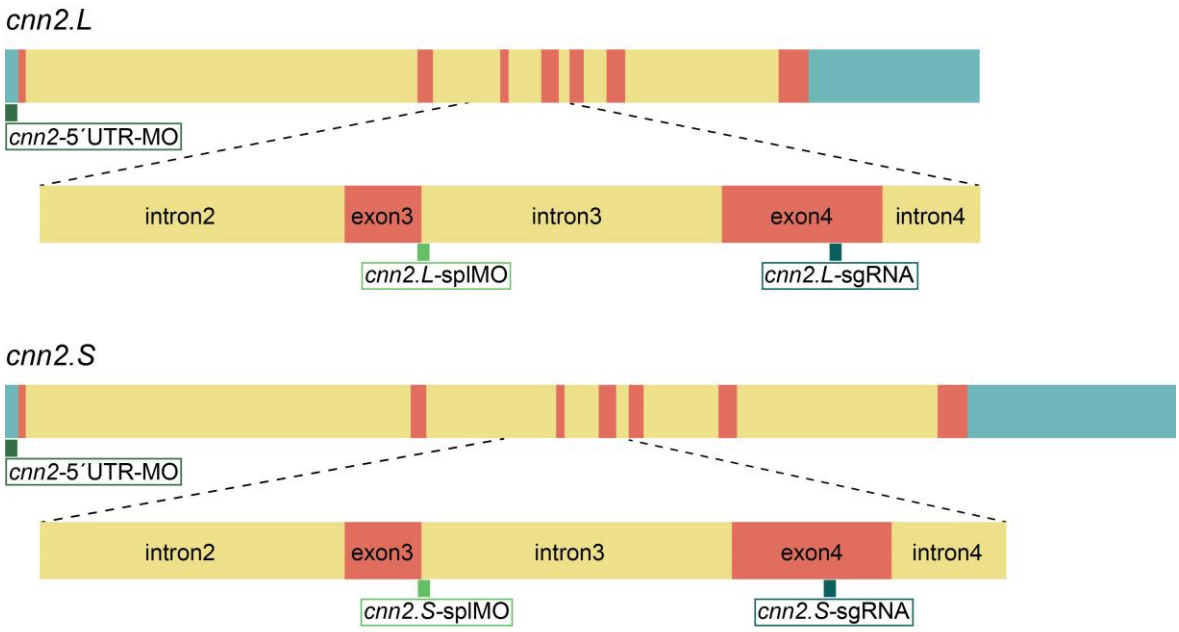

Figure 12: Morpholino and CRISPR target sites.
Schematic representation of *cnn2* precursor messenger RNAs (pre-mRNAs) are shown, *cnn2.L*-form (top) *cnn2.S*-from (bottom). Regulatory 5´(left) and 3´(right) regions indicated in light blue, introns displayed in yellow and exons marked in red. Regions between intron2 and intron5 are visualised in higher magnification (cf. dashed lines). Positions of MO and sgRNA target sites are marked by respective boxes in different shades of green.

2.2.2. Specific knockdown of *cnn2* causes severe developmental defects

Based on the described expression analysis and NCC explant data, MOs were injected unilaterally into 8-cell embryos targeting the NC lineage. The injected region was verified by co-applied LT and the un-treated contralateral side served as an internal control. After injection of 1.2 pmol *cnn2*-5´UTR MO and 1 pmol *cnn2.L*-splMO together with 1 pmol *cnn2.S*-splMO, all specimens were allowed to grow until uninjected controls reached stage 25. Embryos were fixed and analysed by whole-mount *in situ* hybridisation (WMISH) to visualise the expression of *twist*, a marker for migratory NCCs.

All embryos were categorised based on their overall morphology and *twist* expression pattern. Untreated control embryos displayed stage-specific craniofacial development as well as a wildtypic *twist* expression in distinct streams of migratory NCCs. Transversal histological sections confirmed an overall normal development and equally advanced NCC migration on both sides (cf. **Fig. 13 A**-**A´´´**). In morphants, craniofacial development as well as NCC migration was impaired, with embryos showing a range of phenotypes from mild to strong aberrations. The mild phenotype included changes in the craniofacial structure with smaller eye primordium and anterior NTDs on the injected side. Although the expression of *twist* was clearly detectable in those specimens, its pattern was slightly altered. Anterior transversal sections revealed morphological defects of the dorsal-most part of the NT, i.e. neural fusion defects and bending towards the injected side. Compared to the contralateral control side, dorsal to ventral migration of *twist*-positive cells was less advanced after MO-injection, which was accompanied by a disrupted structure of the facial tissue. Sections of the posterior part showed a closed NT and no other developmental defects (cf. **Fig. 13B**-**B´´´**). In the more severe morphant phenotype, anterior NTDs and disrupted facial structures were clearly visible on the injected side, with a smaller eye primordium as well as a reduced cement gland. In addition, *twist* expression was nearly absent and the embryos displayed blastopore closure defects (BPDs). Transversal sections within the anterior part verified an open and bent NT in addition to a strong reduction of *twist* expression together with altered facial tissue structure on the injected side. Posterior sections showed a closed but slightly bent NT and prominent BPDs (cf. **Fig. 13C**-**C´´´**).

The described phenotypes were defined as “mild NTDs” and “strong NTDs” to score the embryos respectively. Overall, 100 % (n=50 / n=55) of all analysed control embryos showed stage-specific craniofacial development and bilateral *twist* expression pattern. Contrary to this, only ~8.2 % (n=4) of morphants injected with *cnn2*-5´UTR-MO displayed wildtypic development, while ~69.4 % (n=34) showed “mild NTDs” and ~22.4 % (n=11) “strong NTDs”. A similar phenotype distribution was observed upon *cnn2*-splMO-injection, with 11.1 % (n=6) of all treated embryos displayed the wild-type phenotype, ~68.5 % (n=37) showing “mild NTDs” and ~20.4 % (n=11) “strong NTDs”. *Cnn2*-5´UTR-MO-injection was carried out in four independent experiments and *cnn2*-splMO was tested in two independent experiments (N=4 / N=2). Statistical analysis of the phenotype distributions attested highly significant differences between control and treated specimens.

To sum this up, the initial LOF experiments carried out by MO-injection into the NC lineage led to distinct developmental defects. Most of the treated embryos showed craniofacial defects (FDs), altered *twist* expression pattern and at least mild anterior NTDs. Some specimens even displayed BPDs. Additionally, it can be stated that both MOs caused the same variety of phenotypes in a similar distribution. Thus, usage of only one MO should be sufficient for further experimental analysis.

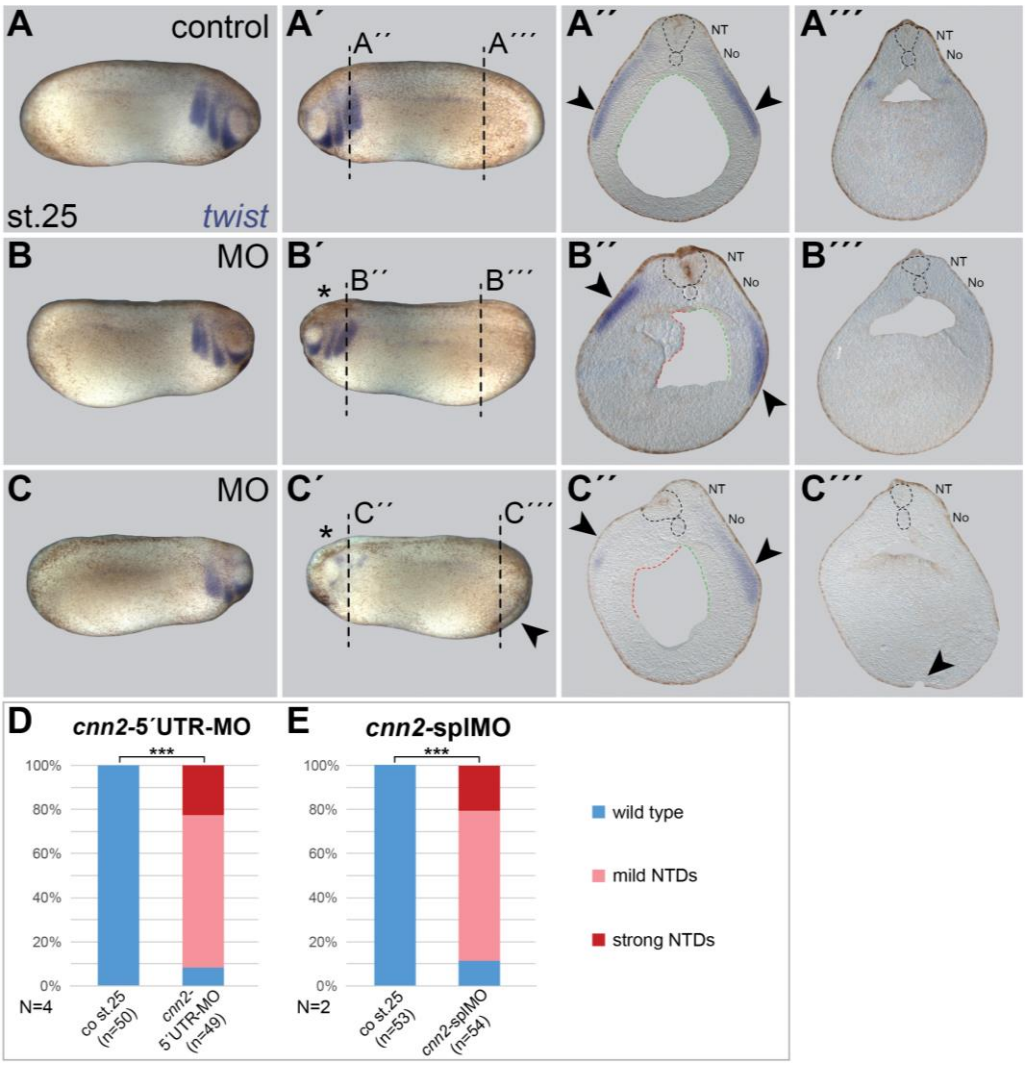

Figure 13: MO-mediated *cnn2* LOF causes craniofacial and anterior neural tube closure defects.

MOs were injected unilaterally into 8-cell embryos targeting the NC lineage. Embryos were fixed at st. 25 and stained via WMISH to visualise *twist* expression pattern. (**A**-**A´´´**) Uninjected controls showed wild-type craniofacial development and *twist* expression on both sides. Transversal sections of anterior and posterior regions attest closed neural tube (=NT, marked by black dashed lines), intact notochord (=No, marked by black dashed lines) along the body axis and bilaterally symmetric *twist* expression (cf. **A´´**, black arrowheads). (**B**-**C**) Unilateral MO-mediated knockdown of *cnn2* led to craniofacial deformations compared to control side (injected side marked by asterisks). (**B**-**B´´´**) Mild phenotype with anterior NTDs and altered *twist* patterning. Respective transversal anterior sections showed NT fusion defects (cf. **B´**, NT), dislocated *twist* expression (cf. **B´**, black arrow heads) and disrupted tissue structures on injected side (cf. **B´**, red dashed lines vs. green). (**C**-**C´´´**) Strong phenotype comprised severe craniofacial defects (FDs), anterior NTDs (cf. **C´´**, NT), reduction of *twist* expression (cf. **C´´** black arrowheads) and BPDs (cf. **C´** and **C´´´**, black arrowheads). (**D**-**E**) Quantitative analysis of phenotype distribution among MO-injected embryos compared to corresponding controls**.** Statistically highly significant difference was affirmed for both set-ups by chi²- students test (***=p≤0.001).

2.2.3. CRISPR/Cas9-mediated genome editing of *cnn2* causes developmental defects

In the next step of LOF experiments, *cnn2* genome editing was introduced using the CRISPR/Cas9 system. C*nn2.L*- and *cnn2.S*-sgRNA were injected as pre-assembled ribonucleoprotein (RNP) complexes, consisting of the Cas9 protein and the individual sgRNAs (Cas9 ribonucleoprotein=CRNP). Injections were performed into early zygote stages to facilitate efficient genome editing in the majority of all embryonic cells later on. Uninjected specimens were set aside at the same time point and incubated under the same conditions. After injections took place all embryos were allowed to grow until controls reached stage 25 to be fixed for WMISH analysing *twist* expression, like it was done in morphants.

In addition to the phenotype analysis, 10 embryos per treatment were lysed to be sequenced for validation of genome editing success and frequency. Samples were prepared for external sequencing services and results were analysed using the SYNTHEGO ICE© analysis tool (cf. **Fig. 14**). Upon injection of *cnn2.L*-CRNPs the sequenced samples displayed an indel percentage up to 84 %. The specific indel nature and their percentage distribution was also predicted, according to that, a loss of 5bp was the most abundant deletion with 39 %. The corresponding knockout-score totalled up to 73 %, meaning that 73 % of the analysed sequences comprised either a frameshift mutation or a fragment deletion of more than 21 bp, thus most likely causing a LOF of the targeted *cnn2.L* allele.

The overall indel percentage was equally high in *cnn2.S*-CRNP-injected specimens with values up to 81 %, although the associated knockout score resided at 48 %. Nevertheless, the specific indel distribution showed deletions of 6 bp in 21 % and 10 %, which might not result in a gene knockout, but possibly change the overall protein conformation due to the deleted amino acids. Those deletions occurred in the sequence segment, which encodes the C-terminal-most part of the CH domain. For both injection batches, the “model fit (R^2)” value was very high with 0.9 and 0.94, which implies that the indel distribution proposed by the algorithm fits well to the Sanger sequence data of the edited samples.

In summary, sequencing analysis attested the successful targeting and editing of the *cnn2* gene.

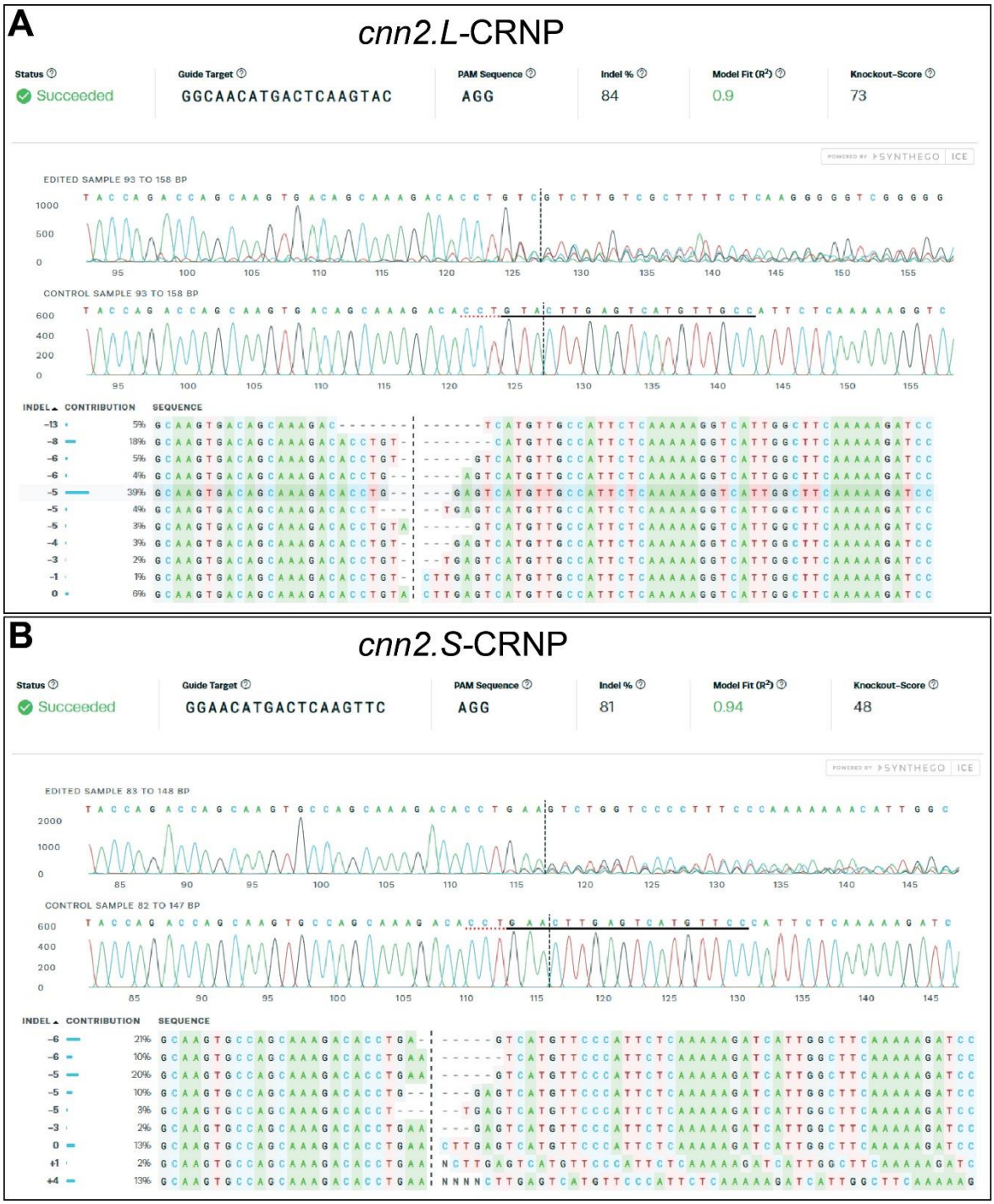

Figure 14: Sequencing of crispant samples attested successful genome editing.
(**A**) Sequencing results of specimens injected with CRNPs targeting the L-allele of *cnn2* analysed with SYNTHEGO ICE©. Upper row gives indel percentage of all sequences, model fit (R^2) value and knockout-score amongst others. Second row displays sequencing results as function of nucleic acids. Below, edited sequences and percentage distribution of respective indels. (**B**) Same analysis and listing as in (**A**) for specimens injected with CRNP targeting the S-allele of *cnn2*.

For the first round of phenotype analysis, both sgRNAs were injected separately and the respective embryos were compared with each other and to untreated controls. All control specimens displayed a stage-specific phenotype (cf. **Fig. 15A**). Upon CRNP-injection however, differently pronounced developmental defects were observed in both treatments. The less severe phenotype, hereafter referred to as “mild FDs”, displayed mild FDs marked by a smaller head and facial region. Additionally, all embryos showed BPDs (cf. **Fig. 15B**). Specimens which resembled the “strong FDs” phenotype, had an even more narrowed craniofacial region with nearly missing eye primordia, a reduced *twist* expression and displayed BPDs (cf. **Fig. 15C**). The most severe phenotype “FDs + NTDs”, included a loss of craniofacial structures, massive NTDs as well as BPDs and reduced body length (cf. **Fig. 15D**). All embryos were categorized and quantified according to the phenotypes described above (cf. **Fig. 15E**). All control specimens (100 %; n=66) displayed a stage-specific, wild type phenotype. Opposing this, only ~33.4 % (n=22) of *cnn2.L*-CRNP-injected embryos were wildtypic, whereas ~43.9 % (n=29) showed mild FDs, ~12.1 % (n=8) strong FDs and ~10.6 % (n=7) had severe NTDs. Upon *cnn2.S*-CRNP-injection, phenotype distribution was similar with ~18.9 % (n=10) of wild-type specimens, ~50.9 % (n=27) displayed mild FDs, ~20.8 % (n=11) strong FDs and ~9.4 % (n=5) severe NTDs. The injection was repeated in two independent experiments (N=2). Statistical analysis of phenotype distributions by chi²- students test confirmed a highly significant difference between controls and either of the injected *cnn2*-CRNPs, the internal relation of which to each other was not significantly different (cf. **Fig. 15E**; ***= p<=0.001, n.s.= p>0.05).

In the second part of *cnn2*-CRNPs-injection experiments, both sgRNAs targeting the L- and S-allele of *cnn2* were injected in a mixture of respective CRNPs. To test the specificity of the sgRNAs, *cnn2* mRNA encoding the wild-type protein was co-injected in a second batch. Uninjected controls were incubated in parallel and all embryos were fixed for WMISH analysis at control stage 25. Following this, specimens were categorised as above and analysed statistically (cf. **Fig. 15F**). In the course of this, ~93.8 % (n=45) of all controls displayed a wild type and ~6.2 % (n=3) a mild phenotype. Embryos injected with the combination of *cnn2.L*- and *cnn2.S*-CRNPs showed no wild type phenotypes at all, with ~53.3 % (n=24) mild FDs, 20 % (n=9) strong FDs and ~6.2 % (n=3) severe NTDs. These distinct defects

were partially rescued upon *cnn2* mRNA co-injection, as ~27,3 % (n=12) of all treated embryos showed wild type phenotype. In the same batch the percentage of specimens with mild FDs was reduced to ~27.3 % (n=12) and ~36.3 % (n=16) displayed strong FDs, while ~9.1 % (n=4) still developed massive NTDs. This rescue experiment was conducted in two independent rounds of injection (N=2). Statistical analysis attested a highly significant difference between untreated control specimens and crispants, as well as between crispants and *cnn2* mRNA co-injected embryos. This rescue effect indicated the specificity of the utilised sgRNAs to target the respective *cnn2* locus and that the induced phenotypes were actually caused by a loss of Cnn2 function.

Taken together, the CRISPR/Cas9-mediated genome editing of *cnn2* led to craniofacial malformations, BPDs, NTDs and a reduction of embryonic body length. When *cnn2.L*- and *cnn2.S*-CRNPs were injected separately, the partial knockout of the S-allele seemed to have a slightly more severe effect. After combined injection of both CRNPs together, more severe alterations were observed, with the complete absence of wild-type specimens. These induced defects were partially rescued by co-injection of *cnn2* mRNA.

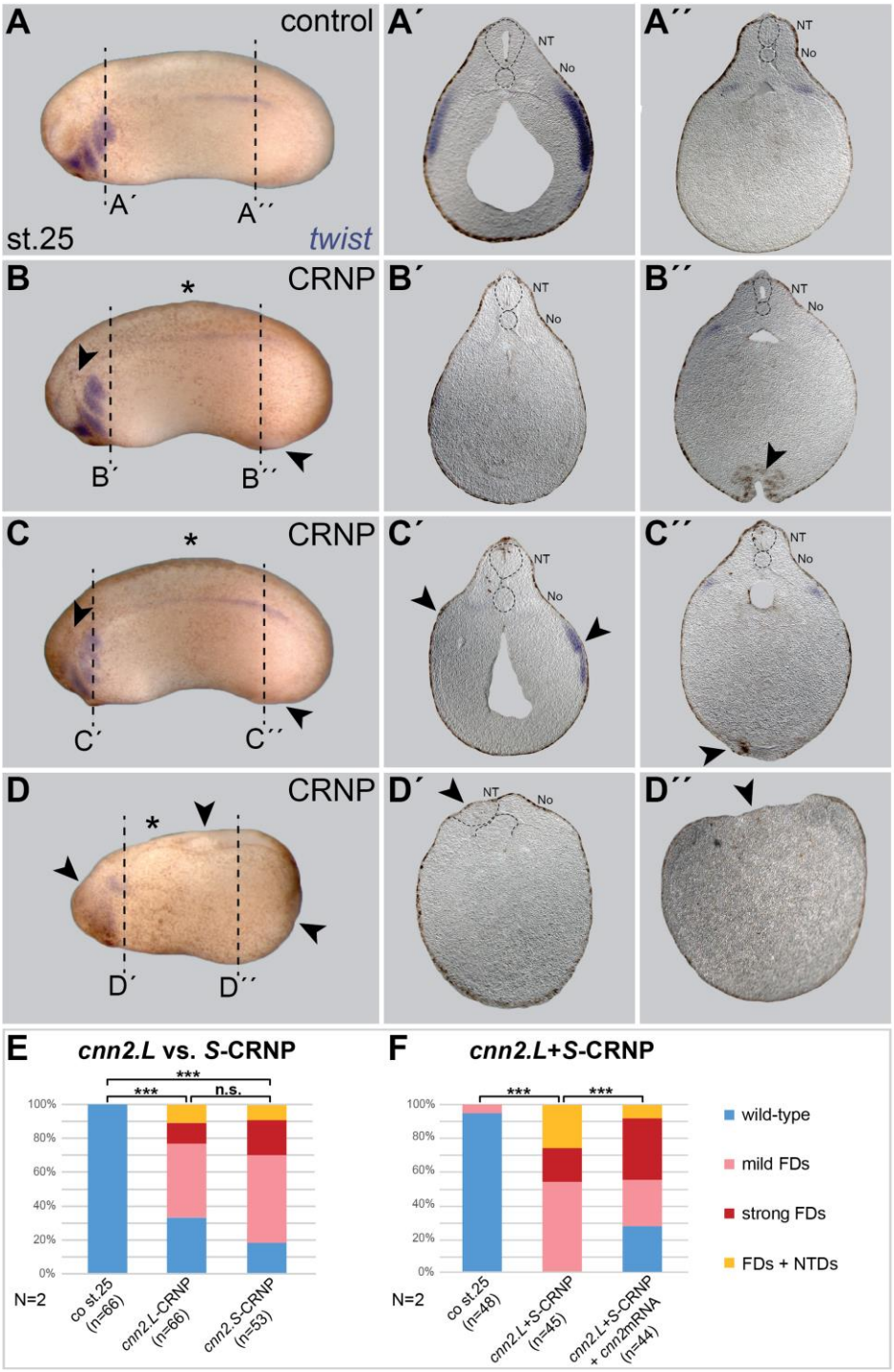

Figure 15: CRISPR/Cas9-mediated genome editing of *cnn2* causes craniofacial and neural tube closure defects.

1-cell embryos were injected, fixed when control specimens reached st. 25 and stained via WMISH to visualise *twist* expression pattern. (**A**-**A´´**) Untreated control embryos with stage-specific morphology and *twist* expression pattern. (**B**-**D**) Specimens injected with *cnn2.L*- and *cnn2.S*-CRNPs displayed distinct phenotypes (marked by asterisks). (**B**-**B´´**) Mild phenotype comprised smaller craniofacial region (=mild FDs) and BPDs (cf. black arrowheads), the neural tube (=NT) was closed (cf. **B´**-**B´´**, cf. black dashed lines; No=notochord). (**C**-**C´´**) Strong FDs occurred combined with partial reduction of *twist* expression and BPDs (cf. black arrowheads). (**D**-**D´´**) Most severe phenotype comprised

massive FDs, BPDs and NTDS (cf. black arrowheads). *Twist* expression and overall body-length was clearly reduced. (**E**) Quantitative distribution of phenotypes in controls compared to crispants injected with *cnn2.L*- or *cnn2.s*-CRNPs. Statistical analysis confirmed highly significant difference between controls and crispants and no significant difference among individual *cnn2*-CRNPS (***= p≤0.001; n.s.= p>0.05). (**F**) Phenotype distribution and statistical analysis of rescue experiments. Highly significant difference among controls and crispants as well as crispants and *cnn2* mRNA co-injection was detected (***=p≤0.001; by chi^2- students test).

2.2.4. Loss of *cnn2* impairs neural crest specification

As experimental knockdown as well as partial knockout of *cnn2* led to morphological defects in the head region of injected embryos, correct specification of the cranial NC was examined more closely.

Embryos were injected with *cnn2*-5´UTR-MO or the *cnn2*-splMO into 8-cell embryos targeting the left NC lineage and allowed to grow until stage 17. They were fixed and analysed by WMISH to detect expression the early cranial NC specification marker *forkhead box D3* (*foxd3*). While untreated control specimens displayed wild type and bilateral expression, *foxd3* expression of morphants was reduced or completely absent on the injected side (cf. **Fig. 16A**-**C**). Phenotype quantification showed that in both experimental set-ups, 100 % (n=27 / n=50) of untreated control embryos resembled the wild type expression pattern. Contrary to this, the wildtypic portion of specimens was reduced to ~14.3 % (n=4) upon *cnn2*-5´UTR-MO-injection, whereas ~64.3 % (n=18) showed a reduced and ~21.4 % (n=6) loss of the *foxd3* expression on the left side. Strikingly, the absence of specific expression correlated with a delay of neural fold formation on the injected side.

A similar phenotype distribution was observed in embryos injected with the *cnn2*-splMO. Here, ~29.8 % (n=14) showed wild type *foxD3* expression, which was reduced in ~61.7 % (n=29) or even absent in ~8.5 % (n=4). Each MO-injection was conducted in two independent clutches (N=2 / N=2). Statistical analysis using the chi²-students test attested highly significant differences between controls and morphants in both cases (cf. **Fig. 16G**-**H**).

In addition, *foxd3* expression in crispants was analysed during neurulation. For this, zygotes were either injected with a mixture of *cnn2.L*- and *cnn2.S*-CRNPs as described above or co-injected with *cnn2* mRNA. All embryos were fixed when uninjected controls had reached stage 15 to be analysed by WMISH. The observed phenotypes were categorised similar to the morphant data as wild type, reduced or absent *foxd3* expression (cf. **Fig. 16D**-**F**). ~94.7 % (n=18) of control embryos displayed stage-specific *foxd3* expression pattern and in ~5.3 % (n=1) no staining was detectable. Upon *cnn2*-CRNP-injection, only ~14.3 % (n=4) showed a wild type expression, while a reduction was observed in ~21.4 % (n=6) and *foxd3* was strongly reduced or absent in ~64.3 % (n=18). This distinct effect was rescued by *cnn2* mRNA co-injection, which resulted in an increase of wild type specimens up

to ~52.4 % (n=11), whereas ~42.9 % (n=9) still displayed a reduced and ~4.7 % (n=1) an absent expression pattern (cf. **Fig. 16I**). The injection experiment was conducted in one clutch (N=1). Overall, an alteration of neurula morphology was observed in both crispant phenotypes, as the neural folds were less prominent or even lost in parallel to the reduction of *foxd3* expression.

Statistical analysis confirmed a highly significant difference between controls and crispants as well as among crispants and *cnn2* mRNA co-injected embryos. Thus the rescue effect was statistically proven and underlined the specificity of the CRNPs in targeting *cnn2*.

In summary, MO-mediated knockdown and the CRISPR/Cas9-mediated genome editing affected expression of the NC specifier *foxd3*. In addition to that, the crispant phenotypes were partially rescued by co-injection of *cnn2* mRNA. Altogether, the observed NC-related phenotypes were accompanied by morphological changes regarding neural fold formation.

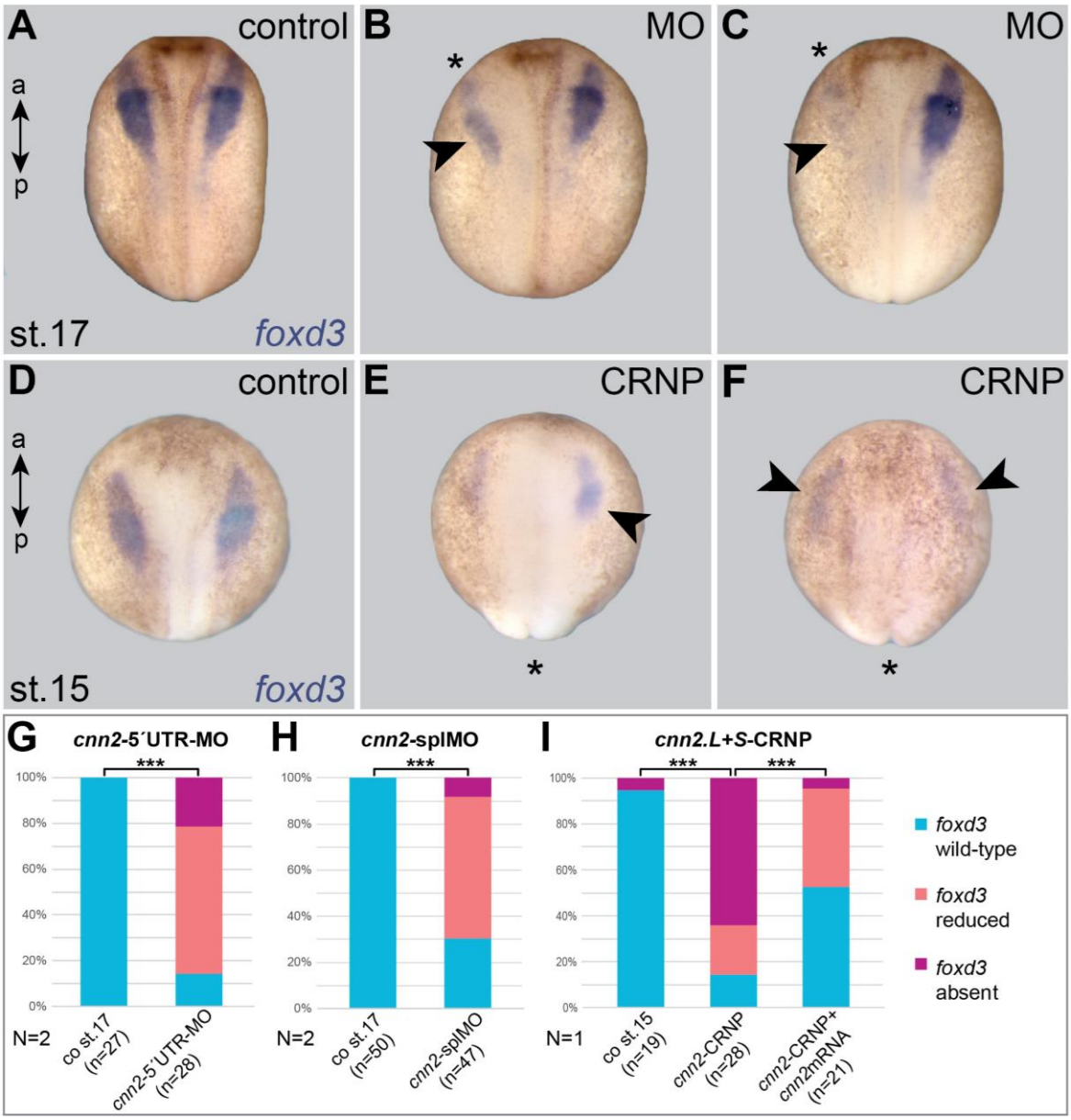

Figure 16: *Cnn2* is required for neural crest specification.
WMISH analysis was performed in morphants and crispants to visualise *foxd3* expression. (**A**) Untreated controls displayed wild-type bilateral expression at st. 17. (**B**-**C**) Expression was reduced or absent on injected side of morphants (cf. black arrowheads). (**D**) Wild-type *foxd3* expression in st. 15 control specimens. (**E**-**F**) Crispants displayed a reduced or nearly absent expression pattern (cf. black arrowheads). Injections were marked by black asterisks. (**G**-**I**) Respective quantitative analysis of phenotype distribution in all conducted injection experiments. Statistical analysis by application of ch^2-students test attested highly significant difference between individual treatments (cf. ***= p<= 0.001).

2.2.5. Loss of *cnn2* affects specification of the anterior head region

Upon *cnn2* LOF, not only defects in the cranial NC, but also malformations in the anterior head region including NTDs, were observed. These phenotypes indicated a possible defect in anterior specification or the NP. Therefore, injected specimens were analysed by towards their expression of *orthodenticle homeobox 2* (*otx2*), a specifier for the anterior head region.

To elucidate the potential role of *cnn2* in the anterior NP, *cnn2*-splMO was injected into the NP lineage on the left side of 8-cell embryos to leave the right NP as a contralateral control. In addition, *cnn2* mRNA was co-injected in a second batch to test the specificity of *cnn2* knockdown in the NP. All injected specimens were incubated until untreated control embryos had reached stage 16. In the following expression analysis, all controls showed a wild-type *otx2* expression pattern (cf. **Fig. 17A**) while it was reduced or absent on the injected side in morphants. Also, it became apparent that neural fold formation was at least partially impaired on the injected sides (cf. **Fig. 17B**-**C**). Quantitative analysis of the respective phenotype distribution showed that 100 % (n=39) of uninjected controls had a wild-type expression pattern. Morphant specimens lost this and displayed in ~63.6 % (n=21) a reduction and in ~36.4 % (n=12) a loss of expression on the injected side. Co-injection of *cnn2* mRNA restored wild type *otx2* expression in 40 % (n=18) of embryos, while in ~33.3 % (n=15) and 26.7 % (n= 12) expression remained reduced or absent, respectively. Statistical analysis with chi^2-students test confirmed a highly significant difference among controls and morphants as well as between morphants and *cnn2* mRNA co-injected specimens (cf. **Fig. 17G**). Injections were performed in two independent experiments (N=2).

In addition to that, a mixture of *cnn2.L*- and *cnn2.S*-CRNPs was injected in a second experimental series to compare the *oxt2* expression upon the CRISPR/Cas9-mediated knockout of *cnn2*. One portion of the crispants was again co-injected with *cnn2* mRNA at 1-cell stage and incubated together with untreated controls until stage 16 to be fixed for WMISH. In the course of expression analysis, most controls displayed a stage-specific *otx2* pattern (cf. **Fig. 17D**). Different from that, crispants showed a reduced and morphologically altered expression pattern, with more diffuse distribution of *otx2*-positive cells. The shape of the NP of these specimens was globally altered with less prominent neural folds. They were also shorter and had

mild BPDs (cf. **Fig. 17E**). In some, diffuse *otx2* expression within the anterior NP was accompanied by gastrulation defects resembling exogastrulae (EG) with *otx2*-positive mesoderm protruding from the blastopore (cf. **Fig. 17F**). Quantitative analysis of phenotype distribution in control specimens showed that 86 % (n=43) displayed a wildtypic expression pattern and morphology and 14 % (n=7) were exogastrulated. In ~34.8 % (n=16) of the crispants, *otx2* expression was reduced and 65.2 % showed the EG phenotype. ~21.7 % (n=10) of crispants, which were co-injected with *cnn2* mRNA displayed a stage-specific phenotype again, while ~52.2 % (n=24) showed reduced and ~26.1 % (n=12) the EG phenotype. Statistical analysis attested a highly significant difference for both comparisons of phenotype distribution, thus *cnn2* mRNA injection led to a significant recovery of the wild-type *otx2* expression pattern (cf. **Fig. 17H**). The injection set-up was repeated twice (N=2).

Taken together, both MO-mediated knockdown and CRISPR/Cas9-mediated partial knockout of *cnn2*, affected the expression pattern of *otx2*. The induced phenotypes were partially rescued by co-injecting *cnn2* mRNA in all experiments. These results underlined the specificity of the *cnn2*-splMO as well as the *cnn2*-CRNPs in targeting the *cnn2* gene.

Additionally, morphological changes were observed upon loss of *cnn2*, concerning neural fold formation of embryos, either restricted to the injected side of morphants or throughout the entire NP of crispants.

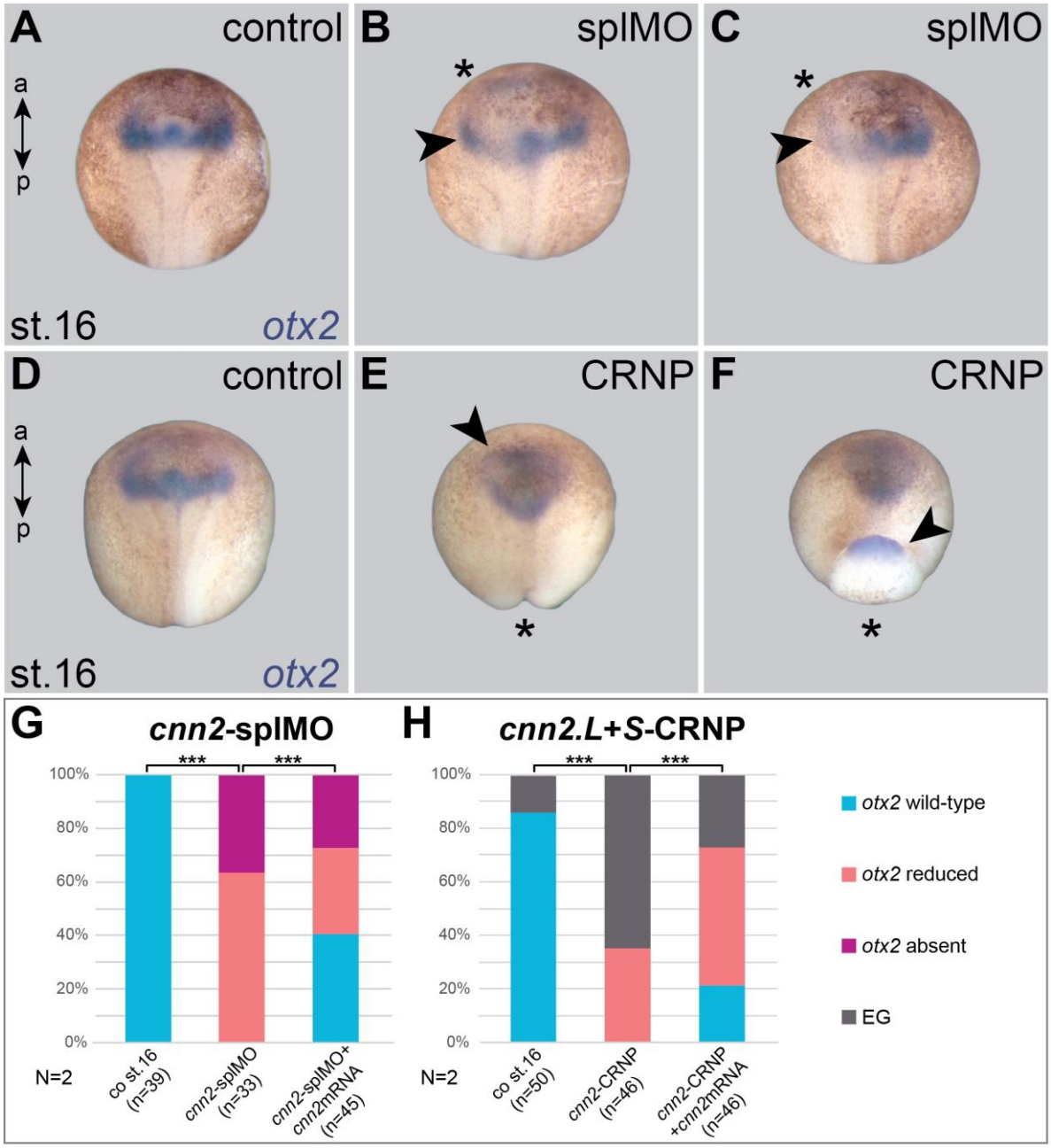

Figure 17: *Cnn2* is required for patterning of the anterior neural plate.
WMISH analysis was performed in morphants and crispants to visualise *otx2* expression. (**A** and **D**) Corresponding untreated controls displayed wild type expression pattern at st. 16. (**B**-**C**) Expression was reduced or absent plus the neural folds were reduced on injected side of morphants (cf. black arrowheads). (**E**) Some crispants displayed a reduced and indistinct expression pattern (cf. black arrowhead) or (**F**) resembled exogastrulae (=EG; cf. black arrowhead). Injections were marked by black asterisks. (**G**-**H**) Respective quantitative analysis of phenotype distribution in all conducted injection experiments. Statistical analysis by applied ch^2-students test affirmed a highly significant difference between individual treatments (cf. ***= p<= 0.001).

In order to summarise the second part of the presented work, it can be stated that a loss of Cnn2 function caused a variety of morphological defects, including craniofacial malformations, anterior NTDs and BPDs. These phenotypes could be observed upon MO-mediated LOF targeting the presumptive NC as well as after global CRISPR/Cas9-mediated genome editing, whereas CRNP-injection also led to severe gastrulation defects and reduction in embryonic body length. The rescue effect by additionally injected *cnn2* mRNA and the sequencing of crispant specimens, underlined the specificity of all applied molecular tools in targeting *cnn2* and approved that the occurred phenotypes were caused by loss of Cnn2.

Additional analysis of morphant and crispant neurula stages revealed an effect on NC specification marked by an altered *foxd3* expression. Together with the LOF phenotypes in older stages, regarding facial structure and *twist* expression, not only the role of Cnn2 in NCCs was confirmed indicated by MTCnn2 localisation in explants, but also its early function for correct specification of the NC was revealed. The loss of *cnn2* function in the NP affected the expression pattern of the anterior head specifier *otx2* as well as the morphology in that region. This indicates a role of Cnn2 for the specification or proper shaping of the anterior NP.

Overall, during the analysis of these last LOF experiments, it became apparent that impaired Cnn2 function led to neurulation defects suggesting a respective function during this morphological process. Therefore, the specific role of Cnn2 within the NP and during neural fold formation was analysed more closely in the following.

2.3. Calponin2 in the neural plate

2.3.1. *Calponin2* is expressed within the early neural plate

Calponin2 is expressed throughout neurulation within the NP (c.f. **Fig. 18A** and **B**). Its expression pattern was analysed by WMISH from the onset of neurulation at stage 13 to 14 until stage 16 to 17. *Cnn2* mRNA expression was first detected at the midline and in the developing anterior neural folds (c.f. **Fig. 18A**). At stage 16 the signal got stronger in the entire NP (c.f. **Fig. 18B**), probably due to condensation of the tissue. Histological sections of the respective fore- and hindbrain regions revealed the restriction of mRNA expression to the superficial cell layers, representing the cells involved in the formation of the dorsolateral- and medial hinge points as well as finally contributing to the NT. Additionally, *cnn2* mRNA expression was observed in the notochord, confirming already described expression data in older stages (see **Fig. 6**; Ulmer et al., 2013).

Overall, *cnn2* mRNA was clearly expressed in the neuroectoderm, which undergoes dramatic morphological changes in the course of neurulation concluding with the formation of the NT. The notochord represents a second tissue underlying shape-changing strains, i.e. convergent extension, where *cnn2* mRNA expression was observed.

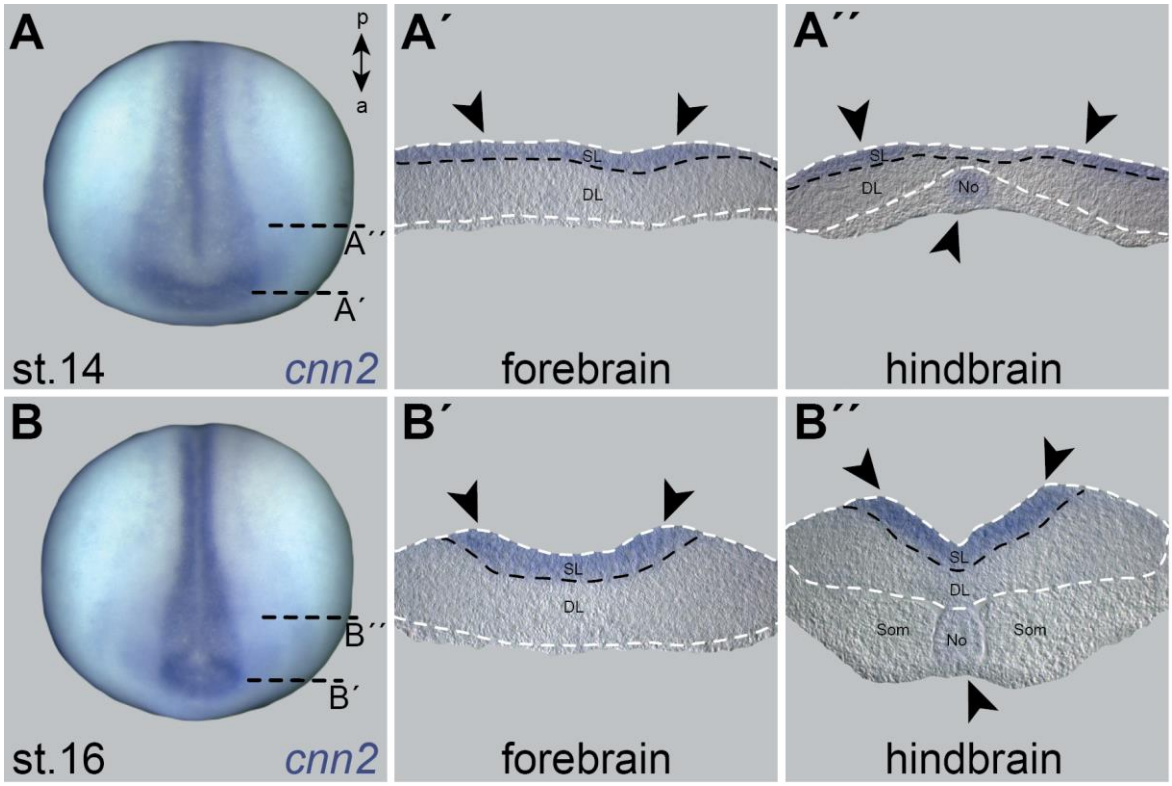

Figure 18: *Cnn2* is expressed in superficial cells of the neural plate.
Expression pattern of *cnn2* mRNA was detected via WMISH at st. 14-16. (**A**) at st. 14 *cnn2* was expressed in the midline of the forming neural groove, in developing anterior neural folds and in the anterior neural ridge. (**A´**-**A´´**) Histological sections of whole-mount embryos exhibited limitation of expression to the superficial layer (=SL) in contrast to non-stained deep layer (=DL) (border between SL and DL marked by black dashed line; arrowheads above point to expression). (**B**) At st. 16, expression became stronger in the entire NP but remained confined to the superficial cell layers (cf. **B´**-**B´´**, black dashed line and upper arrowheads). Expression was also detected in the notochord (=No) throughout neurulation (cf. **A´´** and **B´´**, lower arrowheads). Neural tissue marked white dashed lines, somites(=Som).

2.3.2. Cnn2 has a tissue-specific function within the anterior neural plate

To analyse the distinct function of Cnn2 within the NP, MO-mediated LOF experiments were conducted. Therefore, the already described *cnn2*-splMO was injected into 8-cell stage embryos precisely targeting either NP or NC lineage to compare possible tissue-specific effects (cf. **Fig. 19A**). A low dose, i.e. 0.5pmol of *cnn2.L*- and *cnn2.S*-splMO each, was injected unilaterally into the dorsal blastomeres to target the NP region (→ a1 injection) or the NC (→ a2 injection). The associated uninjected dorsal blastomere served as an untreated contralateral control. In a first step of analysis, the neurulation movements of differently injected specimens were monitored simultaneously comparing the two injection set-ups to each other and to uninjected control embryos by recording time-lapse movies (cf. **Movie 1**). To assure correct targeting of the MO treatment, co-injected green fluorescently labelled dextran served as LT and was detected in the specific regions before the onset of neural fold elevation (cf. **Fig. 19B**; green signal). Evaluation of time-lapse movies showed a clear differential impact of *cnn2* LOF on neurulation in a1-injected embryos compared to controls and a2-injected specimens. Stills of one movie are shown as representative pictures at the starting point (t=0´), after 204 minutes (t=204´) of neurulation at room temperature and after 305 minutes (t=305´), when the uninjected control embryo had completed NTC. During the whole time frame, the control underwent a normal neurulation process with bilateral formation and elevation of the neural folds as well as formation of hinge points within the anterior NP, terminating in the dorsal fusion of the neural folds along the entire body axis. The same movements were observed upon a2-injection, although the left NC was clearly hit by the morpholino injection. Both sides went through a similar neurulation process as the control, yet the injected side displayed a slight delay in anterior NTC. On the contrary, the a1-injected embryo completely failed to form neural folds on the injected side, resulting in a unilaterally exposed anterior NP at the end of the recorded time frame (cf. **Fig. 19C**-**E**).

Subsequently, embryos were allowed to develop until stage 24 to be analysed for the individual progress of neurulation. In the course of a categorised analysis, three different phenotypes were distinguished. Firstly, the stage-specific phenotype with a completely closed NT, hereafter referred to as wild type (= wt; cf. **Fig. 19G**). Secondly, anterior NTDs (cf. **Fig. 19H**) were observed, in particular an open NT on

the injected side resembling the anterior NTDs already recorded in the course of time-lapse analysis. Thirdly, malformations concerning overall head morphology occurred, affecting NC-derived structures on the injected side and resulted in reduced pharyngeal arches as well as a bending of the entire embryo towards the injected side. However, in such specimens, the NT appeared to be closed (= NC defects; cf. **Fig. 19I**). While 100 % (n=61) of uninjected controls reflected the wild-type phenotype, 91.7 % (n=55) of a1-injected embryos had clear anterior NTDs on the injected side and 8.3 % (n=5) showed NC defects. Contrary to this, only 13.6 % (n=8) of a2-injected embryos displayed anterior NTDs and 86.4 % (n=51) of them had NC defects. The injection was repeated in three independent experiments (N=3). The distribution of the analysed phenotypes differed clearly between the individual treatments and their statistical analysis utilising the chi^2-students test gave a high significance for each comparison (cf. **Fig. 19F**; ***= p <= 0,001). These results underlined the differential effects of the tissue-specific LOF.

In addition, representative embryos of each observed phenotype were sectioned and stained using red-labelled phalloidin to visualise global tissue morphology in connection with the localisation of fluorescently labelled green LT (cf. **Fig. 19J**-**L**). Cutting edges were analysed by confocal laser scanning microscopy (LSM). The corresponding sections of control embryos confirmed the proper formation of a closed NT, covered dorsally by an intact epidermis. In a1-injected specimens, the cells of the left dorsal floorplate were positive for green fluorescent LT, while the imaged NT failed to fuse at its dorsal most part as well as the overlaying epidermis (cf. **Fig. 19K**; marked by white arrowhead). As a result of a2-injection with the *cnn2*-splMO, sectioned embryos displayed bending towards the injected tissue. The NT, clearly not targeted, folded up and was covered by enclosed epidermis (cf. **Fig. 19L**; white arrowhead).

In summary, the specific knockdown of *cnn2* mRNA within the anterior NP led to respective NTDs. Time-lapse movies of neurulation, as well as subsequent analysis of tailbud stages, revealed a loss of neural fold formation on the injected side resulting in complete failure of anterior NTC, possibly due to an effect on the tissue responsible for hinge point formation. In contrast to that, the *cnn2* LOF in the developing NC led to FDs and only few anterior NTDs. The latter might result from

a slight effect of injected morpholino on the neighbouring tissue forming the NP. Overall, these results indicated a differential function of Cnn2 in the NP vs. NC.

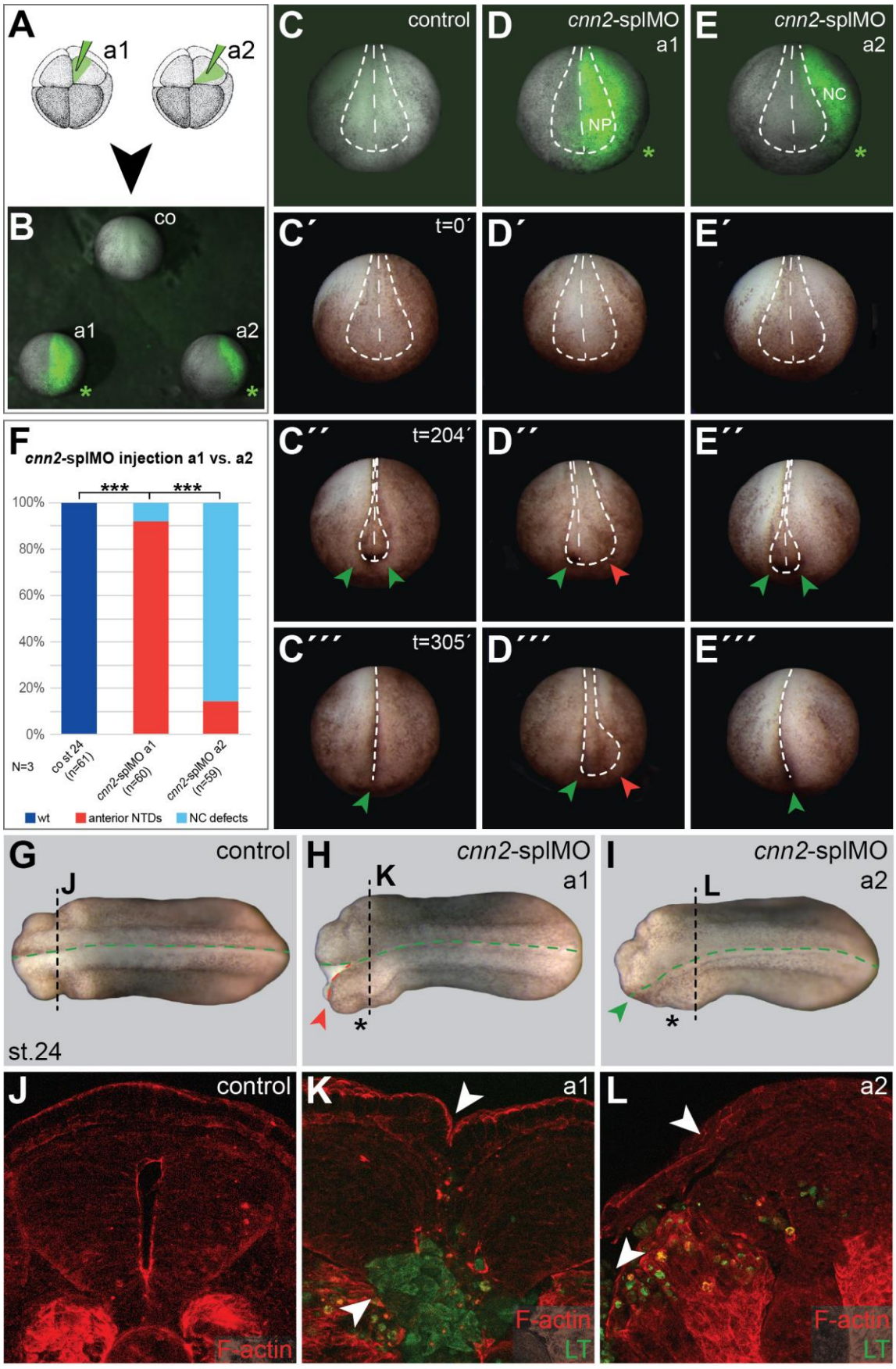

Figure 19: Cnn2 has a specific function within the anterior neural plate.

(**A**) Experimental set-up, *cnn2*-splMO was injected in 8-cell embryos stage into the future anterior NP (green arrowhead, a1) or NC (green arrowhead, a2; sketch of 8-cell embryo from Nieuwkoop & Faber, 1994). (**B**) Specimens recorded via time-lapse sequence, untreated control embryo on top, a1-injection bottom left, a2-injection bottom right. Affected tissue marked by fluorescently labelled dextran (=green) that served as LT at site of injection (cf. green asterisks). (**C**-**E**) Embryos were separated and magnified. (**C´**-**E´´´**) Stills from time-lapse sequence at start of sequence (t=0´), after 204 (t=204´) and 305 minutes (t= 305´) of recording. Dorsal midlines and corresponding NP regions highlighted by white dashed lines. While control NP and a2-injected NPs narrowed and closed completely, a1-injection impaired narrowing and resulted in open anterior NPs (cf. green vs red arrowheads). (**F**) Neurulation phenotypes were analysed at st. 24 and quantified for different injection sites. Differences between the distribution of phenotypes was statistically analysed (chi^2-students test; ***=p<=0.001). Representative embryos for each phenotype shown in (**G**; control→ wt), (**H**; a1→ anterior NTDs) and (**I**; a2→ NC defects), side of injection marked by asterisk, midline highlighted by green and anterior NTD by red dashed line (cf. green and red arrowheads). (**J**-**L**) Respective specimens were hemisectioned (sectional planes marked by dashed lines in **G**-**I**) and stained with fluorescently labelled phalloidin (=red signal, F-actin). LT was limited to targeted tissue (cf. **K**-**L**, green signal; marked by lower white arrowhead). NT remained open (cf. **K**, upper white arrowhead) or closed (cf. **L**, upper white arrowhead).

2.3.3. Neural plate morphogenesis depends on the presence of Cnn2

To examine the specific role of Cnn2 within the NP further, *cnn2*-splMO was targeted to the future NP (a1 injection) into 8-cell embryos to analyse its morphology in neurula stages. Therefore, the expression pattern of *SRY box 3* (*sox3*), a pan-neural marker gene, was analysed in fixed specimens using WMISH. In a first step, *cnn2* LOF was induced bilaterally by injecting into both dorsal blastomeres. Embryos were allowed to grow until stage 17 to be fixed, stained and scored regarding the width of the *sox3*-positive NPs (cf. **Fig. 20A-D**). In all untreated controls (100 %, n=50) the NP was narrow posteriorly and wider at the anterior end (**Fig. 20A**). Upon injection of 0.5 pmol MO, the anterior NP was massively widened in all specimens (100 %, n=39; **Fig. 20B**). Increasing the MO dose aggravated the phenotype, as 26.7 % (n=12) of these embryos had a wide NP along the entire anterior-posterior axis (**Fig. 20C**). Injection was performed in three different clutches (N=3) and statistical analysis using chi^2-students attested highly significant difference between all treatments (cf. **Fig. 20D**; ***= p <= 0,001).

These results implied a dose-dependent effect of the *cnn2*-splMO on NP narrowing and neural fold approximation.

To quantify the impact on the NP morphology, injection experiments were repeated by applying 0.5 pmol *cnn2*-splMO each in a unilateral manner, thereby leaving the contralateral side as a direct internal control for measurements. In addition to the MO treatment, one portion of the embryos were co-injected with *cnn2* mRNA to perform a rescue experiment. Following this, embryos were incubated, fixed and stained as described above. Afterwards, the width of either side of the anterior NP, marked by *sox3*-expression, was measured and the individual ratio between injected and uninjected side was calculated (cf. **Fig. 20E**-**H**). This was achieved by dividing the width of the injected side by the corresponding value of the untreated control side. For control embryos, ratios ranged from 0.95 to 1.04 with a mean value of 1 (n=60; ratio~1), as both sides displayed a similar NP region width on either side of the midline (cf. **Fig. 20E**). Ratios were increased in injected specimens ranging mainly between values of 1.15 to 1.3 and averaged at 1.22 (n=61; ratio~1.22) as the injected sides were expanded compared to their control sides (cf. **Fig. 20F**). The co-injection of *cnn2* mRNA led to a normalisation of ratios around 1.02 (n=49; ratio~1.02), thus restoring the narrowing of the NP on the injected side (cf. **Fig.**

20G). Ratios were calculated from three independent experiments (N=3). Statistical analysis of the boxplot results using Wilcoxon paired test, attested a highly significant difference between the calculated ratios of controls and morphants, as well as between morphants and embryos co-injected with *cnn2* mRNA (cf. **Fig. 20H**). This rescue effect confirmed the specificity of the *cnn2*-splMO.

In summary, these results demonstrated a function of Cnn2 during specifically morphological changes of the NP in the course of neurulation.

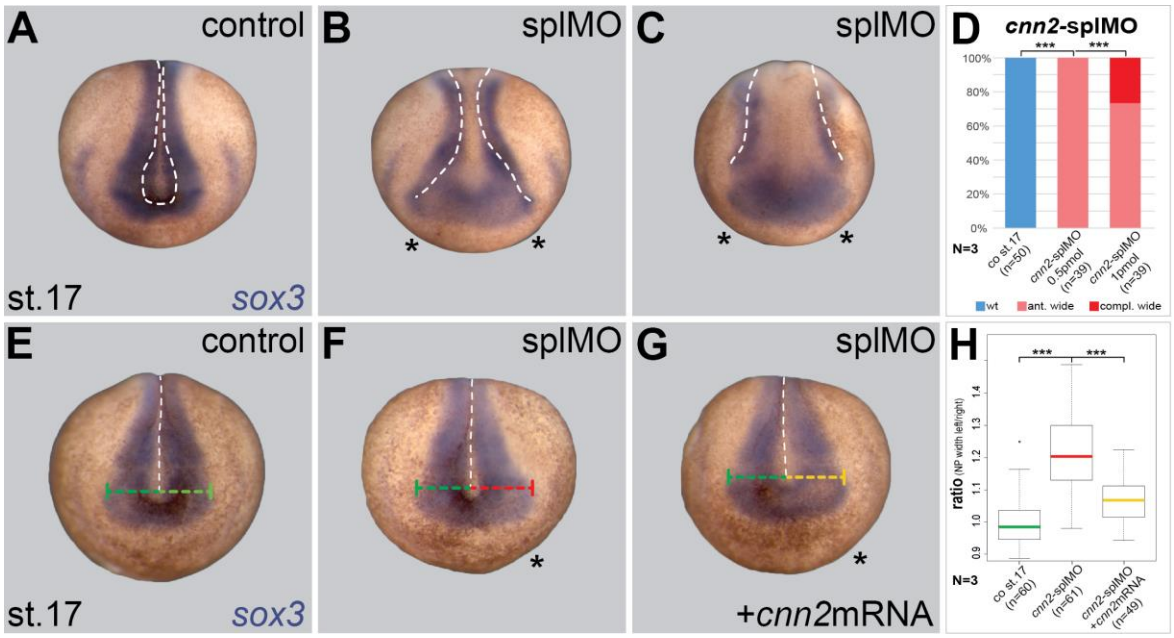

Figure 20: Loss of *cnn2* function impairs correct neural plate morphogenesis.
NP width was visualised by WMISH of *sox3* (purple staining). (**A**-**D**) *cnn2*-splMO (0.5 pmol / 1pmol each) was injected bilaterally into NP lineage of 8-cell embryos. (**A**) Untreated control (co) embryos displayed normally shaped NPs at st. 17 (=wt) compared to morphants (**B**-**C**), either showing widening of the anterior (=ant. wide, **B**) or entire NP (=compl. wide, **C**). Border between neural and non-neural ectoderm (hinge points) marked by white dashed lines, injected sites indicated by asterisks. (**D**) Quantification of phenotypes comparing different MO concentrations (0,5 pmol vs 1 pmol) with untreated controls. Highly significant difference between treatments attested by chi^2-students test (***=p≤0.001).
(**E**-**H**) *cnn2*-splMO was injected unilaterally into 8-cell embryos targeting NP lineage. At co st. 17, NP width was measured on either side of the midline (cf. coloured dashed lines, midlines marked with white) and ratios were calculated. (**E**) NP was equally wide on both sides in co embryos, resulting in ratios around 1. (**F**) Morphants displayed wider NPs on injected sites (marked by asterisk), an effect that was rescued by co-injection of 25 ng/µl *cnn2* mRNA (**G**). (**H**) Boxplot displaying distribution of all calculated ratios. Statistical analysis via paired samples Wilcoxon test confirmed highly significant difference between all treatments (***=p≤0.001). Injection experiments were conducted in three independent round of injection each (N=3).

2.3.4. Phenotypes resulting from *cnn2* CRISPR/Cas9-mediated geome editing confirm specificity of the MO

In addition to MO-mediated knockdown, a *cnn2* LOF was induced by genome editing utilising the CRISPR/Cas9 system. Cnn2-CRNPs were injected into, embryos were allowed to grow until stage 16 and fixed to analyse *sox3* expression by WMISH. Uninjected specimens of each clutch served as controls. Phenotypes were categorised and counted for each treatment. Three different phenotypes were observed (cf. **Fig. 21A**-**C**). First, the stage-specific phenotype with narrow posterior and wider anterior NP. Embryos of the second category displayed a NP which was wide along the entire anterior-posterior axis without any narrowing of the *sox3*-positive tissue. Those embryos were also shorter, indicating an impaired axis elongation during gastrulation. Thirdly, gastrulation defects occurred, i.e. exogastrulae, due to not internalised yolk plugs.

In a first step, uninjected controls were compared with *cnn2*-CRNP-injected specimens in four independent experiments (cf. **Fig. 21D**). While 71.9 % (n=92) of the analysed controls showed the stage-specific phenotype, 24 % (n=31) displayed a widening of the NP and 3.9 % (n=5) were exogastrulating. As opposed to this, only 9.9 % (n=12) of the sgRNA-injected specimens revealed a stage-specific phenotype, 52.9 % (n=64) exhibited a completely broad NP and 37.2 % (n=45) were exogastrulae. Statistical analysis of phenotype distribution comparing both treatments confirmed highly significant differences between controls and crispants.

Rescue experiments were also conducted in crispants. For this, *cnn2* mRNA was co-injected with *cnn2*-CRNPs into zygote stages, which were allowed to grow until neurulation together with *cnn2*-CRNP-injections and untreated specimens serving as controls. Phenotype analysis and categorisation were carried out as described above (cf. **Fig. 21E**). Of controls, 90.5 % (n=57) were wild type and 9.5 % were exogastrulating. On the other hand, only in 7.5 % (n=5) of crispants, NP morphogenesis was normal, whereas it was clearly broadened in 53.7 % (n=36) and 38.8 % (=26) had gastrulation defects. This phenotype distribution was rescued upon *cnn2* mRNA co-injection, so that 48.6 % (n=35) of specimens showed stage-specific narrowing of the NP opposing to 30.6 % (n=22) with a wide NP and exogastrulation in 20.8 % (n=15). Total numbers were obtained from three independent rounds of injection (N=3). Statistical analysis of the phenotype

distributions testified highly significant differences between controls and crispants as well as for comparison of crispants and co-injected embryos with *cnn2*mRNA, thus confirming the rescue effect.

In summary, CRISPR/Cas9-mediated genome editing of *cnn2* induced a widening of the NP and severe gastrulation phenotypes. Furthermore, the crispants indicated a slight reduction in their overall body-length. These phenotypes were partially rescued by additional *cnn2* mRNA injection, confirming sgRNA specificity in targeting *cnn2*.

As widening of the NP in crispants clearly resembles the phenotype of bilaterally injected morphants (see **Fig. 20B** and **C**), CRISPR/Cas9-mediated genome editing confirmed the specificity of the *cnn2*-splMO.

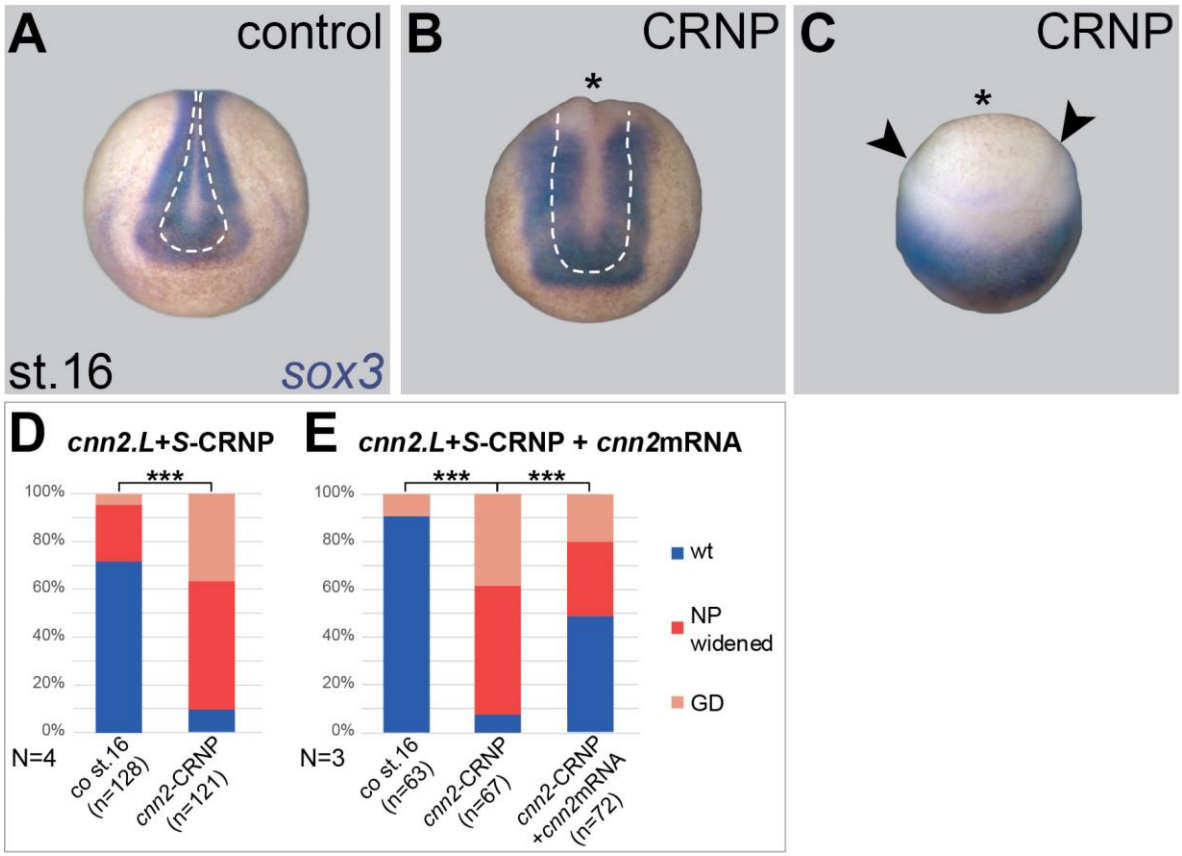

Figure 21: CRISPR/Cas9-mediated genome editing of *cnn2* confirms the morphant phenotype.

CRNPs were injected into zygotes. (**A** – **C**) NP morphology was analysed towards *sox3* expression via WMISH at control st. 16 (blue staining). (**A**) Uninjected control embryos displayed stage-specific NP shape (=wt) Border between neural and non-neural ectoderm (hinge points) marked by white dashed lines. (**B**-**C**) Specimens injected with *cnn2*-CRNPs (marked by asterisk) showed uniformly wide NP along the anterior-posterior body axis (=NP widened; note white dashed lines compared to control) or gastrulation defects (=GDs; marked by arrowheads). (**D**-**E**) Quantitative analysis of phenotype distribution in two different experimental sequences. (**D**) Statistical analysis of comparison between crispants and controls attested highly significant disparity (***=p≤0.001). (**E**) Amount of wt embryos increased upon co-injection of *cnn2* mRNA compared to *cnn2*-CRNP injection. Phenotype distribution differed highly significantly between all treatments (***=p≤0.001). Statistical analysis was performed using chi² students test.

2.3.5. *Cnn2* is required for apical constriction

As both LOF approaches clearly indicated a function of Cnn2 in properly shaping the NP, morphogenetic mechanisms underlying neurulation movements were examined more closely. One critical step in that process is accomplished by regionalised AC of NP cells to achieve dynamic shape changes of the entire tissue. Considering this, unilateral MO-mediated knockdown of *cnn2* as well as the corresponding rescue experiments were repeated to analyse the apical shape of cells within the anterior NP thereafter.

Therefore, 8-cell embryos were injected unilaterally and allowed to develop until controls reached stage 17. Specimens were then fixed stained with fluorescently labelled red phalloidin to visualise F-actin along the cell borders. Fixable green fluorescein dextran was co-injected to mark treated cells for the following LSM analysis of NPs (cf. **Fig. 22A**-**C**). Anterior NP cells of uninjected control embryos displayed similar surface sizes on either side of the midline (cf. **Fig. 22A**). Contrary to this, the dextran-positive NP cells in morphants were larger than uninjected cells (**Fig. 22B**, **D**). This phenotype was rescued by co-injection of 0.1 ng *cnn2* mRNA (**Fig. 22C**). To better visualise the overall cell morphology, the F-actin signal was checked separately in the corresponding channel devoid of colour (cf. **Fig. 22A´**-**C´**). In untreated control specimens, the signal intensity was evenly distributed throughout the entire NP. Opposing this, morphants displayed a clear reduction of signal strength on the injected side, indicating a relaxation of the apical actin network in those cells. Upon *cnn2* mRNA co-injection the signal was restored again on both sites of the anterior NP.

The area of the imaged apical cell surfaces was measured on both sides of the respective NPs and ratios were calculated of the average cell sizes each. Sixty cells were measured per embryo, thirty per side. In controls, cells were of similar size on either side, resulting in ratios between 1 and 1.15, with a mean value of 1.05. Upon *cnn2*-splMO injection, the average surface area of treated cells increased considerably, which raised calculated ratios up to values ranging from 1.65 to 2.5 and gave a median of 2.01. It is noteworthy that the increase of size was only measurable in LT-positive cells, indicating a cell-autonomous effect. Contrary to this, NP cells of embryos co-injected with *cnn2* mRNA showed almost unchanged surface areas compared to untreated control cells. This led to a reduction of the

corresponding ratios, which contained values of 1.01 up to 1.5 and an average of 1.2. Ratios were plotted accordingly and statistical analysis using Wilcoxon paired test confirmed highly significant differences for each comparison (cf. **Fig. 22E**). Thus, apical cell surface was notably increased in size upon *cnn2*-splMO injection, an effect that was rescued by additional injection of *cnn2* mRNA.

In summary, these results clearly indicate that the knockdown of *cnn2* had an effect on AC processes in the anterior NP, which could be rescued by applying *cnn2* mRNA supplementary.

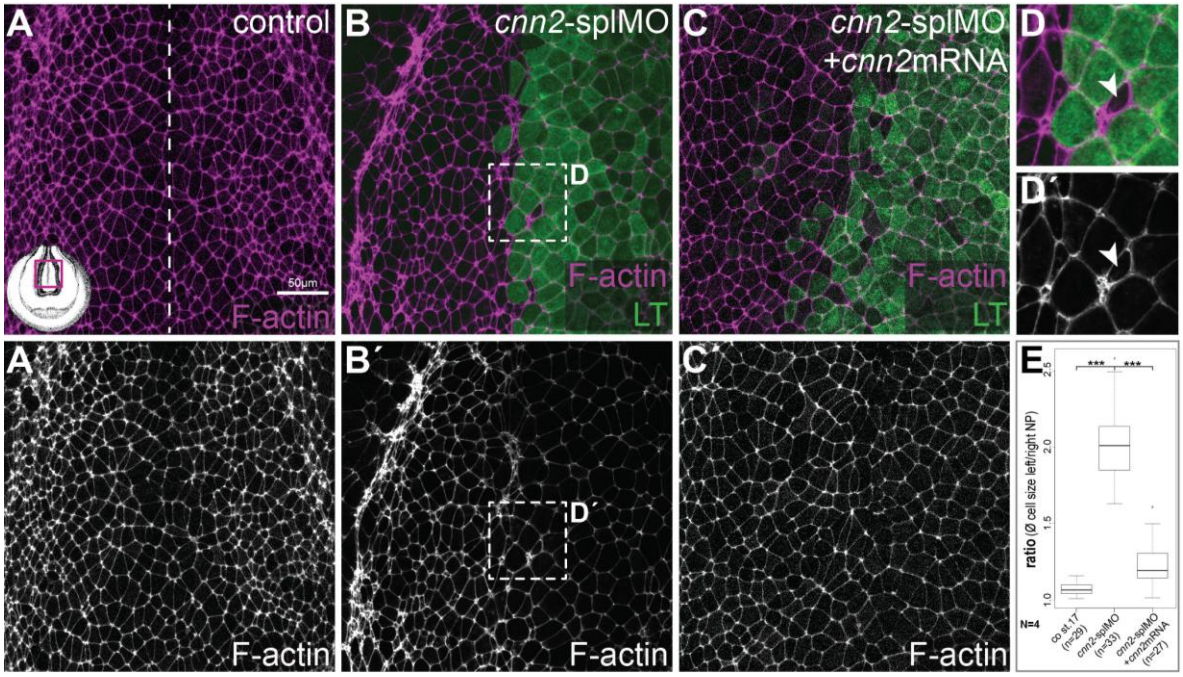

Figure 22: MO-mediated *cnn2* LOF induces apical constriction defects within the anterior neural plate.

MO (0.5 pmol each) was injected into 8-cell embryos targeting NP lineage. (**A**-**C**) Anterior NPs analysed by LSM, cell borders marked by fluorescently labelled phalloidin staining (=magenta signal), injected cells marked by green fluorescein dextran serving as LT (=green signal). (**A**) Sketch of st. 17 embryo (inset on lower left side, from Nieuwkoop & Faber, 1994, magenta rectangle marks visualised NP regions). (**A**) Untreated controls displayed same average cell surface size on both sites (midline indicated by white dashed line; scale bar equals 50µm, note white line at bottom right corner) F-actin staining highlighted in white revealed equal signal intensity on either side (cf. **A´**). (**B**) *Cnn2*-splMO injection induced cell-autonomous enlargement of targeted cells, compared to smaller untreated cells (cf. **D**, **D´**, magnification; white arrowhead), actin signal intensity was reduced in injected cells (cf. **B´**). (**C**) Co-injection of 0.1 ng *cnn2* mRNA normalised cell

surface expanse in injected cells again and F-actin signal strength was restored on injected side (cf. **C´**). (**E**) Cell surface areas were measured in 30 cells on each side of the anterior NPs (left side/injected side vs right side/uninjected control side) to calculate corresponding ratios. Distribution of ratio values of four independent experiments (N=4) was plotted and analysed via paired samples Wilcoxon test, which testified highly significant differences between the analysed treatments (***=p≤0.001).

Comparable to the cell surface analysis of morphant embryos, the same region within the anterior NP was examined upon CRISPR/Cas9-mediated genome editing of *cnn2.* Again, *cnn2*-CRNPs were injected into zygotes and specimens incubated until uninjected controls reached stage 16. After fixation, all embryos were stained using fluorescently labelled phalloidin to visualise the cell borders within the anterior NPs.

While untreated controls displayed stage-specific NP morphology with apically constricting cells, crispants had clearly enlarged NP cell (cf. **Fig. 23A** vs. **B**). This increase in size was limited to the anterior NP, as AC was observable in the more posterior region (cf. **Fig. 23B**; upper white arrowhead). To quantify the observed effect, the surface areas of 30 NP cells each were measured of the control as well as of the crispant embryo and value distribution was blotted accordingly (cf. **Fig. 23C**). The average size in control cells lay around ~11 μm^2 compared to the average crispant cell size of ~20.5 μm^2. Statistical analysis by Wilcoxon paired test confirmed a highly significant difference between both treatments. According to that, the CRISPR/Cas9-mediated *cnn2* LOF also led to a measurable enlargement of anterior NP cells.

Closer examination of the F-actin signal showed a reduction in strength in crispant cells of the anterior NP region compared with control cells (cf. **Fig. 23A´** vs. **B´**), like it was observed in morphants.

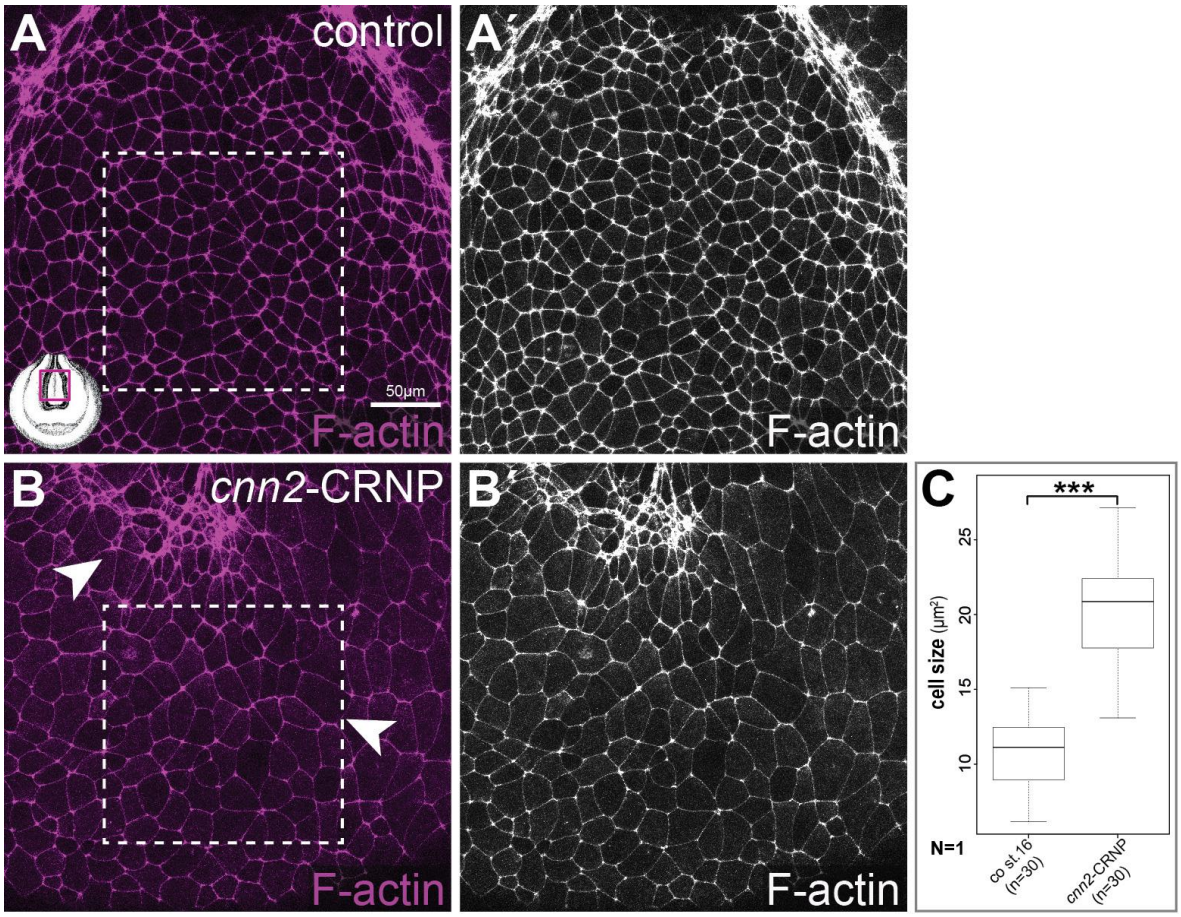

Figure 23: CRISPR/Cas9-mediated genome editing of *cnn2* induces apical constriction defects within the anterior neural plate.

CRNPs were injected into zygotes (**A**-**B**) untreated embryos and crispants were fixed at control st. 16 and analysed by staining of cell boarders with fluorescently labelled phalloidin (=magenta signal). (**A**) cells in the anterior NP of control embryos displayed stage-specific cell size (inset on lower left side, from Nieuwkoop & Faber, 1994, magenta rectangle marks visualised NP regions; scale bar equals 50µm, note white line bottom right corner). (**B**) corresponding cells of crispants were enlarged, while posterior cells underwent AC (cf. white arrowhead bottom vs. top). Cell surface size of 30 anterior NP cells was measured in control and crispant (analysed area marked by white dashed quadrats). (**A´** vs **B´**) Actin signal was overall weaker in crispant embryo compared to control (=white signal). (**C**) Distribution of measured cell sizes was plotted and paired samples Wilcoxon test confirmed highly significant differences between both treatments (***=p≤0.001). 20 embryos were checked for each treatment (n=20) in one injection experiment (N=1).

Overall, the loss of *cnn2* function, either induced by MO- or CRNP-injection, led to severe AC defects within the anterior NP. Together with the rescue effect upon co-injection of *cnn2* mRNA in morphants, these results indicated a specific role of Cnn2 for the proper regulation of neural AC.

2.3.6. Cnn2 function in apical constriction depends on domains that regulate actin binding

The next step was to determine whether the association with F-actin is essential for Cnn2 function in the context of AC. Therefore, respective MTCnn2 deletion contructs missing individual domains that mediate actin binding (see **Fig. 7**), were analysed towards their capacity to rescue the impairment of AC upon Cnn2 LOF.
As described before, 8-cell embryos were injected into the left dorsal blastomere to maintain a contralateral internal control side. Embryos were fixed when controls had reached stage 17 and F-actin was stained with fluorescently labelled phalloidin to be analysed by confocal microscopy (cf. **Fig. 24A**-**I**).
Again, the apical cell surface extent of 30 cells per side was measured and ratios of average values were calculated for each embryo. All constructs were injected into at least three different clutches (N=3), together with *cnn2*-splMO and accompanied by untreated control specimens. While morphants displayed an enlargement of the anterior NP cells with main ratio values between 1.76 and 1.96 compared to untreated controls, the co-injection of *MTcnn2* mRNA rescued this phenotype and led again to a significant reduction of the calculated ratios ranging mainly from 1.05 to 1.22 (cf. **Fig. 24A**-**C**). A similar rescue effect was observed in embryos co-injected with *MTcnn2ΔABD1* or *-ΔClik3* mRNA, whose ratios levelled around 1.16 to 1.36 and 1.1 to 1.19 (cf. **Fig. 24E**, **H**). Contrary to this, the additional injection of *MTcnn2ΔClik1*, *-ΔClik2* and *-ΔCterm* mRNA did not result in significant ratio reduction with corresponding values between 1.72 to 1.88, 1.59 to 1.84 and 1.68 to 2.12 (cf. **Fig. 24F**, **G**, **I**). Statistical analysis using Wilcoxon paired test confirmed highly significant difference between ratio distributions of morphants and *MTcnn2*, *MTcnn2ΔABD1* and *-ΔClik3* mRNA-injected specimens, while no significant difference was given between morphants and *MTcnn2ΔClik*, *-ΔClik2* or *-ΔCterm* mRNA-injections (cf. **Fig. 24J**)
Thus, deletion of the ABD1 or Clik3 domain did not impair the rescue ability of Cnn2, whereas the lack of Clik1, Clik2 or the C-terminus abrogated proper Cnn2 function.

In summary, these results clearly showed that the mRNA encoding the full-length MTCnn2 construct was able to rescue the morphant phenotype just like the untagged *cnn2* mRNA before (see **Fig. 22**), indicating an equal function in the cellular context. In addition to this, the deletion of the ABD1- or the Clik3 domain had no impact on the rescue potential, which in turn implied that the critical domains responsible for the regulation of AC during neurulation must be located to Clik1, Clik2 and the C-terminus. Therefore, these domains seem to be required for mediation of Cnn2 function, possibly by regulating its association with the actin cytoskeleton.

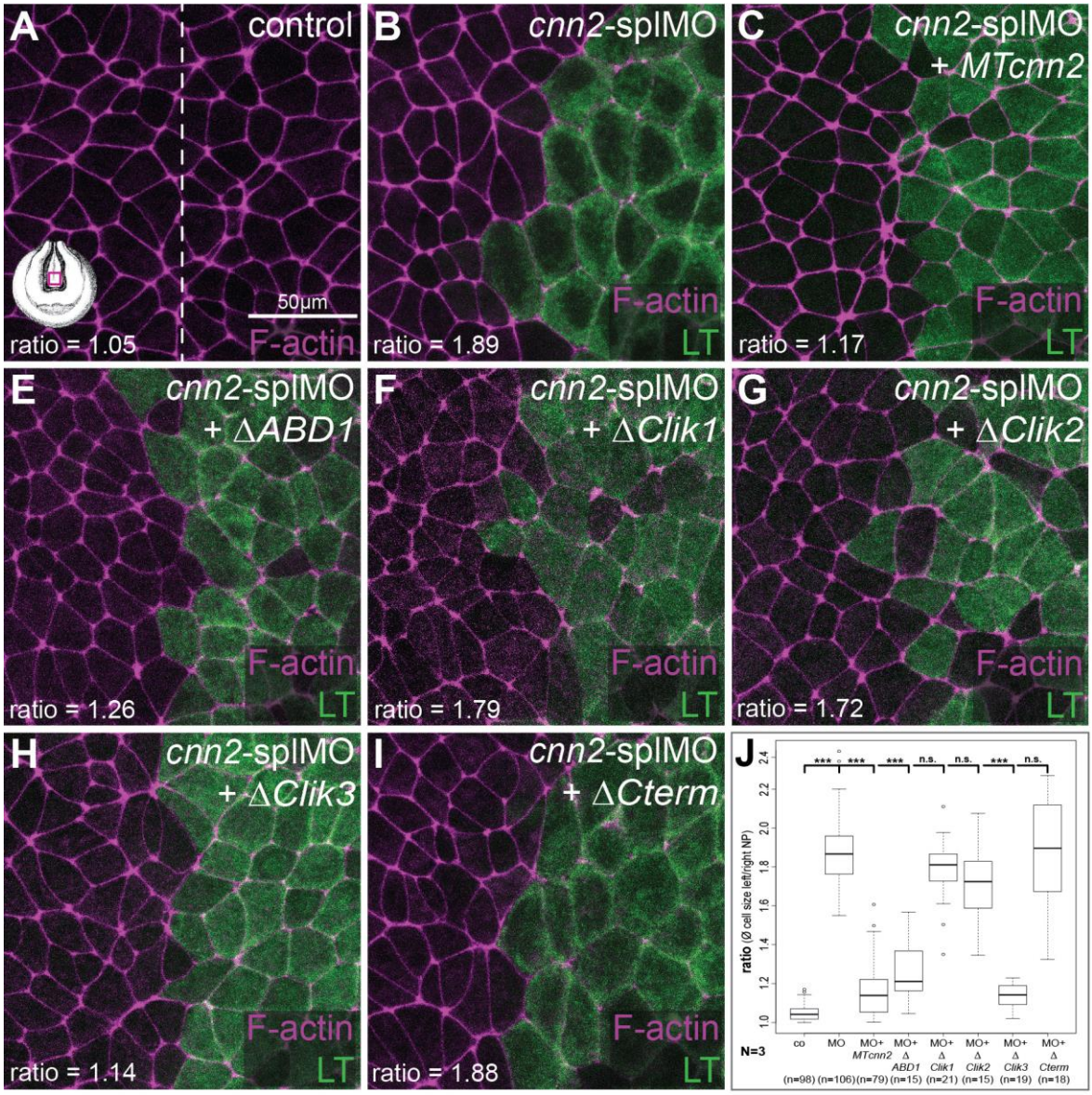

Figure 24: Specific protein domains are critical for Cnn2 function during apical constriction.

Cnn2-splMO (0.5pmol each) and *MTcnn2* mRNA (0.1 ng) constructs were injected into left NP lineage and analysed at control st. 17 using confocal microscopy. Phalloidin marked cell borders (F-actin=magenta signal) and fluorescein dextran served as LT (=green signal). (**A-N**) Magnifications of representative anterior NP regions for each injection composition, corresponding average ratios at bottom left corners. Analysed NP region indicated in sketch on bottom left corner (cf. **A**, magenta quadrat; stage sketch from Nieuwkoop & Faber, 1994). (**A**) Cells of uninjected control specimen exhibited equally sized cell surfaces on both sides (split by dashed line). (**B**) Injection of *cnn2*-splMO led to enlarged surfaces in injected cells (note green cells compared to control side). (**C**, **E**, **H**) Upon co-injection of mRNA encoding MTCnn2, MTCnn2ΔABD1 or -ΔClik3, morphant phenotype was rescued. (**F**, **G**, **I**) Co-injection of mRNA encoding MTCnn2ΔClik1, -ΔClik2 or -ΔCterm constructs showed no rescue effects in treated cells. (**J**) Surfaces of 30 cells were measured on each side of the midline (left side/injected side vs right side/uninjected control side) to calculate ratios. Value distribution for each treatment was blotted and statistically analysed. Highly significant differences were confirmed between MO-injection and *MTcnn2*, *MTcnn2ΔABD1* or *-ΔClik3*

mRNA co-injection (=***) and no significant differences compared to morphants upon co-injection of *MTcnn2ΔClik1*, *-ΔClik2* or *-ΔCterm* mRNA (=n.s.). Each construct was tested in at least 3 independent injection experiments (N=3). Statistical analysis was accomplished by paired samples Wilcoxon test (n.s.=p≥0.05; ***=p≤0.001).

2.3.7. Cnn2 is differentailly expressed in neural plate cells

According to the performed LOF experiments, Cnn2 is required for neural AC and its function thereby is mediated by specific domains that are responsible for actin binding. As AC is highly dynamic both temporally and spatially, the temporospatial dynamics of Cnn2 expression during the course of neurulation were analysed in the following.

In the first step intracellular Cnn2 localisation was examined more closely within NP cells. Therefore, 8-cell stage embryos were injected unilaterally with *MTcnn2* mRNA targeting the NP lineage and allowed to grow until neurulation. Early neurula stages were fixed between 14 and 16 subjected to IF staining and analysed by confocal microscopy. Like in NCC explants, the N-terminal MT was visualised by primary anti-c-myc antibody together with red-fluorescing secondary antibody. Cytoskeletal F-actin was stained in green with fluorescently labelled phalloidin and co-injected Cascade Blue^{TM} served as LT.

In early neurula stages, MTCnn2 was expressed in a salt and pepper-like pattern (cf. **Fig. 25A**). Although the LT was evenly distributed on the injected NP side, only a small proportion of cells showed a strong MTCnn2 expression. All analysed embryos (n=12; N=4) displayed this phenotype. Apical surface size of NP cells with the highest expression intensity, were smaller compared to MTCnn2-negative cells. Orthogonal optical sections of these NPs attested a dome-like shape of MTCnn2-expressing cells, whereas neighbouring LT-positive cells were flat (cf. **Fig. 25A´**). Eight embryos out of the described twelve were analysed and all displayed the same correlation between apical cell shape and MTCnn2 expression level.

Additionally, embryos between stage 15 to 16 were dissected transversally to analyse the MTCnn2 localisation within NP cells further. Thereby, injected cells of the superficial layer either displayed a MTCnn2 localisation around the cortex of the entire cells or no expression at all (cf. **Fig. 25B**). Four embryos out of two independent experiments were analysed and all specimens showed this cortical localisation of MTCnn2 (n=4; N=2).

In summary, Cnn2 is differentially expressed in superficial NP cells of early neurula stages. Higher expression levels were detected in cells that bulge outwards, thus in actively constricting NP cells. The missing MTCnn2 expression in several LT-positive cells indicated a degradation of Cnn2, like it was observed in NCC explants.

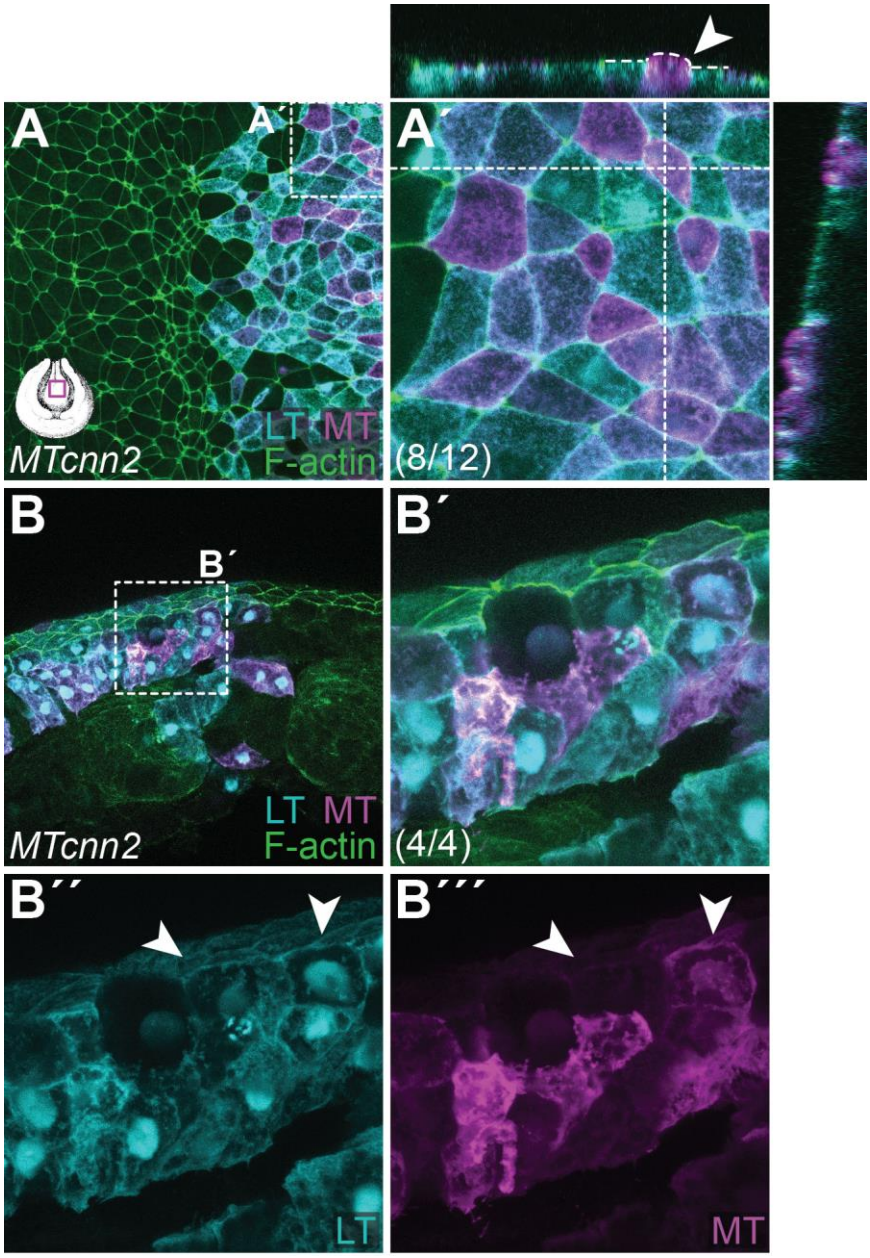

Figure 25: Cnn2 is expressed in actively constricting neural plate cells.
MTCnn2 mRNA (0.1 ng) was injected unilaterally into 8-cell embryos to analyse Cnn2 localisation within the anterior NP via IF staining of fixed st. 15 embryos. MTCnn2 was visualised by anti-c-myc 1st combined with red fluorescing 2nd antibody (=magenta signal), F-actin along cell borders was marked by fluorescently labelled phalloidin (=green signal), Cascade BlueTM served as LT (=cyan signal). (**A**) NP of st. 15 neurula displayed strong MT signal in small proportion of injected cells (analysed NP region indicated by draft bottom left; cf. magenta quadrat; st. 15 sketch from Nieuwkoop & Faber, 1994). (**A´**) Multilayer z-stack scan in higher magnification showed limitation of strongest MTCnn2 expression to dome-like shaped cells (cf. orthogonal views on top and right side, sectional planes marked by white dashed lines; note dome-shape vs flat neighbouring cells marked by white dashed lines and arrowhead). (**B**) Transversal section of st. 16 embryo displayed weak MTCnn2-signal in superficial cell layer. (**B´**-**B´´´**) Close-up view of LT signal attested general targeting of analysed tissue (cf. **B´´**; white arrowheads). MTCnn2 was localised to the entire cell cortex in superficial cells (cf. **B´´´**; right white arrowhead).

As the first localisation analysis of MTCnn2 indicated a differential regulation and possible degradation of the protein within the anterior NP, this characteristic was examined more closely. To assess the regulation of Cnn2 during the course of neurulation, *MTcnn2* mRNA t was injected again as described and treated embryos were fixed at successive neurula stages to be analysed towards their protein expression levels by IF staining (cf. **Fig. 26**). Experimental set-up, including LT usage and subsequent staining, was conducted as described before.

The following analysis showed that NP cells at early neurula stages (st. 14 and 15), clearly expressed MTCnn2 in some injected cells. Stronger signals appeared to be limited to cells, which were already slightly reduced in cell surface size, thus undergoing AC. With advancing neurulation, the overall MTCnn2 expression was reduced and finally almost lost in stage 17 embryos.

In summary, the second part of this analysis revealed temporal dynamics of MTCnn2 expression within the NP. The observed decrease over time implied a precise regulation of Cnn2 levels and that the protein undergoes degradation.

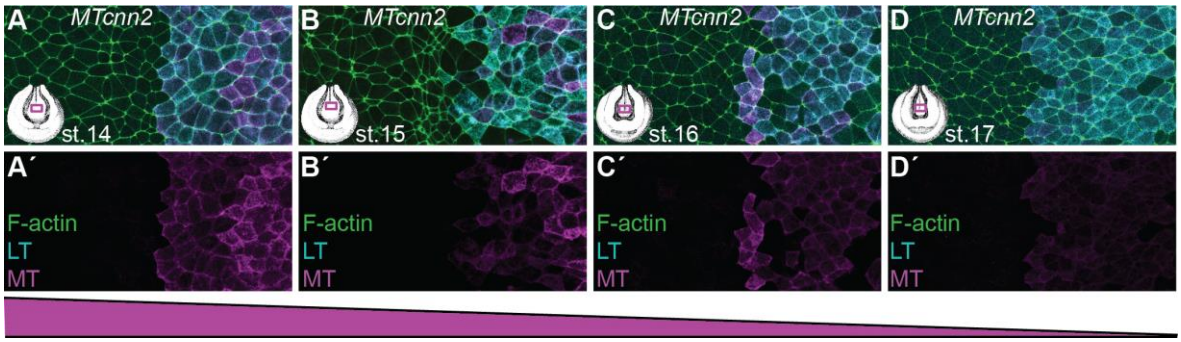

Figure 26: Cnn2 expression levels decrease during the course of neurulation.
MTCnn2 mRNA (0.1 ng) was injected into left NP lineage of 8-cell embryos. Treated specimens were fixed between st. 14 and 17 analysed by IF staining. MTCnn2 was visualised by anti-c-myc 1st combined with red fluorescing 2nd antibody (=magenta signal), F-actin along cell borders was marked by fluorescently labelled phalloidin (=green signal), Cascade BlueTM served as LT (=cyan signal). (**A**-**D**) Magnifications of analysed NPs, examined stages were indicated (cf. stage drafts bottom left corners, from Nieuwkoop & Faber, 1994 with respective regions marked by magenta rectangle). (**A**) MTCnn2 was clearly expressed at st. 14 with higher expression levels several cells (cf. **A´**, MT signal separated). (**B**) At st. 15 the signal was reduced but still prominent in smaller cells (cf. **B´**). (**C**) St. 16 embryos displayed even lower MTCnn2 expression levels (cf. **C´**). (**D**) Expression was almost absent in st. 17 specimens (cf. **D´**). Proceeding reduction of MT signal indicated by magenta triangle below.

2.3.8. Expression levels of Cnn2 within the neural plate are controlled by domains that regulate actin binding

The so far obtained data suggested that neural AC requires Cnn2, but for efficient progression the protein needs to be eliminated. This was implied by the decreasing MTCnn2 levels which are concomitant with the progression of AC movements from stage 14 to 17. As conducted rescue experiments showed that the different domains in Cnn2 confer the physiological function of the protein, their different functionality may stem from differential expression levels. Therefore, embryos were analysed at stage 17 towards their expression levels of the different MTCnn2 deletion constructs.

Of each mRNA construct, 0.1ng were injected unilaterally into the NP lineage of 8-cell stage embryos to subsequently analyse MTCnn2 expression and localisation in NP cells. Injection experiments were performed as described before and specimens fixed at when controls had reached stage 17 to be analysed via IF detection of the N-terminal MT. To identify targeted cells, Cascade Blue^{TM} was co-injected as LT and cell borders were visualised using fluorescently labelled phalloidin (cf. **Fig. 27**).

As expected, injection of the full-length *MTcnn2* construct resulted in a very weak MTCnn2 signal, which indicated a degradation of the protein just resembling the observed phenotype in formerly analysed NP cells as well as in NCC explants (cf. **Fig. 27A**). This low expression level was detectable in 19 out of 24 embryos. The analysis of *MTcnn2ΔABD1* and especially *-ΔClik3* mRNA-injected specimens gave similar results, as the MTCnn2 expression was weak in most treated cells although the LT was evenly distributed (cf. **Fig. 27B**, **E**). Results were obtained by analysis of 10 and 11 specimens, whereas 7 and 8 showed the described phenotype. Opposing this, the expression of MTCnn2ΔClik1, -ΔClik2 and -ΔCterm was intense in most injected cells (cf. **Fig. 27C**, **D**, **F**). These strong expression levels were detectable in 9 out of 11, 9 out of 10 and 8 out of 11 samples respectively.

In summary, the differential expression of Cnn2 upon the deletion of specific domains, implies a function of Clik1, Clik2 and the C-terminus for the regulated degradation of the protein which might be mediated by actin binding. As these domains were also critical for the rescue ability of Cnn2 in the course of AC, proper function of the protein seems to correlate with its tightly regulated expression levels. Thus, a loss of degradation would lead to a loss of Cnn2 function.

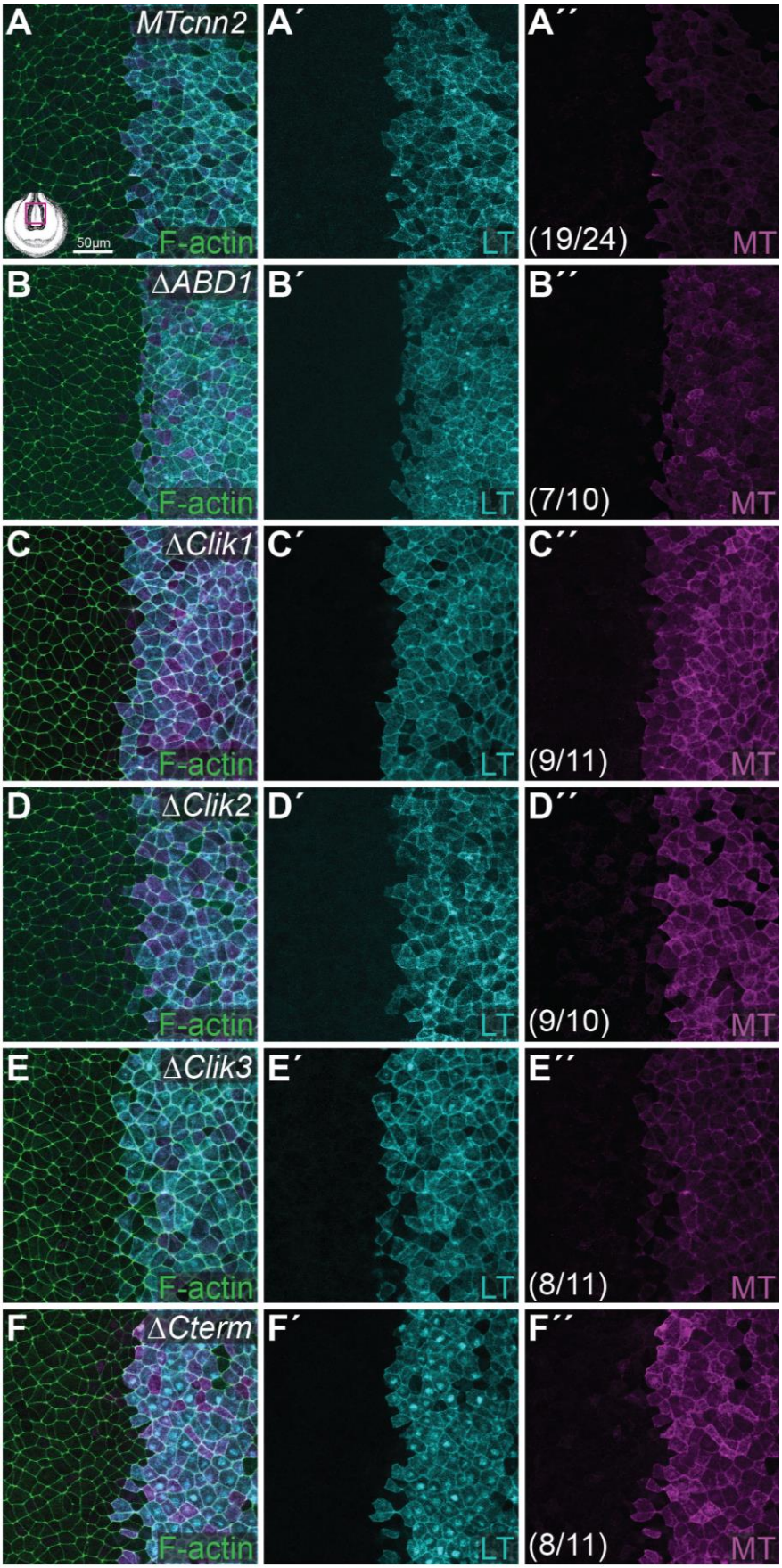

Figure 27: Cnn2 expression levels within the anterior neural plate are controlled by protein domains that mediate actin binding.

MTcnn2 mRNA constructs were injected unilaterally to analyse their localisation within the anterior NP via IF staining. MTCnn2 was visualised by anti-c-myc 1st combined with red fluorescing 2nd antibody (=magenta signal), F-actin along cell borders was marked by fluorescently labelled phalloidin (=green signal), Cascade BlueTM served as LT (=cyan signal). Analysed NP region and stage indicated by draft (cf. **A**, on bottom left corner; magenta quadrat; st. 17 sketch from Nieuwkoop & Faber, 1994). (**A-A´´**) *MTcnn2* mRNA-injected cells were LT-positive but displayed very weak MTCnn2 signal. (**B-B´´**) *MTcnn2ΔABD1* mRNA-injection was detectable by strong LT signal and resulted in comparably low MTCnn2ΔABD1 expression levels. (**C-C´´**) Injection of *MTcnn2ΔClik1* mRNA led to strong expression of the protein in nearly all treated cells. (**D-D´´**) *MTcnn2ΔClik2* mRNA-injection gave similar results as *MTcnn2ΔClik1*. (**E-E´´**) Cells injected with *MTcnn2ΔClik3* mRNA showed clearly reduced expression levels. (**F-F´´**) Injection of *MTcnn2ΔCterm* mRNA led to high MTCnn2ΔCterm levels in almost all hit cells. Protein localisation and expression of full-length MTCnn2 was analysed in 5 clutches (N=5) and in 2 clutches each (N=2) regarding the deletion constructs. Absolute numbers of specimens matching depicted expression phenotypes (X) out of total number analysed (Y) (cf. **A´´-F´´**, (X/Y); bottom left corner).

2.3.9. Cnn2 influnces apical contriction within the neural plate in a level-dependent manner

Based on the assumption that the regulated degradation of Cnn2 and consequently the correctly balanced amount of protein within the anterior NP is critical for AC, two different doses of all *MTcnn2* mRNA constructs were finally tested in this context. In order to introduce distinct expression levels, either 0.1 ng (low dose) or 0.3 ng (high dose) of mRNA were injected unilaterally into NP lineage of 8-cell stage embryos, together with green-labelled fluorescein dextran serving as LT. Specimens were allowed to grow, fixed when uninjected controls reached stage 17 and stained with fluorescently labelled phalloidin for confocal LSM analysis (cf. **Fig. 28A**-**M**). Again, cell sizes were measured of treated cells marked by LT and compared to sizes of controls cells. Sixty cells per embryo were measured, thirty cells on each side of the midline and ratios were calculated by dividing the corresponding mean sizes. Uninjected controls showed similar NP cell sizes on both sites, which resulted in ratio levels mainly ranging between 1.02 and 1.07.

Upon the injection of low *MTcnn2* mRNA doses of any construct, no difference in NP cells size was observed between treated and control sites. Respective ratios of all low dose-treatments reached from 1.02 to 1.16 (cf. **Fig. 28B**, **D**, **F**, **H**, **J**, **L**). Contrary to this, high mRNA doses affected the apical size of treated cells. NP cells injected with full-length *MTcnn2* or *MTcnn2 ΔClik3* construct displayed a reduction of surface size, which resulted in ratio values of 0.71 to 1.02 and 0.79 to 1.03 respectively (cf. **Fig. 28C**, **K**). Upon the injection of high *MTcnn2ΔABD1* mRNA dose, treated cells showed sizes similar to controls with ratios from 0.91 to 1.16 (cf. **Fig. 28E**). Meanwhile, led the injection of *MTcnn2ΔClik1*, *-ΔClik2* and *-ΔCterm* mRNA to a clear increase of cell surface size as mean ratios levelled between 1.39 and 1.52, 1.36 and 1.53 as well as 1.31 and 1.60 (cf. **Fig. 28G**, **I**, **M**).

Statistical analysis, by Wilcoxon paired test, comparing ratio distributions of uninjected controls with mRNA-injected specimens attested a highly significant difference for all high dose-injections, except for *MTΔABD1* mRNA. Along with all low dose- injections, this treatment led to no statistically significant alteration of cell surface size compared to controls (cf. **Fig. 28N**).

Overall, these data indicate an effect of Cnn2 on AC, which depends on its expression levels as well as on the presence of distinct protein domains, which mediate actin binding. Whereas the injection of low mRNA doses had no impact on AC of NP cells, higher levels of the full-length Cnn2 or a protein version missing the Clik3 domain caused a reduction of the cell surface area. Opposing this, higher levels of Cnn2 without Clik1, Clik2 or the C-terminus affected the cell size in a contradictory manner by inducing a measurable enlargement compared to control cells. As these three domains were also shown to be critical for the rescue ability of Cnn2 during the course of AC as well as for its regulated degradation within the NP, this last gain-of-function approach underlines the requirement of balanced protein levels for Cnn2 proper function.

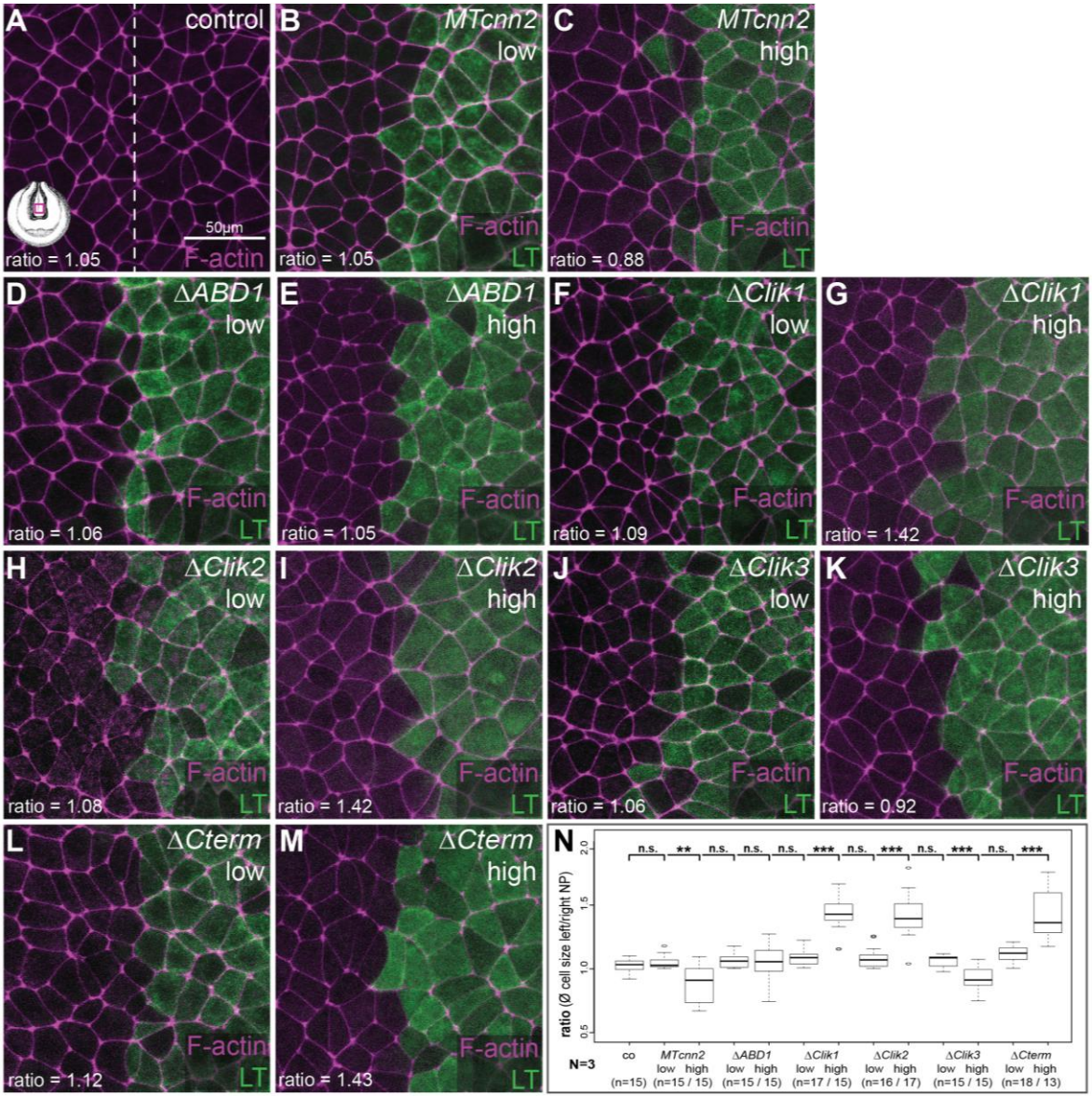

Figure 28: High doses of *MTcnn2* mRNA have an impact on neural apical constriction. *MTcnn2*mRNA constructs ("low" dose =0.1 ng; "high" dose =0.3 ng) were injected into 8-cell embryos targeting the left NP lineage and fixed for LSM analysis, when uninjected controls reached st. 17. F-actin along the cell borders was stained with fluorescently labelled phalloidin (=magenta signal) and green-labelled fluorescein dextran served as LT (=green signal). (**A**-**M**) Magnifications of representative anterior NP regions for each injection, corresponding average ratios at bottom left corners. Analysed NP region indicated in sketch on bottom left corner (cf. **A**; magenta quadrat; stage draft from Nieuwkoop & Faber, 1994). (**A**) Cells of uninjected control specimen exhibited equal surfaces sizes on both sites of the midline (split by white dashed line). (**B, D, F, H, J, L**) Low dose injection of all mRNA constructs as well as high dose of *MTcnn2ΔABD1* mRNA (**E**) had no effect on NP cell sizes compared to uninjected cells. (**C, K**) High doses of *MTcnn2* and *MTcnn2ΔClik3* mRNA led to a reduction of cell surface size. (**G**, **I**, **M**) Cells injected with *MTcnn2ΔClik1-*, *-ΔClik2* or *–ΔCterm* mRNA displayed an increase in surface size. (**N**) Cell surfaces were measured in 30 cells on each side of analysed NPs (left side/injected side vs right side/uninjected control side) to calculate ratios. Distribution of ratio values comparing controls and mRNA-injected specimens. No significant difference was attested between controls and all low dose as well

as high dose *MTcnn2ΔABD1* mRNA-injection (=n.s.). Highly significant differences were noticed comparing controls and remaining high dose-injections (=**/***), except for *MTcnn2ΔABD1* which led to no significant change in ratios (=n.s.). Injections were conducted in 3 independent experiments (N=3). Statistical analysis was carried out by using paired samples Wilcoxon test (n.s.=p≥0.05; **=p≤0.01; ***=p≤0.001).

In order to summarise this last part, *cnn2* mRNA was clearly expressed in the entire NP throughout neurulation.

Different LOF approaches demonstrated a region-specific function of Cnn2 for proper neurulation movements, in addition to its role for the NC.

The morphological shape changes of the NP induced by loss of *cnn2* function, were caused by a dysregulation of AC in the respective cells.

It was also shown that the ability of Cnn2 to rescue this AC phenotype depends on actin binding-mediating domains, i.e. Clik1, Clik2 and the C-terminus. Performed localisation assays revealed strong Cnn2 expression in cells undergoing AC as well as a highly regulated and stage-dependent degradation of the protein within the anterior NP, which was lost upon deletion of Clik1, Clik2 or the C-terminal domain. Thereafter, the rescue ability of Cnn2 correlated with its degradability. Injections of high doses of respective deletion constructs had also an impact on AC within the anterior NP, which underlined the necessity of balanced protein levels for correct actin regulation during this process.

Overall, Clik1, Clik2 and the C-terminus seem to be critical for correct Cnn2 function as well as for its degradation. As these domains are involved in actin binding, the regulated filament association might be the crucial step in this morphological context.

3. Discussion

Calponins constitute a conserved F-actin binding protein family, displaying an isoform-specific expression pattern that indicates different functions dependent on the cellular context. Although numerous studies already focused on these proteins, most analyses regarding the structure and function of Calponin (Cnn) were conducted by utilising chicken gizzard Cnn, an orthologue of mammalian Cnn1, mainly analysing smooth muscle contraction or differentiation (Liu & Jin, 2016).
This work provides new insights into the specific function of Cnn2 during the early development of *Xenopus laevis*. It enables a closer look on the intracellular localisation of this isoform in cells undergoing dramatic shape changes and analyses its function in the course of neurulation, which is regulated by single Cnn2 protein domains.

3.1. Loss of *cnn2* affects specification of the neural crest

One early effect induced by *cnn2* LOF is the defective specification of the NC indicated by reduced *foxd3* expression. Upon the morpholino-mediated LOF either by utilising *cnn2*-5´UTR-MO or *cnn2*-splMO as well as upon CRISPR/Cas9-mediated genome editing, a clear reduction up to complete absence of the early NC specifier expression was detectable. Splice MOs and CRISPR/Cas9 only interfere with zygotic gene expression but not maternally displaced mRNA. This indicates that *cnn2* mRNA is expressed upon activation of the zygotic genome following mid-blastula transition (MBT) and that loss of zygotic *cnn2* function induces the NC specification phenotype. The consistency of phenotypes among morphants as well as crispants and the rescue by co-injected *cnn2* mRNA underline the function of Cnn2 in the course of early NC specification. Previous studies already demonstrated an early expression of *cnn2* in gastrula stages within the presumptive neural and non-neural ectoderm as well as in the pre-involuting mesodermal and ectodermal tissue. The reduced *cnn2* mRNA signal in the latter, after passing through the blastopore, implies a down-regulation in the involuting cells (Schmalholz, 2008). This correlates with the time point of NC induction towards the end of gastrulation and during early NP stage (Pla & Monsoro-Burq, 2018).

The NC arises from the NB region, where its induction program is initiated by the two NB-TFs Pax3 and Zic1 (Milet et al., 2013). Expression of *pax3* in turn is induced in the lateral neural ectoderm at late gastrula stages by signals emanating from the underlying paraxial and intermediate mesoderm (Bang et al., 1999). Pax3 and Zic1 are at the very top of the NC induction Gene Regulatory Network (GRN) with FoxD3 as one downstream factor. Taking all this into consideration, it is possible that Cnn2 or its precise regulation during gastrulation is necessary to correctly position the mesoderm and neuroectoderm with respect to each other enable correct inter-tissue signal transduction and trigger the NC-GRN. This would explain the crispant phenotype which displayed a global *foxd3* reduction and faulty gastrulation, indicated by BPDs, as well as the morphant phenotype if the targeted neuroectoderm is shifted in its position upon unilateral knockdown.

As the altered expression pattern in morphants correlated with morphological changes in neural fold formation on the injected side, an actin-based function of Cnn2 in cell shaping is also conceivable. In this context, the altered NP morphology would influence the expression of NC specifiers directly. It is well understood that spatial tissue organisation mediated by morphogens is a prerequisite of embryonic development. But it still needs to be figured out, whether cell tension is able to modify morphogen signalling. Most recently, studies in human embryonic stem cells (hESCs) indicated that direct application of force by mechanical stretching promotes Wnt/ß-catenin signalling in “gastrulation-like” nodes of BMP-induced mesoderm cells (Muncie et al., 2020). Enhanced cell adhesion-induced tension led to conformational changes of ß-catenin, which permitted its phosphorylation and eventually caused its release from adherens junctions. This enabled ß-catenin nuclear translocation and eventually promoted mesoderm specification (Muncie et al., 2020). Hence, cell fate specification in hESCs can be influenced by tension-mediated reinforcement of Wnt/ß-catenin signalling. Interestingly, studies of murine embryonic stem cells described a direct regulative cooperation between Wnt/ß-catenin and BMP signalling in the course of *msx2* induction (Hussein et al., 2003). The *msx* homeobox genes in turn, are involved in the mediation of BMP4-dependent neural fate specification of the *Xenopus* ectoderm, as *msx1* overexpression promotes epidermal cell fate (Suzuki et al, 1997). Overall, these data imply that cell tension could directly influence Wnt/ß-catenin signalling, which in turn is able to

modulate BMP levels and thus downstream target genes involved in cell fate specification. Therefore, a function of Cnn2 in organising the actin-cytoskeleton of the respective ectodermal cells to mediate cell tension is possible. If the mechanical forces in the presumptive NC tissue are not correctly coordinated, this could lead to defective regulation of Wnt signalling as well as BMP levels and eventually result in the observed loss of NC specifier expression. A hint for an actual shape effect in the targeted cells is the altered neural fold morphology on the injected side.

3.2. Morphological defects in the embryonic head region

The induced loss of *cnn2* function also affected expression pattern of the head specifier *otx2.* Although its expression domain was altered upon injection of *cnn2*splMO as well as *cnn2*-CRNPs, the phenotypes differed between both treatments. While *otx2* was reduced on the targeted side in unilaterally injected morphants, crispants showed a more diffuse distribution of *otx2* expression. It should be noted that the loss of *cnn2* consistently altered embryonic morphology, i.e. it induced neurulation defects in all treated specimens as well as additional gastrulation defects in crispants. The unilateral defects in neural fold formation of morphants were enhanced by specifically targeting the NP. These alterations of the overall embryonic morphology could explain the apparent differences of phenotypes between morphants and crispants. It is conceivable that *otx2*-expressing cells are dispersed within unconstructed morphant NP regions. In crispants on the other hand, the completely disarranged expression domain could be explained by the additional gastrulation defects as the inductive mesoendoderm resides outside of the blastopore in exogastrulae. In both cases, the altered expression pattern would not be caused by a loss of *otx2* expression, but by morphological defects of the respective NP tissue.

In this context, Cnn2 could play a role in the cytoskeletal organisation, as indicated in the previous section. An early function of Cnn2 in *otx2* induction is less likely. *Otx2* mRNA deposited maternally and *otx2* expression levels increase shortly before the onset of gastrulation at stage 9.5. This increase in expression levels depends on the positional specification of transcript mediated by the cortical rotation. Only classical UV treatments of respective embryos are capable of abolishing *otx2* expression in the neural ectoderm, whereas experimentally obtained exogastrulae still show a clear mRNA signal (Pannese et al., 1995). On the one hand, these data approve the observed gastrulation-independent *otx2* expression of crispants in the present work. On the other hand, the very early zygotic induction of *otx2* makes it unlikely that *cnn2,* first expressed at late gastrula stages, might have an impact on this preceding process. Still, the precise patterning of *otx2* expression within the anterior neuro-ectoderm relies on spatial signals emanating from the underlying anterior mesoendoderm (Blitz & Cho, 1995). Therefore, the respective expression domain shape depends on correct gastrulation movements, which ensure correct

positioning of the mesodermal tissue. This might be influenced by the loss of *cnn2* function concerning the CE-dependent cell migration and could result in the observed crispant phenotype.

Regarding the shape changes of the NP upon targeted *cnn2* LOF, it is also possible that Cnn2 plays an additional role for tissue rearrangements in the course of neurulation itself. It has been shown that *cnn2* is a potential direct downstream target of *otx2*. By introducing an *otx2-GR* construct in ectodermal explants, Morgan and colleagues were able to rapidly induce *cnn2* expression (Morgan et al., 1999). Besides its function as anterior specifier, *otx2* expression excludes respective cells from undergoing neural CE movements (Pannese et al., 1995). As the overexpression of *XclpH3* mRNA caused CE defects, Morgan et al. claimed that XclpH3 negatively regulates CE downstream of *otx2* in cells expressing the latter. But as it turned out, this Calponin2 construct exhibited two biochemically functional amino acid exchanges within the Clik1 domain (Hagenlocher, 2010). Therefore, the overexpression introduced more likely a faulty protein version of Cnn2, which would resemble the dysregulation of Cnn2 observed in this study upon MTCnn2ΔClik1 injection.

Nevertheless, Cnn2 could play a role in *otx2*-expressing cells as well as in CE by regulating cytoskeletal stability via F-actin binding in a concentration-dependent manner. In this case, Otx2 would enhance *cnn2* expression in the respective cells and thereby prevent CE movements by higher stabilisation, whereas lower levels of Cnn2 in the neighbouring tissues would enable respective cell movements. Thus, the loss of Cnn2 function could remove the underlying regulator of cell movement in both populations, leading to the general changes in morphology which disrupts the pattern of *otx2* expression.

3.3. *Cnn2* LOF cause distinct developmental defects

At stage 25, both morphant and crispant embryos clearly showed morphological malformations such as craniofacial defects, altered *twist* expression as well as neurulation and gastrulation defects with different degrees of severity or a shorter anterior-posterior axis. This crispant phenotype, together with the increased number of gastrulation defects upon *cnn2*-CRNP-injection, indicates an early requirement of Cnn2 for convergent extension (CE) movements. In amphibian embryos, CE is driven by cell migration and intercalation, which requires the formation multidirectional lamellipodia in presumptive mesodermal cells and their correct mediolateral polarisation (Keller et al., 2008). CE movements occur in different tissues such as the future mesoderm or notochord and are a prerequisite for proper gastrulation and neurulation (Keller & Sutherland, 2020). The analysis performed here and in a previous study (Schmalholz, 2008), detected *cnn2* expression in both mesoderm and notochord. Another indication for the function of Cnn2 in CE comes from elongation assays, performed in animal caps of *Xenopus.* Mesodermally induced, elongating caps expressed *cnn2* mRNA in a domain corresponding to notochord tissue and *cnn2* LOF reduced animal cap elongation (Hagenlocher, 2010). The less prominent CE phenotype in the morphants here analysed can be attributed to the unilateral injection targeted to the NC lineage, but not the dorsal mesoderm. Bilateral injections into the DMZ, to target the future floorplate and notochord, also led to a reduced body length (data not shown). This reproduces the phenotype observed by Hagenlocher, following a similar experimental set-up (Hagenlocher, 2010). Taken together, Cnn2 plays a role in CE movements. Its function is indicated by respective expression patterns in critical tissues and by different loss-of-function experiments. As the mediolateral cell movements that drive CE depend on the formation and polarisation of cell protrusions as well as the mediation of traction forces, an involvement of the actin binding protein in the cytoskeletal organisation of these migrating cells is possible.

The blastopore closure and gastrulation defects, observed in all severely affected morphants and crispants as well as NTDs of crispants, could be a consequence of defective CE.

Interestingly, the distribution of altered and reduced *twist* expression matched the proportion of reduced or absent *foxd3* expression. Since Twist is a direct

downstream target of FoxD3 (Pla & Monsoro-Burq, 2018), NC specification was obviously affected in those specimens. Therefore, the altered facial structures could directly be linked to incorrect specification of the NC, whereas the severity of defects correlates with reduction of *foxd3* expression.

NTDs in unilaterally injected morphants could also be caused by impaired NC induction upon loss of *cnn2*. Studies in mouse embryos showed that correct specification of the NB, which gives rise to the NC, is a prerequisite for NTC. According to this, correct fold fusion depends on a balanced and stepwise induction of distinct NCC fates governed by Wnt/ß-catenin signalling (Kimura-Yoshida et al., 2015). As discussed above, NC specification could be influenced by gastrulation defects, but also by morphological changes of the NB. If Wnt/ß-catenin signalling would in turn be affected due to altered tension within the elevating neural folds, the underlying process would constitute kind of a chicken and egg situation. Thereafter, the morphology would be regulated by cell fate induction and cellular shape changes could in turn influence specification via ß-catenin release. Still, Cnn2 could play a role here as key regulator of the cytoskeleton.

3.4. Polarised localisation of Cnn2 in emigrating neural crest cells

First indications for a function of Cnn2 in NCC migration came from overexpression experiments in *Xenopus*. The injection of mRNA encoding a truncated protein version lacking the C-terminal region, caused migration defects of *krox20*-positive cranial NCCs (Ghislain et al., 2003; Schmalholz, 2008). Additionally, *cnn2* expression was found in migratory cranial NCC streams of chick embryos and its knockdown inhibited cranial NCC migration respectively (Ulmer et al., 2013). Together with the expression of *cnn2* within the pharyngeal arches of the frog detected here, this argues for a conserved role of Cnn2 in NCC migration.

In the present study, MTCnn2 was detected in leading edge lamellipodia of individual cells emigrating from NCC explants. MTCnn2 co-localised with actin fibres of the cortical meshwork region. This distinct part of migrating cells is critical for active protrusion formation and subsequent mediation of locomotive forces via mature focal adhesions. The latter are linked to actomyosin cables and their maintenance is precisely regulated until their eventual disassembly at the retracting edge of the moving cell (Mayor & Etienne-Manneville, 2016). Thus, precise regulation of cell adherence to the ECM is crucial for tension-based locomotion. As Cnn2 is expressed in regions of high mechanical tension, it might be important for this tight regulation. A correlation between traction force and Cnn2 expression levels could be observed in human epidermal keratinocytes and fibroblast cell cultures. Higher traction forces caused by growth on stiffer substrates induced an increase in protein expression (Hossain et al., 2005). Upon reduction of cytoskeletal tension by inhibition of myosin-II-motor activities, Cnn2 expression was reduced accordingly (Hossain et al., 2006).

Overall, the polarised localisation of Cnn2 in NCCs indicates a regulated degradation within the explant tissue. Given the negative effect of high *cnn2* mRNA doses and the necessity of proper titration for explant attachment, balanced Cnn2 levels in migrating cells seem to be critical.

A possible upstream regulator of localised degradation is Wnt/PCP signaling. The Rho-associated kinase (ROCK) gets activated at the rear end of migrating NCCs downstream of this pathway (Mayor & Theveneau, 2014). This regionalised kinase activity could be responsible for the polarisation of Cnn2. *In vitro* analyses of the phosphorylation in chicken Cnn1 revealed 5 functional ROCK target sites, i.e. Thr-

170, Ser-175, Thr-180, Thr-184 and Thr-259. Thr-170 and Thr-180 are not reported to be phosphorylated by another kinase so far. Additionally, respective phosphorylation of Cnn1 seemed to inhibit F-actin binding (Kaneko et al., 2000). Indeed, Cnn2 of *Xenopus* displays the first four phosphorylation sites at the same positions. Therefore, it contains potential ROCK target sites and could be degraded accordingly at the rear end of migrating NCCs.

This could also explain the differential localisation of the full-length protein construct compared to MTCnn2ΔABD1. All potential ROCK target sites of Cnn2 lie within the Clik1 domain in direct vicinity to ABD1. The deletion of the latter, which constitutes a surface-exposed region of the protein, could induce a conformational change of Cnn2 (see **Fig. 4**; Rozenblum & Gimona, 2008), such that the phosphorylation sites become inaccessible and polarised degradation of Cnn2 is inhibited.

3.5. Cnn2 has a distinct function in shaping the neural plate

A tissue-specific function of Cnn2 becomes apparent by the direct comparison of its targeted LOF within the presumptive NP vs. NC region. *Cnn2*-splMO-injection into anterior NP lineage led to defective neural fold formation and unilateral NTDs, while targeting of the NC did not elicit NTDs.

Further examination of NP shaping showed that the bilateral knockdown within the future NP and the CRNP-mediated knockout caused more severe NTDs. These resembled gastrulation and CE defects, as the specimens displayed broad NPs along the entire body axis as well as BPDs and exogastrulation in crispants. The severity of defects was most likely caused by doubled splMO dose upon bilateral injection or the global knockout by influencing *cnn2* expression within the more posterior NP and during gastrulation. In the course of this, Wnt/PCP-mediated neural and mesodermal CE movements, which play an important role for posterior neurulation, could be affected (Wallingford & Harland, 2002). Hereby, Cnn2 might be involved in the mediolateral polarisation of NP cell protrusions downstream of Wnt/PCP signalling, similar to the situation in migrating NCCs discussed above.

The unilateral knockdown of *cnn2* within the anterior NP, on the other hand, led to a defective neural fold formation and reduced narrowing of the tissue, restricted to the presumptive head region (see **Fig. 20**). Upon closer examination of these morphants, it was striking that the treated neural fold areas did not show lines of higher pigmentation, which are characteristic for anterior hinge point formation. Therefore, not only the fold formation was impaired, but also the emergence of dorsolateral hingepoints (DLHPs) in addition to the overall constriction of the neural tissue. Taken together, all these phenotypes indicated a loss of apical constriction (AC). Detailed measurements of apical surface areas within the respective region confirmed an affected AC in morphants as well as in crispants. In general, AC is marked by a higher density of the apical actin cortex (Sawyer et al., 2010; Martin & Goldstein, 2014). A reduced actin signal in correlation with the clearly expanded apical cell surface area of treated cells was detectable. Both could be restored by *cnn2* mRNA injection.

MTCnn2 was localised in a salt and pepper distribution of the protein within the early NP. Especially in the apical dome-shaped region of already constricted cells, strong expression was detectable. This indicates a function of Cnn2 for the organisation of

the apical actin network. Spatial control of medioapical contractility is critical for coordinated AC and governed by Wnt/PCP components (Martin & Goldstein, 2014). Polarised recruitment of ROCK towards the circumferential contractile network is required for directed mediolateral actomyosin contraction within neuroepithelial cells during the course of vertebrate neurulation (Nishimura et al., 2012). As potential effector downstream of ROCK activity, Cnn2 might be necessary to mediate circumferential tension at the apical actin cortex. Here, it could accomplish a stabilising function in this dynamically regulated process.

Preceding studies have shown that AC, in the course of NTC, occurs stepwise and is driven by asynchronous cell-autonomous contraction pulses. These are followed by stabilisation steps of the apical surface area (Christodoulou & Skourides, 2015). The pulses are initiated by transient waves of intracellular Ca^{2+} release. Christodoulou and colleagues identified another Ca^{2+}-regulated and stabilising protein, i.e. Calpain. As all Cnns are able to bind calcium within their CH-domain, a stimulation of Cnn2 activity upon pulsatile Ca^{2+} release is conceivable (Winder & Walsh, 1990; Rozenblum & Gimona, 2008). Additionally, *in vitro* studies analysing smooth muscle Cnn1 demonstrated that Calpain is able to degrade Cnn by proteolysis (Tsunekawa et al., 1989). Thus, an interaction between these two during AC is possible.

Another molecular step in neural AC initiation is regulated by Shroom3. It recruits ROCK to apical adherens junctions, where the latter phosphorylates the myosin light chain and thus induces actomyosin contractility (Hildebrand, 2005; Nishimura & Takeichi, 2008). Shroom3 is also responsible for the apical polarisation of microtubules to facilitate apicobasal elongation, another prerequisite for AC of *Xenopus* NP cells (Lee et al., 2007). *In vitro* studies revealed an interaction of Cnn1 with tubulin, which might also be true for Cnn2 (Fujii, 1997). Thus, Cnn2 might not only play a role here in organising the apical actin cytoskeleton, but also for the required tubulin dynamics.

Overall, in relation to this Shroom3-dependent pathway, a downstream regulation of Cnn2 by the apically recruited ROCK could explain its spatially regulated degradation and differential localisation within the NP. Thereby, Cnn2 would be removed from the apical cortex before actomyosin contractility takes place and recruited again to stabilise circumferential tension in the constricted cell apex. This

transient recruitment could be in turn triggered by Ca^{2+} pulses. The reduced signals at later stages, which seem to be restricted to the apical cell surface borders, suggest that balanced levels of Cnn2 are necessary at the apical actin ring to ensure cell shape stabilisation without inhibiting actin dynamics completely.

3.6. Cnn2 influences actin dynamics via specific regulatory domains

Analysis of the MTCnn2 full-length construct demonstrated a decrease of Cnn2 levels in NCC explants as well as in a temporospatial manner throughout the NP.
Expression analysis of individual deletion constructs clearly showed that the temporospatial regulation of Cnn2 levels depends on distinct protein domains.
Both in NCCs and NP cells, MTCnn2ΔClik3 was degraded to levels as low as the full-length construct, while MTCnn2ΔABD1 levels decreased only slightly and MTCnn2ΔClik1, -ΔClik2 or –ΔCterm remained at high expression levels.
For Cnn1 it has been shown that Cnn was highly resistant to Calpain degradation (Tsunekawa et al., 1989), this indicates an enhanced F-actin binding of the deletion constructs which were not degraded properly. The differential expression levels also directly correlated with the physiological function of Cnn2, as only those constructs which were regulated similar to full-length Cnn2 rescued the LOF-induced impairment of AC in NP cells. In addition, deletion constructs that lacked physiological function, i.e. those that were refractory to degradation and maintained high expression levels, impaired AC when overexpressed. Given the F-actin binding ability of Cnn2 and its capacity to regulate actin-myosin dynamics, this suggests that high levels of Cnn2 correlate with increased binding to actin as well as filament stabilization and thus interfere with the physiological function of actin-myosin contraction. A level-dependent interference with proper Cnn2 function was also observed in NCC explants, as higher amounts of injected *MTcnn2* mRNA influenced explant attachment. Thus, balanced Cnn2 protein levels appear to be required for its regulatory function of actin dynamics.
Why is the controlled degradation of Cnn2 critical for neural AC or in migrating NCCs?
As already discussed above, the transient and localised expression within the dome-shaped apex of constricting NP cells and in lamellipodia of moving cells indicates a function in stabilising F-actin fibres as well as for dynamic tension mediation. It has been shown that Cnn2 acts as filament stabilising factor in cell culture of rabbit aortic smooth muscles, where upon enhanced h2-calponin expression, actin filaments were more resistant to cytochalasin B treatment (Hossain et al., 2005). Cytochalasin normally binds to the barbed ends of F-actin and thereby inhibits actin dynamics. It was also demonstrated that Cnn2 plays a role in cell adhesion, as its decreased

expression in prostate cancer cells notably slowed attachment and reduced their spreading area (Hossain et al., 2014). Further localisation studies in fibroblasts, analysing GFP-tagged Cnn2, showed its specific localisation at the end of stress fibres and within peripheral membrane ruffles of lamellipodia, where it regulates tension-based actin dynamics (Danninger & Gimona, 2000). A comparable localisation was observed in human keratinocytes with the same implications about Cnn2 function, concerning the actin cytoskeleton organisation in the region of cell-to-cell junctions (Fukui et al., 1996). Overall, Cnn2 seems to be critical for actin dynamics by transiently regulating F-actin stabilisation and cell adhesion in various cell types.

A direct functional dependency on balanced protein expression levels is not only indicated by the differential degradation and physiological function of Cnn2 deletion constructs identified here, but also by contradictory functions in cell dynamics reported from other studies. In mouse macrophages derived from h2-calponin null-mutants, a higher proliferation rate and faster cell migration was measured (Huang et al., 2008). Opposing this, reduced *cnn2* expression in zebrafish blocked the proper migration of endothelial cells in the course of vessel formation, whereas its overexpression in human endothelial cells enhanced respective migration and accelerated wound healing *in vitro* (Tang et al., 2006). Thus, Cnn2 can not only inhibit but also promote migration, possibly by coordinating cytoskeletal activity and actin dynamics. This strongly suggests that perfectly balanced cellular levels of Cnn2 are required and would explain the negative effect on AC not only in the loss-of-function situation, but also upon the overexpression of specific deletion constructs. Furthermore, higher doses of the full-length construct and MTCnn2ΔABD1 or -ΔClik3 had a minor effect on AC, which presumably demonstrates a very effective regulation of Cnn2 levels.

Considering that the critical domains for the described regulation are constituted by Clik1, Clik2 and the C-terminus, a loss of either of those could lead to the observed phenotypes regarding protein localisation as well as function. Thus, each deletion construct would represent a protein version, whose actin binding cannot properly be regulated anymore and therefore result in the dose-dependent negative effect upon its overexpression. Thereafter, these constructs would be able to displace native

Cnn2, if their intracellular concentration is excessively increased and bind to the actin cytoskeleton in an uncoordinated, not degradable manner.

It has been shown that ABD2 represents the critical domain for actin binding in Cnn2, whereas ABD1 appears to be incapable of actin binding (Burgstaller et al., 2002; Gimona & Mital, 1998). Additionally, *in vitro* analyses of rat smooth muscle cells identified the Clik domain as critical stabiliser to coordinate overall actin dynamics and podosome formation (Gimona et al., 2003). Thus Clik1 and Clik2 could be solely responsible for F-actin binding and stabilisation here. Regarding the missing rescue effect as well as the loss of degradation, combined with the gain of function phenotype upon overexpressing either deletion construct, both domains obviously have to be present to allow the regulated actin binding of Cnn2. Furthermore, it would explain the ability of MTCnn2ΔABD1 to partially rescue the knockdown phenotype, although ABD1 has no function in this context. Its deletion in direct proximity to the critical Clik domain, still could induce conformational changes. These would minimally affect proper actin stabilisation, which then leads to the observed partial rescue effect and not complete degradation of the construct. The balanced stabilisation of F-actin binding, on the other hand, most likely is dependent on an auto-regulatory function of the Cnn2 C-terminus. It has been shown that a deletion of the tail sequence enhances attachment of h2-calponin to the actin cytoskeleton (Danninger & Gimona, 2000). Even a differential localisation upon removal of the C-terminus was observed in rat smooth muscle cell culture, as h2-calponin displayed increased F-actin binding and bundling. It was also displaced from the peripheral cell cortex towards central stress fibres (Burgstaller et al., 2002). Biochemical studies, based on turkey Cnn1, demonstrated a conformational change of the C-terminal domain upon F-actin binding and implied a direct interaction between the actin binding site and the tail region (Bartegi et al., 1999). In accordance with the data generated here, this clearly indicates a direct regulation of Clik1 and Clik2 function by the C-terminus, which influences binding as well as localisation of Cnn2 within the actin cortex.

In summary, Cnn2 actually seems to influence morphogenetic events such as lamellipodia formation and AC by coordinating actin dynamics. Proper F-actin binding and therefore its stabilisation could be achieved by Clik1 and Clik2 together. This cytoskeletal organisation needs to be transient, thus Cnn2 binding and its

expression level should be regulated via C-terminus-dependent degradation. Overall, the first two Clik domains in combination with the C-terminal region appear to form a regulatory unit, which only functions correctly if all three components are present (cf. **Fig**. **29**). In this scenario, a dysregulated deletion construct of Cnn2 would affect both, the spatial and temporal regulation of the actin cytoskeleton by incorrect F-actin binding.

Considering the stabilising function of Cnn2, an irreversible binding of high protein amounts, for example could inhibit actin-myosin contractility within the apical cell cortex by blocking the interaction between actin-bound ATP and myosin motor proteins (Alberts et al., 2015).

As actin dynamics require coordinated filament reorganisation (Winder & Ayscough, 2005), dysregulated F-actin binding by Cnn2 also might interfere with other accessory proteins that are responsible for formation of dendritic or gel-like actin networks in order to adjust individual cell shapes during the course of morphogenetic events, such as lamellipodia formation.

Furthermore, increased Cnn2 localisation towards the end of stress fibres within lamellipodia could stabilise the fibres and enhance their linkage to focal adhesions (Burridge & Guilluy, 2016), thus preventing proper tension transduction and focal adhesion degradation in migrating cells.

Overall, enhanced filament binding by stabilising Cnn2 could interfere with or even block a variety of dynamic processes within the actin cortex.

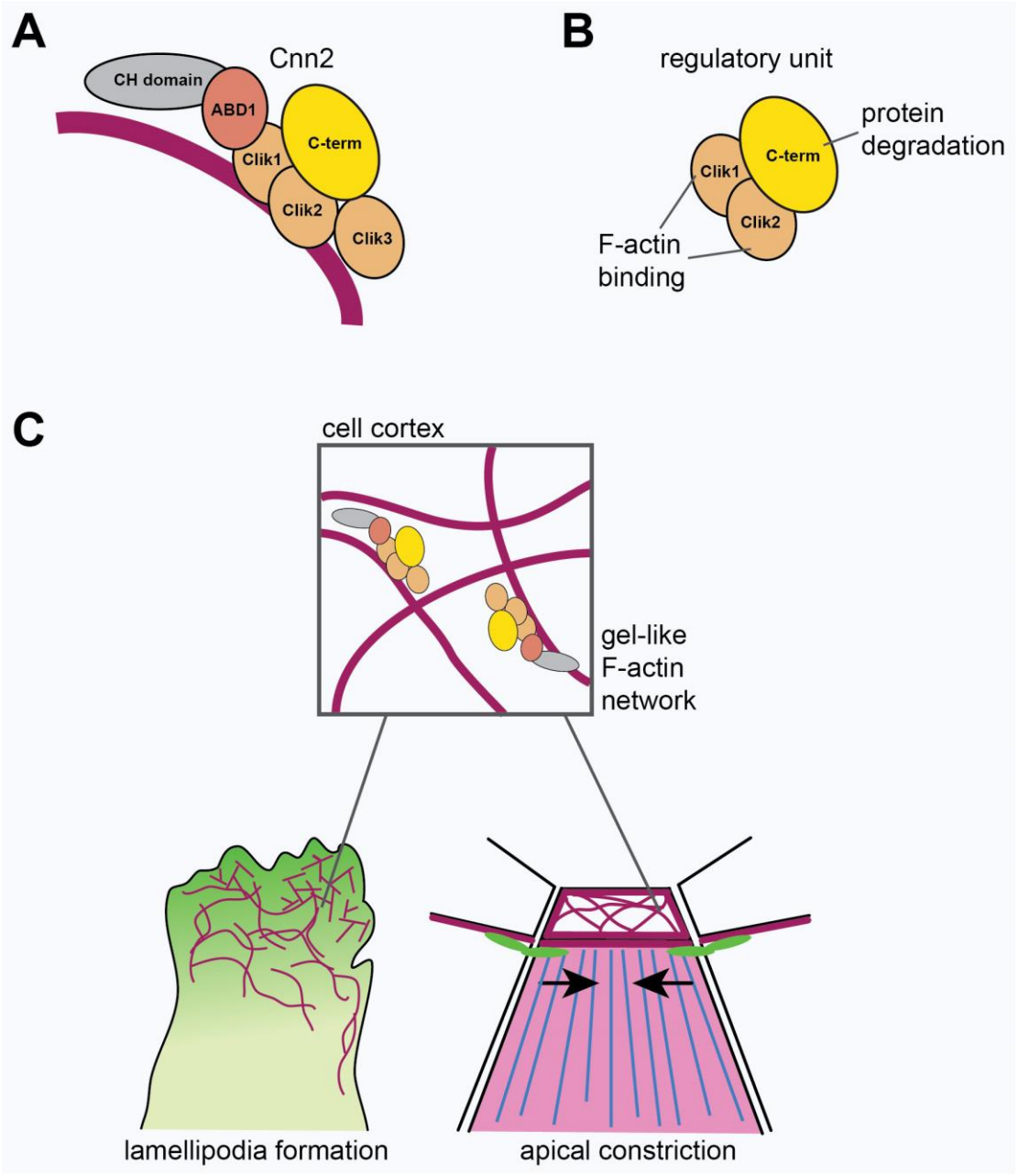

Figure 29: Dynamic actin binding of Cnn2 is mediated by regulating domains
(**A**) Schematic representation of Cnn2 bound to F-actin (magenta line). Protein domains depicted by respectively inscribed circles. Clik1 and Clik2 domain mediate actin binding. The C-terminus interacts with both Clik domains in order to regulate their binding and enable proper degradation of the whole protein. (**B**) All three together components constitute a regulatory unit. (**C**) Regulated dynamic F-actin binding of Cnn2 is crucial for organising the cell cortex in actin-based morphogenetic processes such as lamellipodia formation and apical constriction. Localisation of actin networks potentially regulated by Cnn2 indicated in migrating and apically constricting cells, which correlates with observed MTCnn2 expression (cf. schematic representation of cell regions in question below).

4. Material

4.1. Analysed Model organism

African clawed frog (*Xenopus laevis)* - Utilised eggs and sperm were retrieved from adult frogs kept under species-appropriate conditions, in special tanks designed by AQUA SCHWARZ GmbH with regulated water temperature between 18°C and 20°C, defined salt concentration and a light cycle of 12 hours.

4.2. Chemicals and kits

Product name	**Supplier**
Agar	AppliChem
Agarose LE	Roth
Agarose standard	Genaxxon Bioscience
Agarose low-melt	Roth
Albumin fraction V (BSA)	Roth
Alexa Fluor™ 488 Phalloidin	Thermo Fisher Scientific
Alexa Fluor™ 555 Phalloidin	Thermo Fisher Scientific
Ammonium acetate	Roth
Anti-c-myc monoclonal antibody (mouse)	Sigma
Anti-Digoxigenin-AP Fab Fragments	Roche
Anti-mouse IgG1 (γ1) Alexa Fluor 555 (goat)	Life Technologies
Benzocaine	Sigma
BM-Purple	Roche
Boehringer blocking reagent	Roche
CAS-Block	Life Technologies
Cascade Blue™ dextran (10.000 MW)	Thermo Fisher Scientific
CHAPS	AppliChem
Chloroform	Merck
Cysteine	Roth
Deoxynucleotide triphosphates (dNTPs)	Promega
Digoxigenine-dNTP-labeling mix	Roche
Dithioreitol (DTT)	Promega
DNaseI	Thermo Fisher Scientific
Ethanol	Roth
Ethylenediaminetetraacetic acid (EDTA)	Roth
Fibronectin bovine plasma F1141-1MG	Sigma
Ficoll	Sigma
Fluorescein dextran	Thermo Fisher Scientific
Formaldehyde	Roth
Formamide	Roth

GeneJET Gel Extraction & DNA Clean-up Micro Kit	Thermo Fisher Scientific
Glutaraldehyde	Roth
Glycerol	Roth
Glycine	AppliChem
Heparin	AppliChem
Hepes	AppliChem
High Pure RNA Tissue Kit	Roche
Hoechst	Molecular Probes
Hydrochloric acid (37%)	Merck
Human chorionic gonadotropin (CG hormone)	Sigma
innuPREP DOUBLE pure Gel Extraction Kit	Analytic Jena
Isopropanol	Roth
Loading buffer DNA Orange (6x)	Thermo Fisher Scientific
Lambda ladder	Promega
Magnesium chloride	Merck
Magnesium sulphate	Roth
Maleic acid	Roth
MEGAshortscript™ T7 Transcription Kit	Thermo Fisher Scientific
MEGAclear™ Transcription Clean-UP Kit	Thermo Fisher Scientific
mMESSAGE mMACHINE™ SP6 Transcription Kit	Thermo Fisher Scientific
mMESSAGE mMACHINE™ T7 Transcription Kit	Thermo Fisher Scientific
Methanol	Roth
M-MLV reverse transcriptase	Promega
Mowiol® (4-88)	Roth
N-N-dimethylformamide	AppliChem
Oligonucleotides	Promega
ScientificParaformaldehyd (PFA)	AppliChem
peqGREEN	Peqlab
Pfu DNA Polymerase	Promega
Potassium acetate	Roth
Potassium chloride	AppliChem
Potassium dihydrogen phosphate	AppliChem
Proteinase K	Roth
PureYield™ Plasmid Midiprep System	Promega
RNasin (Rnase inhibitor)	Promega
ROTI®Phenol/Chloroform	Roth
Sodium acetate	Roth
Sodium citrate	Roth

Sodium chloride	AppliChem
Sodium hydrogen carbonate	Merck
Sodium hydroxide	Roth
Sodium dodecyl sulphate (SDS)	AppliChem
Sp6 RNA polymerase	Promega
Transcriptor High Fidelity cDNA synthesis Kit	Roche
T7 RNA polymerase	Promega
Taq DNA polymerase	Promega
Tris	AppliChem
Tris base	Roth
Tween20	Roth

4.3. Chemical solutions and buffers

AP1 buffer
0.1 M Tris buffer (pH 7.5); 5M $MgCl_2$; 0.1 M NaCl (pH 9.6)

Cysteine
2 % cysteine dissolved in dest. H_2O (pH 7.99)

DFA buffer
10.6 ml 5 M NaCl; 5 ml 1 M Na_2CO_3; 1.05 g $C_6H_{11}KO_7$; 6.98 g $C_6H_{11}NaO_7$; 1 ml 1M $CaCl_2$; 1 ml 1 M $MgSO_4$; added dest. H_2O up to 1 l; set pH 8.3 with $C_6H_{13}NO_4$; filtrated; added 1 g BSA; autoclaved; stored at -20 °C

Ficoll
2 % Ficoll dissolved in 1x MBSH

Gurdon´s buffer
88 mM NaCl; 15 mM Hepes; 15 mMTris-HCl; 1 mM KCl; pH 7.6

Hybridisation buffer (1l)
1 g Torula RNA dissolved in 100 ml dest. H_2O stirring at 65 °C; filtered; 10 g Boehringer blocking reagent in 500 ml CH_3NO and 250 ml 20xSSC (pH 7.0) stirring at 65 °C; adding 120 ml dest. H_2O; dissolved Torula RNA; 100 mg Heparin in 2 ml 1xSSC and 10 ml 0,5 M EDTA; 1 g CHAPS in 10 ml dest. H_2O; 5 ml Tween

LB (lysogeny broth) medium
10 g/l tryptone; 12.2 mM NaCl; 5 g/l yeast extract; pH 7.0

Lysis buffer for crispants
50 mN Tris (pH 8.8); 1 mM EDTA; 0.5 % Tween 20; added 200 µg/ml proteinase K

MAB
100 mM $C_4H_4O_4$; 150 mM NaCl; pH 7.5

MAB blocking
1 % Boehringer blocking reagent in MAB; dissolved at 70 °C; added 0.1 % Tween (pH 7.4)

MABw
MAB, 0.1 %Tween

5x MBSH (1l)
25.7 g NaCl; 0.375 g KCl; 1 g $NaHCO_3$; 1 g $MgSO_4/7H_2O$; 0.39 g $(CaNO_3)_2/4\ H_2O$; 0.3 g CaCl/2HO; 11.9 g HEPES; 5 ml Pen-Strep

10x MEMFA
Stock (1 l): 500 ml 2 M MOPS (pH 7,4); 200 ml 100 mM EGTA; 10 ml 1M $MgSO_4$
Working solution: 10 % MEMFA; 10 % formaldehyde (37 %ig); 80% H_2O

10xPBS$^-$
1.5 mM KH_2PO_4; 137 mM NaCl; 2.7 mM KCl; 5 mM Na_2HPO_4 (pH 7.3)

Mowiol
30 g Mowiol®; 120 ml 1xPBS-; stirring overnight. at 60 °C; 75 ml glycerine; 1 thymol crystals; filtered; stored at 4 °C

PBST
1xPBS$^-$ + 0.1 % TritonX-100 (pH 7.4)

PBSw
1xPBS$^-$ + 0.1 % Tween (pH 7.4)

4 % PFA with 0,2 % Glutaraldehyde (100ml)
4 g PFA in 100 ml PBS$^-$ dissolved stirring at 70 °C;
pH 7.4; kept on ice; added 0.2 % Glutaraldehyde

8 % PFA (100 ml)
8g PFA in 100 ml PBS$^-$ dissolved stirring at 70 °C

P1 (resuspension) buffer
50 mM Tris-HCl; 10 mM EDTA (pH 8.0); 100 µg/mL RNAse A; stored at 4 °C

P2 (lysis) buffer
0.2 M NaOH; 1 % (v/v) SDS

P3 (neutralisation) buffer
3 M CH_3CO_2K (pH 5.1)

20x SSC (1 l)
175.3 g NaCl; 88.2 g $Na_3C_6H_5O_7$ dissolved in 800 ml dest. H_2O; pH 7.0; added up to 1 l; autoclaved

SOC medium (super optimal catabolite repression medium)
20 g/l tryptone; 10 mM MgSO4; 10 mM MgCl2; 10 mM NaCl; 5 g/l Hefeextrakt; 2.5 mM KCl; 3.6 g/l $C_6H_{12}O_6$

50x TAE buffer (Tris acetate EDTA electrophoresis buffer)
2 M Tris (pH=8.5); 1 M CH_3COOH; 50 mM EDTA (pH = 8.0); pH 8.5

Vib mix
2.2 g gelatine dissolved in 450 ml 1xPBS^- at 65 °C; cool down; added 135 g BSA stirring; stored at -20 °C

5. Methods

5.1. *In vitro* fertilization

Egg deposition by adult *Xenopus laevis* females was induced by subcutaneous injection of human chorionic gonadotropin (CG hormone). Therefore, about 50 µl of hormone were injected 1 week in advance followed by a second dose of 400-600 µl 12 hours before clutch retrieval. Utilised sperm for *in vitro* fertilisation came from dissected testicles, kept in 1xMBSH at 4 °C up to two weeks before usage. 2 mm^2 thick pieces of testis were macerated within 1 ml 1xMBSH per clutch. Sperm solution was added via pipette and softly distributed between the eggs. Immotile sperm was activated by adding 0.1xMBSH thereby increasing the overall salt concentration. 45 minutes after fertilisation, the jelly envelope was removed from the clutches by incubation in cysteine for 5 minutes. Cysteine was removed by washing for at least 4 times in 0,1xMBSH and 2 times in 1xMBSH using a beaker. Embryos were left in 1xMBSH petri dishes until requested stage was reached for fixation or injection.

5.2. PCR design and cloning of mRNA constructs

All deletions were obtained by overlap PCR technique and subsequent ligation into CS2+MT plasmid to enable amplification in respectively transfected *E. coli* bacteria (XL1-Blue Competent Cells). As template severed *Xcnn2.L* sequence, which was linearized from the *Xcnn2MT* Midi provided by Schmalholz, 2010.
PCR was performed in two steps. In the first round *cnn2* fragments were amplified just missing the domain sequences, which should be deleted. Those fragments were then combined and served as templates for the final amplification step with specific primers designed to put the single sequence parts together, encoding one deletion construct each. The general FW and RV primers, positioned at the 5´ and 3´ end of the *Xcnn2.L,* were complemented by an additional XhoI target site (marked by yellow) and one KpnI target site within the FW primer sequence to enable subsequent linearization as well as restriction reaction to test the construct orientation within the plasmid upon cloning.

No.	Primer name	Sequence (5´-3´)
1	XCnn2_FW	GGCCTCTCGAGGGTACCATGAGCTCCCAGTTTAACAAGGGC
2	XCnn2_RV	CCGCGCTCGAGGAAGTCCTGCTGGTACTGTTCTTGT
3	XCnn2_delABD1_FW	GGTTTGCAGAGTGTAGACATCGGGATTGGGCTGCAGATGGGC
4	XCnn2_delABD1_RV	CCCGATGTCTACACTCTGCAAACC

5	XCnn2_delClik1_FW	GATGATAATACAAAGAAAGCAGGAAACTGTGTCAGCCTACAGATGGGCAGCAAC
6	XCnn2_delClik1_RV	GACACAGTTTCCTGCTTTCTTTGTATTATCATC
7	XCnn2_delClik2_FW	CCAAGAACACAATCCTACCACCAATGGACACCAAGTCTGGAACTGAGAAGTG
8	XCnn2_delClik2_RV	CATTGGTGGTAGGATTGTGTTCTTGG
9	XCnn2_delClik3_FW	TGGAACTGAGAAGTGTGACAATTCATCTGACCCAAAATACTGCCCCACG
10	XCnn2_delClik3_RV	AGATGAATTGTCACACTTCTCAGTTCCA
11	XCnn2_delCterm_RV	CCGCGCTCGAGATAGATCTGCCTGCCAAGCCC

Fragments were obtained by combination of primer No. 1 with each RV primer separately and primer No. 2 with each FW primer.

PCR reaction (25 µl)		PCR program	
1 µl	FW primer (10 µM)	110 °C	pre-heat lid
1 µl	RV primer (10 µM)	95 °C	for 2 min
1 µl	DNA fragment (~25 µg/ml)	35 cycles:	
5 µl	Polymerase buffer	95 °C	for 30 sec
0.2 µl	Pfu DNA Polymerase	60 °C	for 30 sec
2.5 µl	dNTPs (2 mM)	73 °C	for 1 min
14.3 µl	DNase-free H_2O	final: 73 °C for 5 min	

Overlap PCR was performed after re-amplification step with doubled reaction volume for some fragments. Therefore, specific del fragments (e.g. for delABD1 obtained by primer combination 1+4 and 2+3) served in combination as template and PCR reaction were set up again with primer No.1 and 2 as FW and RW primers for all reactions.

Overlap PCR reaction (50 µl)		PCR program	
2 µl	FW primer (10 µM)	110 °C	pre-heat lid
2 µl	RV primer (10 µM)	95 °C	for 2 min
5 + 5 µl	del fragments	40 cycles:	
5 µl	Polymerase buffer	95 °C	for 30 sec
0.6 µl	Pfu DNA Polymerase	55 – 58 °C	for 30 sec
1 µl	dNTPs (10 mM)	73 °C	for 1 min 36 sec
29.4 µl	DNase-free H_2O	final: 73 °C	for 5 min

PCR reactions were purified by using innuPREP DOUBLE pure Kit according to protocol provided by manufacturer. CS2+MT plasmid and reaction were linearised overnight at 37°C.

Linearisation CS2+MT plasmid (0.5 µg/µl)		Linearization PCR products	
20 µl	plasmid	~18 µl	PCR reaction (total)
10 µl	Buffer D (Promega)	5 µl	Buffer D (Promega)
1 µl	BSA	0.5 µl	BSA
3 µl	Xho1 enzyme (Promega)	1.5 µl	Xho1 enzyme (Promega)
66 µl	H_2O (autoclaved)	25 µl	H_2O (autoclaved)

Linearization reactions were cleaned by adding 10 µl 5 M NH_4 acetate and 220 µl 100 % EtOH at -20 °C for 15 minutes and centrifuged at 4 °C and maximum spin. Obtained DNA pellets were dried at RT and re-suspended in 30 µl RNase-free H_2O. Following this, ligation reactions were incubated overnight at 4 °C.

Ligation	
0.5 µl	linearised CS2+MT plasmid
5 µl	DNA
1 µl	10x T4 DNA Ligase Buffer
1 µl	T4 DNA Ligase
2.5 µl	H_2O (autoclaved)

For transformation 100 µl of competent *E. coli* were thawed on ice and incubated with 5 µl of ligation solution for 30 minutes on ice. Afterwards, samples were heat shocked for 90 seconds at 42 °C then chilled on ice for 2 minutes and finally incubated in 400 µl SOC medium for 1 hour shacking at 300 rpm at 37 °C. Bacteria were plated onto LB-agarose plates containing 0.01 % ampicillin and left to grow at 37 °C overnight. Selected bacteria colonies were picked and incubated in 3 ml LB medium containing ampicillin rocking at 37 °C overnight. DNA was extracted from 1.5 ml of each bacteria suspension by centrifugation at 5000 rpm for 5 minutes. Pellets were re-suspended in 100 µl P1 buffer and vortexed. 200 µl P2 buffer were added and samples incubated for 5 minutes at RT after shacking briefly. Finally, 150 µl P3 buffer were added and incubated for 20 minutes on ice. Upon subsequent centrifugation at 14000 rpm for 10 minutes at 4 °C, supernatants were transferred into new eppi tubes and vortexed with 1 ml cold 100% EtOH (-20 °C). DNA was left to participate overnight at -20 °C. To test cloning success, all samples were digested again with XhoI enzyme in 20 µl reactions at 37 °C for ~6 hours. Left 1.5 ml of positive colony suspensions were transferred into 100 ml LB medium containing ampicillin and left growing again overnight at 37 °C. Plasmid DNA was extracted utilising PureYield™ Plasmid Midiprep System and finally sent to macrogen for sequencing. Seqeuncing reactions contained 200 ng/µl DNA, 5µl SP6 or T7 primer and were added up to 40 µl total volume by H_2O (autoclaved).

5.3. mRNA synthesis

To prepare mRNA constructs for injection into the embryo, 10 µg of plasmid DNA were linearized overnight at 37 °C. Synthesis reactions were set up after successful linearisation using mMESSAGE mMACHINE™ SP6 Transcription Kit.

Linearisation (50 µl total reaction)	Synthesis reaction
10 µg plasmid DNA	10 µl 2xNTP
5 µl Buffer D (Promega)	2 µl 10x reaction buffer
2 µl NotI enzyme (Promega)	2 µl SP6 enzyme mix
X µl H_2O (autoclaved)	2 µl linear DNA template
	4 µl RNase-free H_2O

Synthesis reactions were incubated at 37 °C for 2 hours. DNA was removed by adding 1 µl TURBO DNase for 15 minutes at 37 °C. After this, 115 µl RNase-free H_2O and 15 µl NH_4 acetate (kit) were added followed by 150 µl ROTI®Phenol/Chloroform. Samples were vortexed after each step. Supernatant was retrieved after 5 minutes of centrifugation and vortexed with 150 µl chloroform and again centrifuged. Upper phase was transferred into clean eppi tube and incubated with 150 µl isopropanol after vortex at -20 °C overnight. Precipitated mRNA was obtained as pellet upon final centrifugation step and re-suspended in 20 µl RNase-free H_2O. Quality and concentration of mRNA was measured via photometry and on a 1 % agarose gel. Aliquots of 1µl were stored at -80 °C ready-to-use.

5.4. Morpholinos

Morpholino antisense oligos (MOs) were designed upon request and produced by Gene Tools, LLC (1001 Summerton Way Philomath, OR 97370 USA). MOs arrived freeze-dried and were dissolved in RNase-free H_2O for 10 minutes at 65 °C. Stock solutions with a concentration of 1 mM were stored at RT. Aliquots were heated again shortly before usage to optimise MO activity.

MO name	Sequence (5´-3´)
Cnn2_5PrimeUTR_Blocking	CACTCCCTTCCACTTGCTCAG
Cnn2.L_SplMO	AATAAAGTTCCCTTTCTCACCTGGT
Cnn2.S_SplMO	TAAAGTCAAGTCCCCATCTCACCTG

5.5. sgRNA synthesis, CRNP preparation KO evaluation

Sequences for sgRNA were predicted and respective oligos designed with CRISPRscan (https://www.crisprscan.org/). HPLC purified DNA oligos were subsequently ordered from Sigma-Aldrich to synthesise designed sgRNAs. Oligos were diluted according to provided data sheet and incubated st 55 °C for 30 minutes before storage at -20 °C. Oligo extension was performed by PCR.

Forward oligo sgRNA_cnn2.L_exon4:
GCAGCTAATACGACTCACTATAGGGCAACATGACTCAAGTACGTTTTAGAGCTAGAAATAGCAAG

Forward oligo sgRNA_cnn2.L_exon4:
GCAGCTAATACGACTCACTATAGGGGAACATGACTCAAGTTCGTTTTAGAGCTAGAAATAGCAAG

Utilised sgRNA-reverse oligo:
AAAAGCACCGACTCGGTGCCACTTTTTCAAGTTGATAACGGACTAGCCTTATTTTAACTTGCTATTTCTAGCTCTAAAAC

PCR reaction	PCR program (by William Ratzan)
83 µl RNase-free H_2O	98 °C for 30 sec
10 µl 10x Polymerase buffer	10 cycles:
2 µl dNTPs (10 mM each)	98 °C for 10 sec
1 µl forward oligo	62 °C for 20 sec
1 µl reverse oligo	72 °C for 20 sec
1 µl Pfu DNA Polymerase	25 cycles:
Annealing control mix	98 °C for 10 sec
98 µl RNase-free H_2O	72 °C for 30 sec
1 µl forward oligo	final: 72 °C for 5 min
1 µl reverse oligo	

2µl of synthesised sgRNA templates were checked versus annealing control on 1.5% agarose gel. Left proportion was purified using the GeneJET Gel Extraction & DNA Clean-up Micro Kit and final concentration was measured by photometric measurements before storage at -20°C.
Final sgRNA synthesis was done by using MEGAshortscript T7 Transcription Kit.

Reaction mix (20 µl total reaction)	
2 µl	10x Buffer
2 µl	ATP, CTP, GTP, UTP (each)
2 µl	T7 RNA polymerase
300 ng	sgRNA template
X µl	RNase-free H_2O

Incubated reaction for 4.5 hours at 37 °C. Added 1 µl DNase and incubated again for at 37 °C for 15 minutes. Reactions were purified with the MEGAclear™ Transcription Clean-Up Kit. Cleaned sgRNA was again checked on 1.5 % agarose gel and via photometric measurement to check final concentration. 1 µl aliquots were stored at -80 °C ready-to-use.
In order to prepare CRNP-injection, sgRNAs were incubated at 70 °C for 2 minutes, followed by chilling on ice. PNA Bio Cas9 (CP01-50) was dissolved in advance with a concentration of 0.5 mg/ml in H_2O and stored at -80 °C à 1 µl. To assemble RNP complexes respectively, sgRNA was added to Cas9 aliquot, in required concentration and together with 2µl RNase-free H_2O. Mix was incubated at 37 °C for 5 minutes and finally left on ice till injection. In all performed CRNP-injection experiments single *cnn2.L*- and *cnn2.S*-sgRNAs were prepared separately and respective CRNPs mixed shortly before usage.
KO evaluation was done by direct sequencing of PCR amplicons according to Nakayama et al., 2014. Therefore, injected specimens were transferred into crispant lysis buffer supplemented by proteinase K (200 µg/ml final concentration) and incubated at 56 °C overnight. DNA was extracted as supernatant after 3 centrifugation steps and stored at -20 °C to be finally pooled for test PCR.

Test primer name	Sequence (5´-3´)
test primer_cnn2.L_Fw	AGGCAATGGAAATTCTGAAGCA
test primer_cnn2.L_Rv	CCCCGATGTCTACACTCTGC
test primer_cnn2.S_Fw	AGGAAAATCAATTAGACGGGCA
test primer_cnn2.S_Rv	TGCAAACCTTGTGTCTTTGCC

PCR reaction (100 µl)		Standard Taq PCR program	
20 µl	5x Taq buffer	110 °C	pre-heat lid
10 µl	dNTPs (2 mM)	95 °C	for 2 min
4 µl	Fw primer	35 cycles:	
4 µl	Rv primer	95 °C	for 30 sec
8 µl	crispant DNA	60 °C	for 30 sec
53.2 µl	nuclease-free H_2O	73 °C	for 1 min
0.8 µl	Taq DNA polymerase	final: 73 °C for 5 min	

Again PCR reaction were cleaned using GeneJET Gel Extraction & DNA Clean-up Micro Kit, followed by photometric concentration measurement and DNA sample were send to external sequencing facility. Sequencing reactions contained 10 ng/µl DNA, 5µl of respective Fw or Rv primer, finally added up to 10 µl total volume by H_2O (autoclaved).

5.6. Microinjection

Needles were pulled from glass capillaries with 1 mm diameter by using a Micropipette Puller (P-87Flaming/Brown, Sutter Instrument). Injections were performed with the Medical Systems Pico-Injector (PLI-100A, Harvard Apparatus Medical Systems) in combination with a stereomicroscope and suitable micromanipulator. Single injection dose was calibrated by manual truncation of the needle to get correct drop size measured with CELL-VU® counting chamber. Drop size amounted 4 nl for injection of MOs and 8 nl for CRNPs. Embryos were put into Ficoll-filled 1xMBSH-agarose petri dishes and injected as described at 4-8 cell stage with MOs or at zygote stage with CRNPs. Treated specimens were left in Ficoll for at least 30 minutes, before they were transferred into 0.1xMBSH in corresponding agarose petri dishes for final incubation until they reached requested stages.

5.7. Fixation of different embryonic stages

Treated embryos plus controls were allowed to grow at 16 °C or at RT, depending on requested stage and given time frame.
For further IF analysis or fluorescent staining procedures, embryos were fixed in 4 % PFA by using 5 ml glass vials, either rolling at RT for 1 hour or at ~5 °C softly shaking overnight.
For WMISH, specimens were fixed in 1xMEMFA shaking overnight or over the weekend at ~5 °C and finally stored in 100 % EtOH at -20 °C till further analysis.

5.8. NCC explant culture

Coverslips for explant culture were cleaned in advance by rinsing 3 times with distilled H_2O and subsequent incubation in 100 % EtOH for 2 hours rocking at RT. After that, coverslips were rinsed again with distilled and autoclaved H_2O and treated with 65 % nitric acid for 24 hours at RT to be finally rinsed again 4-6 times shaking at 5 °C. Cleaned coverslips were transferred into sterile 12-well-plates and let dry for 30 minutes at 37 °C.
For coating, 20 µl fibronectin in 980 µl PBS^- were applied per coverslip and left to dry at 37 °C for ~1 hour. Dried fibronectin crystals were washed off with PBS^-, 3 times and gently rocking at RT. Finally, 2 ml DFA buffer were added per well.
Embryos were checked at stage 14 for correct targeting of the NC lineage and transferred into 1xMBSH petri dishes to remove their vitelline membrane. Before dissection, specimens were put into DFA-filled 1xMBSH-agarose petri dishes. NCC explants were dissected at stage 17-18 with an eye-brow tools and fine forceps and transferred onto coated coverslips by using a BSA-coated pipette. All explants were finally incubated for ~21 hours at 17 °C. Fixation was achieved by adding 2 ml 8 % PFA per well overnight at ~5 °C.

5.9. Immunofluorescence staining (IF) and Phalloidin staining

Before specific staining, PFA was washed off with PBS^-. Whole mount embryos were removed from their vitelline membrane and cut, if needed. NCC explants remained within well-plates. All samples were washed 3 times in PBST and blocked in CAS-Block™ in PBST (1:10) overnight at ~5 °C. Specific Anti-c-myc monoclonal antibody produced in mouse was incubated in Cas-Block™ (1:1000) overnight or over the weekend at ~5 °C. Primary antibody was removed by several washing steps with PBS^-. Secondary Anti-mouse IgG1 (γ1) Alexa Fluor 555 produced in goat (1:1000) was incubated together with Alexa Fluor™ 488 Phalloidin (1:200) and Hoechst (1:10000) in Cas-Block™ for 2 hours at RT or overnight at ~5 °C.
For Phalloidin staining of whole mount embryos, PFA was washed off as well with PBS^-, followed by vitelline membrane removal and PBST wash 3 times for 15 minutes each. Finally, specimens were incubated in Alexa Fluor™ 555 Phalloidin in Cas-Block™ (1:100) overnight or over the weekend till eventual analysis.

5.10. Gene expression analysis via *in situ* hybridisation

The following method enables the expression analysis of specific genes. Therefore, digoxigenin-labelled RNA probes are utilised, which attaches to complementary mRNA sequences within the analysed tissues. Digoxigenin gets detected by respective antibody coupled with an enzyme that converts a substrate, like BM-Purple®, into blue staining thereby marking gene activity.
All used RNA probes, namely *cnn2, twist, foxd3* and *otx2*, were newly synthesised for this project from plasmids provided by the Department of Zoology. In the first step respective plasmids were linearised overnight at 37 °C.

Linearisation (100 µl total reaction)	
10 µg	plasmid DNA
10 µl	10x enzyme buffer
1 µl	100x BSA
3 µl	Restriction enzyme
X µl	H_2O (autoclaved)

Linearised DNA was purified by incubating in 10 µl 5 M NH_4 acetate and 220µl 100 % EtOH at -20 °C for 30 minutes. Upon centrifugation at 4°C for 20 minutes, DNA pellet was re-suspended in nuclease-free H_2O and stored at -20 °C. *In vitro* transcription was performed by using either T7 or SP6 RNA polymerase, depending on the sequence orientation within the plasmids. Incubation was done for 2 hours at 37 °C.

In vitro transcription	
2 µl	linearised plasmid
4 µl	5x transcription buffer
0.5 µl	RNase inhibitor
2 µl	Digoxigenine-dNTP-labeling mix
2 µl	DTT (100 mM)
2 µl	RNA polymerase
7.5 µl	RNase-free H_2O

To remove the template, 1µl TURBO DNase was added to each reaction for 15 minutes at 37 °C. Finally, RNA probes were purified by adding 30 µl RNase-free H_2O 5 µl 5 M NH_4 acetate and 165 µl 100 % EtOH for 30 minutes at -20 °C. After final centrifugation for 25 minutes at 4 °C, RNA pellet was washed with 500 µl 70 % EtOH and dissolved in 50 µl formamide in RNase-free H_2O (1:1) and stored at -80 °C.

Whole-mount *in situ* hybridization (WMISH) was performed based on the protocol designed by Harland et al., 2000. During the first day, all steps were performed under sterile conditions and on ice. Embryos were rehydrated stepwise and eventually washed with PBS^-. Small incisions were made in neurula stages to open embryonic body cavities for overall treatment. Several PBSw washing steps followed. After that, embryonic membranes were made more permeable by proteinase K (1 µl/ml in PBSw) treatment at RT for 15 minutes. Reaction was stopped by adding glycine (2 mg/ml in PBSw) and subsequent washing steps. Specimens were fixed again in 4 % PFA and 0.2 % glutaraldehyde in PBSw for 15 minutes. After additional PBSw washing steps, the embryos were transferred into hybridization buffer in PBSw (50:50) and finally incubated in pure buffer for 3 hours at 65 °C. Probes were applied overnight at 70 °C.

Probes were recycled and specimens washed in fresh hybridization buffer at 70 °C. Then the pH was gradually increased by washing steps in 2xSSC (pH 4.5) and 2xSSC (pH 7.0), all performed at 70 °C. Following this, samples were washed twice in MABw and blocked in MAB blocking solution for 1 hour at RT. Incubation in Anti-Digoxigenin-AP Fab Fragments in MAB blocking (1:10000) was done overnight rocking st ~5 °C.

Finally, the antibody solution was washed off with MABw and embryos were treated several times with AP1 buffer, before they were incubated in BM-Purpel staining solution at RT to enable colour reaction.

After staining intensity was sufficient, the reaction was stopped by final PBS^- wash and embryos were stored in 100 % EtOH at -20 °C until analysis

5.11. Histological vibratome sections

Embryos were equilibrated in Vib mix. In order to prepare a sample block, metal squares were used as mould. First, 1ml Vib mix was mixed with 80 µl glutaraldehyde and transferred into the mould to form a solid base. Specimens were placed on that based and oriented, before adding another milliliter of Vib mix plus glutaraldehyde. The cured blocks were trimmed and glued onto sample plate, which was placed into a PSB^- -filled chamber of the vibratome (Leica VT 1000). Histological sections measured 32µm and were mounted in Mowiol® on microscope slides.

5.12. Analysis and photo documentation

5.12.1. Examination of LT signals

Localisation of co-injected fluorescent LTs was verified utilising the fluorescence stereomicroscope Leica MZ FLII. Photo documentation (cf. **Fig. 19**) was done with AxioVision Release 4.5(12/2005) software by Zeiss.

5.12.2. Documentation IF and Phalloidin staining

Stained embryos were mounted either in low-melt agarose (cf. NP analyses) or specifically moulded modelling clay combined with Mowiol®. NCC explants were mounted in Mowiol® on microscope slides. All samples were analysed via laser scanning microscopy with the Zeiss LSM 700. Laser intensity and contrast were adjusted by ZEN 2011 program. Scale bares were directly applied by using the software.

5.12.3. Documentation WMISH

Stored embryos were rehydrated stepwise in PBS^- and transferred into PBS^- -agarose petri dishes and analysed under the stereomicroscope Zeiss SteREO Discovery V.12. Photo documentation was done by using the Zeiss AxioCam HRc“, controlled with AxioVision Rel. 4.6 software. Images were saved as TIF files

5.12.4. Documentation histological sections

Mounted sections were documented with the stereomicroscope Zeiss Axioskop 2 mot plus and saved as TIF files by using AxioVision Rel. 4.6 software.

5.12.5. Creation of figures

Recorded TIF files were cut and embryos were extracted with Adobe Photoshop CS6. Colouring of the embryos was not changed. Arrangement of photo panels, as well as labelling and addition of arrow heads was done in Adobe Illustrator CS6.

5.13. Measurements

Width of NPs and apical cell surface areas were measured in ImageJ (NIH). Corresponding values were saved in Microsoft Excel to calculate the required ratios.

5.14. Statistical analysis

Bar graphs were designed and phenotype distributions compared by using chi²-students test in Microsoft Excel.

Boxplots were created and statistically analysed via Wilcoxon paired test in Rstudio (PBC).

Levels of significance	p values, labelling
not significant	p>0,05, n.s.
significant	p<0,05, *
high significant	p<0,01, **
highly significant	p<0,001, ***

List of references

A. Represa, H. Trabelsi-Terzidis, M. Plantier, A. Fattoum, I. Jorquera, C. Agassandian, Y. B.-A. and E. der T. (1995). *Distribution of caldesmon and of the acidic isoform of calponin in cultured cerebellar neurons and in different regions of the rat brain: an immunofluorescence and confocal microscopy study*. *Experimenta* (Vol. 221). https://doi.org/https://doi.org/10.1006/excr.1995.1383

Alberts, B., Johnson, A., Lewis, J., Morgan, D., Raff, M., Roberts, K., & Walter, P. (2015). *Molecular Biology of The Cell, 6th Edition*. *Garland Science*.

Archer, T. C., Jin, J., & Casey, E. S. (2011). Interaction of Sox1, Sox2, Sox3 and Oct4 during primary neurogenesis. *Developmental Biology*, *350*(2), 429–440. https://doi.org/10.1016/j.ydbio.2010.12.013

Bang, A. G., Papalopulu, N., Goulding, M. D., & Kintner, C. (1999). Expression of Pax-3 in the lateral neural plate is dependent on a Wnt- mediated signal from posterior nonaxial mesoderm. *Developmental Biology*, *212*(2), 366–380. https://doi.org/10.1006/dbio.1999.9319

Bartegi, A., Roustan, C., Kassab, R., & Fattoum, A. (1999). Fluorescence studies of the carboxyl-terminal domain of smooth muscle calponin: Effects of F-actin and salts. *European Journal of Biochemistry*, *262*(2), 335–341. https://doi.org/10.1046/j.1432-1327.1999.00390.x

Basch, M. L., García-Castro, M. I., & Bronner-Fraser, M. (2004). Molecular mechanisms of neural crest induction. *Birth Defects Research Part C - Embryo Today: Reviews*, *72*(2), 109–123. https://doi.org/10.1002/bdrc.20015

Blitz, I. L., & Cho, K. W. Y. (1995). Anterior neurectoderm is progressively induced during gastrulation: The role of the Xenopus homeobox gene orthodenticle. *Development*, *121*(4), 993–1004. https://doi.org/10.1242/dev.121.4.993

Bouwmeester, T. (2001). The Spemann-Mangold organizer: The control of fate specification and morphogenetic rearrangements during gastrulation in Xenopus. *International Journal of Developmental Biology*, *45*(1), 251–258. https://doi.org/10.1387/ijdb.11291854

Brechner, E., Dinkelaker, B., & Dreesmann, D. (2001). *Kompaktlexikon der Biologie*. Spektrum Akademischer Verlag, Heidelberg. https://doi.org/https://www.spektrum.de/lexikon/biologie-kompakt/morphogenese/7781

Briscoe, J., & Ericson, J. (1999). The specification of neuronal identity by graded sonic hedgehog signalling. *Seminars in Cell and Developmental Biology*, *10*(3), 353–362. https://doi.org/10.1006/scdb.1999.0295

Burgstaller, G., Kranewitter, W. J., & Gimona, M. (2002). The molecular basis for the autoregulation of calponin by isoform-specific C-terminal tail sequences. *Journal of Cell Science*, *115*(10), 2021–2029. https://doi.org/10.1242/jcs.115.10.2021

Burridge, K., & Guilluy, C. (2016). Focal adhesions , stress fi bers and mechanical tension. *Experimental Cell Research*, *343*(1), 14–20. https://doi.org/10.1016/j.yexcr.2015.10.029

C. Agassandian, M. Plantier, A. Fattoum, A. R. and E. der T. (2000). Subcellular distribution of calponin and caldesmon in rat hippocampus. *Brain Research*, *887*(2), 444–449. https://doi.org/10.1016/S0006-8993(00)03030-4

Cha, B. J., & Gard, D. L. (1999). XMAP230 is required for the organization of cortical microtubules and patterning of the dorsoventral axis in fertilized Xenopus eggs. *Developmental Biology*, *205*(2), 275–286. https://doi.org/10.1006/dbio.1998.9123

Christodoulou, N., & Skourides, P. A. A. (2015). Cell-Autonomous Ca2+ Flashes Elicit Pulsed Contractions of an Apical Actin Network to Drive Apical Constriction during Neural Tube Closure. *Cell Reports*, *13*(10), 2189–2202. https://doi.org/10.1016/j.celrep.2015.11.017

Dady, A., Havis, E., Escriou, V., Catala, M., & Duband, J. L. (2014). Junctional Neurulation: A unique developmental program shaping a discrete region of the spinal cord highly susceptible to neural tube defects. *Journal of Neuroscience*, *34*(39), 13208–13221. https://doi.org/10.1523/JNEUROSCI.1850-14.2014

Danninger, C., & Gimona, M. (2000). Live dynamics of GFP-calponin: isoform-specific modulation of the actin cytoskeleton and autoregulation by C-terminal sequences. *Journal of Cell Science*, *113 Pt 21*, 3725–3736. Retrieved from http://www.ncbi.nlm.nih.gov/pubmed/11034901

Darken, R. S., Scola, A. M., & Rakeman, A. S. (2002). The planar polarity gene strabismus regulates convergent extension movements in Xenopus. *EMBO Journal*, *21*(5), 976–985. https://doi.org/10.1093/emboj/21.5.976

De Souza, F. S. J., & Niehrs, C. (2000). Anterior endoderm and head induction in early vertebrate embryos. *Cell and Tissue Research*, *300*(2), 207–217. https://doi.org/10.1007/s004410000204

Durston, A. J., Jansen, H. J., & Wacker, S. A. (2010). Review: Time-space translation regulates trunk axial patterning in the early vertebrate embryo. *Genomics*, *95*(5), 250–255. https://doi.org/10.1016/j.ygeno.2009.11.002

Eagleson, G. W., & Dempewolf, R. D. (2002). The role of the anterior neural ridge and Fgf-8 in early forebrain patterning and regionalization in Xenopus laevis. *Comparative Biochemistry and Physiology - B Biochemistry and Molecular Biology*, *132*(1), 179–189. https://doi.org/10.1016/S1096-4959(01)00521-8

Edlund, A. F., Davidson, L. A., & Keller, R. E. (2013). Cell segregation, mixing, and tissue pattern in the spinal cord of the xenopus laevis neurula. *Developmental Dynamics*, *242*(10), 1134–1146. https://doi.org/10.1002/dvdy.24004

El-Mezgueldi, M. (1996). Calponin. *International Journal of Biochemistry and Cell Biology*, *28*(11), 1185–1189. https://doi.org/10.1016/S1357-2725(96)00085-4

Elul, T., Koehl, M. A. R., & Keller, R. (1997). Cellular mechanism underlying neural convergent extension in Xenopus laevis embryos. *Developmental Biology*, *191*(2), 243–258. https://doi.org/10.1006/dbio.1997.8711

Ezin, A. M., Skoglund, P., & Keller, R. (2003). The midline (notochord and notoplate) patterns the cell motility underlying convergence and extension of the Xenopus neural plate. *Developmental Biology*, *256*(1), 101–114. https://doi.org/10.1016/S0012-

1606(02)00130-6

Ezin, A. M., Skoglund, P., & Keller, R. (2006). The presumptive floor plate (notoplate) induces behaviors associated with convergent extension in medial but not lateral neural plate cells of Xenopus. *Developmental Biology*, *300*(2), 670–686. https://doi.org/10.1016/j.ydbio.2006.09.004

Ferhat, Lofti, Esclapez, M., Represa, A., Fattoum, A., Shirao, T., & Ben-Ari, Y. (2003). Increased levels of acidic calponin during dendritic spine plasticity after pilocarpine-induced seizures. *Hippocampus*, *13*(7), 845–858. https://doi.org/10.1002/hipo.10136

Ferhat, Lotfi, Charton, G., Represa, A., Ben-Ari, Y., Der Terrossian, E., & Khrestchatisky, M. (1996). Acidic calponin cloned from neural cells is differentially expressed during rat brain development. *European Journal of Neuroscience*, *8*(7), 1501–1509. https://doi.org/10.1111/j.1460-9568.1996.tb01612.x

Flemming, A., Huang, Q.-Q., Jin, J.-P., Jumaa, H., & Herzog, S. (2015). A Conditional Knockout Mouse Model Reveals That Calponin-3 Is Dispensable for Early B Cell Development. *Plos One*, *10*(6), e0128385. https://doi.org/10.1371/journal.pone.0128385

Fujii, T., Hiromori, T., Hamamoto, M., & Suzuki, T. (1997). Interaction of Chicken Gizzard Smooth Muscle Calponin with Brain Microtubules. *Journal of Biochemistry*, *351*(2), 344–351. https://doi.org/10.1093/oxfordjournals.jbchem.a021759

Fukui, Y., Masuda, H., Takagi, M., Takahashi, K., & Kiyokane, K. (1996). The presence of h2-calponin in human keratinocyte. *Journal of Dermatological Science*, *14*(1), 29–36. https://doi.org/10.1016/S0923-1811(96)00545-2

Fürst, S. (2016). Die Rolle des Aktin-Bindeproteins Calponin3 (Cnn3) während der Neurogenese im afrikanischen Krallenfrosch Xenopus laevis. *Masterthesis Im Studiengang Biologie Master of Science*.

Gammill, L. S., & Bronner-Fraser, M. (2003). Neural crest specification: Migrating into genomics. *Nature Reviews Neuroscience*, *4*(10), 795–805. https://doi.org/10.1038/nrn1219

Ghislain, J., Desmarquet-Trin-Dinh, C., Gilardi-Hebenstreit, P., Charnay, P., & Frain, M. (2003). Neural crest patterning: Autoregulatory and crest-specific elements co-operate for Krox20 transcriptional control. *Development*, *130*(5), 941–953. https://doi.org/10.1242/dev.00318

Gilbert, S. F. (2014). Developmental Biology. Andrew D. Sinauer (10th edition).

Gilbert, S. F., & Barresi, M. J. F. (2016). *Developmental biology* (11th edition). Sinauer Associates. https://doi.org/lccn-loc.gov/2016012601

Gimona, M., Kaverina, I., Resch, G. P., Vignal, E., & Burgstaller, G. (2003). Calponin repeats regulate actin filament stbility and formation of podosomes in smooth muscle cells. *Molecular Biology of the Cell*, *14*(February), 2372–2384. https://doi.org/10.1091/mbc.E02

Gimona, M., & Mital, R. (1998). The single CH domain of calponin is neither sufficient nor necessary for F-actin binding. *Journal of Cell Science*, *111*(13), 1813–1821.

https://doi.org/10.1242/jcs.111.13.1813

Goodson, H. V, & Jonasson, E. M. (2018). Microtubules and Microtubule-Associated Proteins. *Cold Spring Harb Perspectives Biology*, *10*(1). https://doi.org/10.1101/cshperspect.a022608

Goto, T., & Keller, R. (2002). The planar cell polarity gene Strabismus regulates convergence and extension and neural fold closure in Xenopus. *Developmental Biology*, *247*(1), 165–181. https://doi.org/10.1006/dbio.2002.0673

Gradl, D. (2019). *Xenopus laevis (Südafrikanischer Krallenfrosch)*. Springer-Verlag GmbH Deutschland. https://doi.org/10.1007/978-3-662-54868-4

Greene, N. D. E., & Copp, A. J. (2014). Neural tube defects. *Annual Review of Neuroscience*, *37*, 221–242. https://doi.org/10.1146/annurev-neuro-062012-170354

Hagenlocher, C. (2010). Differenzielle Rolle der Aktinbindeproteine Calponi -2 und -3 auf die konvergente Extension von Neuroektoderm und Mesoderm während der Embryonalentwicklung von Xenopus laevis. *Diplomarbeit Im Studiengang Biologie*

Haigo, S. L., Hildebrand, J. D., Harland, R. M., & Wallingford, J. B. (2003). Shroom Induces Apical Constriction and Is Required for Hingepoint Formation during Neural Tube Closure. *Current Biology*, *13*(24), 2125–2137. https://doi.org/10.1016/j.cub.2003.11.054

Hall, B. K. (2000). The neural crest as a fourth germ layer and vertebrates as quadroblastic not triploblastic. *Evolution and Development*, *2*(1), 3–5. https://doi.org/10.1046/j.1525-142X.2000.00032.x

Harada, H., Sato, T., & Nakamura, H. (2016). Fgf8 signaling for development of the midbrain and hindbrain. *Development Growth and Differentiation*, *58*(5), 437–445. https://doi.org/10.1111/dgd.12293

Harland, R. M. (1994). Neural induction in Xenopus. *Current Opinion in Genetics and Development*, *4*(4), 543–549. https://doi.org/10.1016/0959-437X(94)90070-J

Harland, R., Sive, H., & Grainger, R. (2000). Early Development of Xenopus Laevis: A Laboratory Manual (pp. 249–297). New York: Cold Spring Harbor Laboratory Press.

Harrington, M. J., Hong, E., & Brewster, R. (2009). Comparative analysis of neurulation: First impressions do not count. *Molecular Reproduction and Development*, *76*(10), 954–965. https://doi.org/10.1002/mrd.21085

Hildebrand, J. D. (2005). Shroom regulates epithelial cell shape via the apical positioning of an actomyosin network. *Journal of Cell Science*, *118*(22), 5191–5203. https://doi.org/10.1242/jcs.02626

Hossain, M. M., Crish, J. F., Eckert, R. L., Lin, J. J. C., & Jin, J. P. (2005). H2-Calponin Is Regulated By Mechanical Tension and Modifies the Function of Actin Cytoskeleton. *Journal of Biological Chemistry*, *280*(51), 42442–42453. https://doi.org/10.1074/jbc.M509952200

Hossain, M. M., Hwang, D. Y., Huang, Q. Q., Sasaki, Y., & Jin, J. P. (2003). Developmentally regulated expression of calponin isoforms and the effect of h2-

calponin on cell proliferation. *American Journal of Physiology - Cell Physiology*, *284*(153-1), 156–167. https://doi.org/10.1152/ajpcell.00233.2002

Hossain, M. M., Smith, P. G., Wu, K., & Jin, J. P. (2006). Cytoskeletal tension regulates both expression and degradation of h2-calponin in lung alveolar cells. *Biochemistry*, *45*(51), 15670–15683. https://doi.org/10.1021/bi061718f

Hossain, M. M., Wang, X., Bergan, R. C., & Jin, J. P. (2014). Diminished expression of h2-calponin in prostate cancer cells promotes cell proliferation, migration and the dependence of cell adhesion on substrate stiffness. *FEBS Open Bio*, *4*, 627–636. https://doi.org/10.1016/j.fob.2014.06.003

Housden, B. E., Muhar, M., Gemberling, M., Gersbach, C. A., Stainier, D. Y. R., Seydoux, G., … Perrimon, N. (2017). Loss-of-function genetic tools for animal models: cross-species and cross-platform differences. *Nature Reviews. Genetics*, *18*(1), 24–40. https://doi.org/10.1038/nrg.2016.118.Loss-of-function

Huang, Q. Q., Hossain, M. M., Wu, K., Parai, K., Pope, R. M., & Jin, J. P. (2008). Role of H2-calponin in regulating macrophage motility and phagocytosis. *Journal of Biological Chemistry*, *283*(38), 25887–25899. https://doi.org/10.1074/jbc.M801163200

Hussein, S. M., Duff, E. K., & Sirard, C. (2003). Smad4 and β-catenin co-activators functionally interact with lymphoid-enhancing factor to regulate graded expression of Msx2. *Journal of Biological Chemistry*, *278*(49), 48805–48814. https://doi.org/10.1074/jbc.M305472200

Ibrahim, H., & Winklbauer, R. (2001). Mechanisms of mesendoderm internalization in the Xenopus gastrula: lessons from the ventral side. *Developmental Biology*, *240*(1), 108–122. https://doi.org/10.1006/dbio.2001.0459

Iemura, S. I., Yamamoto, T. S., Takagi, C., Uchiyama, H., Natsume, T., Shimasaki, S., … Ueno, N. (1998). Direct binding of follistatin to a complex of bone-morphogenetic protein and its receptor inhibits ventral and epidermal cell fates in early Xenopus embryo. *Proceedings of the National Academy of Sciences of the United States of America*, *95*(16), 9337–9342. https://doi.org/10.1073/pnas.95.16.9337

Janesick, A., Nguyen, T. T. L., Aisaki, K., Igarashi, Katsuhide Kitajima, Satoshi Chandraratna, R. A. S., Kanno, J., & Blumberg, B. (2014). Active repression by RARγ signaling is required for vertebrate axial elongation. *Development*, *141*(11), 2260–2270. Retrieved from https://doi.org/10.1242/dev.103705%0A

Ji, T., Ma, F., Huo, L., Guo, X., Chen, B., & Zhou, Q. (2015). Calponin-h2 is upregulated in the tissues and plasma of patients with breast cancer. *Molecular Medicine Reports*, *12*(2), 2886–2892. https://doi.org/10.3892/mmr.2015.3782

Junghans, D., & Herzog, S. (2018). Cnn3 regulates neural tube morphogenesis and neuronal stem cell properties. *FEBS Journal*, *285*(2), 325–338. https://doi.org/10.1111/febs.14338

Kaneko, T., Amano, M., Maeda, A., Goto, H., Takahashi, K., Ito, M., & Kaibuchi, K. (2000). Identification of calponin as a novel substrate of Rho-kinase. *Biochemical and Biophysical Research Communications*, *273*(1), 110–116. https://doi.org/10.1006/bbrc.2000.2901

Keller, R. E. (1981). An experimental analysis of the role of bottle cells and the deep marginal zone in gastrulation of Xenopus laevis. *Journal of Experimental Zoology*, *216*(1), 81–101. https://doi.org/10.1002/jez.1402160109

Keller, R., Shih, J., & Sater, A. (1992). The cellular basis of the convergence and extension of the Xenopus neural plate. *Developmental Dynamics*, *193*(3), 199–217. https://doi.org/10.1002/aja.1001930302

Keller, R., Shook, D., & Skoglund, P. (2008). The forces that shape embryos: physical aspects of convergent extension by cell intercalation. *Physical Biology*, *5*(1), 015007. https://doi.org/10.1088/1478-3975/5/1/015007

Keller, R., & Sutherland, A. (2020). *Convergent Extension in the Amphibian, Xenopus laevis. Curr Top Dev Biol.* (Vol. 136). 2020 Elsevier Inc. All rights reserved. https://doi.org/10.1016/bs.ctdb.2019.11.013.

Keller, Raymond E. (1975). Vital dye mapping of the gastrula and neurula of Xenopus laevis. I. Prospective areas and morphogenetic movements of the superficial layer. *Developmental Biology*, *42*(1), 222–241. https://doi.org/10.1016/0012-1606(76)90127-5

Keller, Raymond E. (1976). Vital dye mapping of the gastrula and neurula of Xenopus laevis. II. Prospective areas and morphogenetic movements of the deep layer. *Developmental Biology*, *51*(1), 118–137. https://doi.org/10.1016/0012-1606(76)90127-5

Keller, Raymond E., & Schoenwolf, G. C. (1977). An SEM study of cellular morphology, contact, and arrangement, as related to gastrulation in Xenopus laevis. *Wilhelm Roux's Archives of Developmental Biology*, *182*(2), 165–186. https://doi.org/10.1007/BF00848055

Kimura-Yoshida, C., Mochida, K., Ellwanger, K., Niehrs, C., & Matsuo, I. (2015). Fate Specification of Neural Plate Border by Canonical Wnt Signaling and Grhl3 is Crucial for Neural Tube Closure. *EBioMedicine*, *2*(6), 513–527. https://doi.org/10.1016/j.ebiom.2015.04.012

Kloc, M., & Kubiak, J. Z. (2014). *Xenopus Development*. *Xenopus Development* (Vol. 9781118492). https://doi.org/10.1002/9781118492833

Kolakowski, J., Makuch, R., Stepkowski, D., & Dabrowska, R. (1995). Interaction of calponin with actin and its functional implications. *Biochemical Journal*, *306*(1), 199–204. https://doi.org/10.1042/bj3060199

Lecuit, T., Lenne, P. F., & Munro, E. (2011). Force generation, transmission, and integration during cell and tissue morphogenesis. *Annual Review of Cell and Developmental Biology*, *27*, 157–184. https://doi.org/10.1146/annurev-cellbio-100109-104027

Lee, C., Scherr, H. M., & Wallingford, J. B. (2007). Shroom family proteins regulate γ-tubulin distribution and microtubule architecture during epithelial cell shape change. *Development*, *134*(7), 1431–1441. https://doi.org/10.1242/dev.02828

Lee, J. Y., & Harland, R. M. (2007). Actomyosin contractility and microtubules drive apical constriction in Xenopus bottle cells. *Developmental Biology*, *311*(1), 40–52. https://doi.org/10.1016/j.ydbio.2007.08.010

Lindqvist, M., Horn, Z., Bryja, V., Schulte, G., Papachristou, P., Ajima, R., … Ringstedt, T. (2010). Vang-like protein 2 and Rac1 interact to regulate adherens junctions. *Journal of Cell Science*, *123*(3), 472–483. https://doi.org/10.1242/jcs.048074

Liu, R., & Jin, J. P. (2016). Calponin isoforms CNN1, CNN2 and CNN3: Regulators for actin cytoskeleton functions in smooth muscle and non-muscle cells. *Gene*, *585*(1), 143–153. https://doi.org/10.1016/j.gene.2016.02.040

Lobikin, M., Wang, G., Xu, J., Hsieh, Y. W., Chuang, C. F., Lemire, J. M., & Levin, M. (2012). Early, nonciliary role for microtubule proteins in left-right patterning is conserved across kingdoms. *Proceedings of the National Academy of Sciences of the United States of America*, *109*(31), 12586–12591. https://doi.org/10.1073/pnas.1202659109

Loges, N. (2008). Die Funktion von Calponin-2 und -3 während der Embryonalentwicklung von Xenopus laevis: eine Funktionsverluststudie. *Diplomarbeit Im Studiengang Biologie Diplom*.

Lowery, L. A., & Sive, H. (2004). Strategies of vertebrate neurulation and a re-evaluation of teleost neural tube formation. *Mechanisms of Development*, *121*(10), 1189–1197. https://doi.org/10.1016/j.mod.2004.04.022

Maller, J. L., Gross, S. D., Schwab, M. S., Finkielstein, C. V., Taieb, F. E., & Qian, Y. W. (2001). Cell cycle transitions in early Xenopus development. *Novartis Foundation Symposium*, *237*, 58–78. https://doi.org/10.1002/0470846666.ch6

Martin, A. C., & Goldstein, B. (2014). Apical constriction: themes and variations on a cellular mechanism driving morphogenesis. *Development (Cambridge, England)*, *141*(10), 1987–1998. https://doi.org/10.1242/dev.102228

Martinez-Ferre, A., & Martinez, S. (2012). Molecular regionalization of the diencephalon. *Frontiers in Neuroscience*, *6*(MAY), 1–10. https://doi.org/10.3389/fnins.2012.00073

Mason, F. M., & Martin, A. C. (2011). Tuning cell shape change with contractile ratchets. *Current Opinion in Genetics and Development*, *21*(5), 671–679. https://doi.org/10.1016/j.gde.2011.08.002

Masuda, H., Tanaka, K., Takagi, M., Ohgami, K., Sakamaki, T., Shibata, N., & Takahashi, K. (1996). Molecular Cloning and Characterization of Human Non-Smooth Muscle Calponin. *Journal of Biological Chemistry*, *120*, 415–424. https://doi.org/10.1093/oxfordjournals.jbchem.a021428

Mayor, R., & Etienne-Manneville, S. (2016). The front and rear of collective cell migration. *Nature Reviews Molecular Cell Biology*, *17*(2), 97–109. https://doi.org/10.1038/nrm.2015.14

Mayor, R., & Theveneau, E. (2014). The role of the non-canonical Wnt-planar cell polarity pathway in neural crest migration. *The Biochemical Journal*, *457*(1), 19–26. https://doi.org/10.1042/BJ20131182

Miano, J. M., & Olson, E. N. (1996). Expression of the smooth muscle cell calponin gene marks the early cardiac and smooth muscle cell lineages during mouse embryogenesis. *Journal of Biological Chemistry*, *271*(12), 7095–7103. https://doi.org/10.1074/jbc.271.12.7095

Milet, C., Maczkowiak, F., Roche, D. D., & Monsoro-Burq, A. H. (2013). Pax3 and Zic1 drive induction and differentiation of multipotent , migratory , and functional neural crest in Xenopus embryos. *PNAS*, *110*(14), 5528–5533. https://doi.org/10.1073/pnas.1219124110

Morgan, R., Hooiveld, M. H. W., Pannese, M., Dati, G., Broders, F., Thiery, J., … Durston, A. J. (1999). Calponin modulates the exclusion of Otx -expressing cells from convergence extension movements. *Nature Cell Biology*, *1*(7), 404–408. https://doi.org/10.1038/15635

Muncie, J. M., Ayad, N. M. E., Lakins, J. N., Xue, X., Fu, J., Weaver, V. M., … Fu, J. (2020). Article Mechanical Tension Promotes Formation of Gastrulation-like Nodes and Patterns Mesoderm Specification in Human Embryonic Stem Cells Article Mechanical Tension Promotes Formation of Gastrulation-like Nodes and Patterns Mesoderm Specification in Huma. *Developmental Cell*, 1–16. https://doi.org/10.1016/j.devcel.2020.10.015

Naka, M., Kureishi, Y., Muroga, Y., Takahashi, K., Ito, M., & Tanaka, T. (1990). Modulation of smooth muscle calponin by protein kinase C and calmodulin. *BIOCHEMICAL AND BIOPHYSICAL RESEARCH COMMUNICATIONS*, *171*(3), 933–937. https://doi.org/10.1016/0006-291x(90)90773-g

Nakayama, T., Blitz, I. L., Fish, M. B., Odeleye, Akinleye O. Manohar, S., Cho, K. W. Y., & Grainger, R. M. (2014). Chapter Seventeen - Cas9-Based Genome Editing in Xenopus tropicalis. *Methods in Enzymology*, *546*, 355–375. https://doi.org/https://doi.org/10.doi:10.1016/B978-0-12-801185-0.00017-9

Nikolopoulou, E., Galea, G. L., Rolo, A., Greene, N. D. E., & Copp, A. J. (2017). Neural tube closure: Cellular, molecular and biomechanical mechanisms. *Development (Cambridge)*, *144*(4), 552–566. https://doi.org/10.1242/dev.145904

Nishimura, T., Honda, H., & Takeichi, M. (2012). Planar cell polarity links axes of spatial dynamics in neural-tube closure. *Cell*, *149*(5), 1084–1097. https://doi.org/10.1016/j.cell.2012.04.021

Nishimura, T., & Takeichi, M. (2008). Shroom3-mediated recruitment of Rho kinases to the apical cell junctions regulates epithelial and neuroepithelial planar remodeling. *Development*, *135*(8), 1493–1502. https://doi.org/10.1242/dev.019646

Ossipova, O., Kim, K., Lake, B. B., Itoh, K., Ioannou, A., & Sokol, S. Y. (2014). Role of Rab11 in planar cell polarity and apical constriction during vertebrate neural tube closure. *Nature Communications*, *5*(3734). https://doi.org/10.1038/ncomms4734

Ossipova, O., Kim, K., & Soko, S. Y. (2015). Planar polarization of vangl2 in the vertebrate neural plate is controlled by wnt and myosin II signaling. *Biology Open*, *4*(6), 722–730. https://doi.org/10.1242/bio.201511676

Pannese, M., Polo, C., Andreazzoli, M., Vignali, R., Kablar, B., Barsacchi, G., & Boncinelli, E. (1995). The Xenopus homologue of Otx2 is a maternal homeobox gene that demarcates and specifies anterior body regions. *Development*, *121*(3), 707–720. https://doi.org/10.1242/dev.121.3.707

Piccolo, S., Sasai, Y., Lu, B., & De Robertis, E. M. (1996). Dorsoventral Patterning in Xenopus: Inhibition of Ventral Signals by Direct Binding of Chordin to BMP-4. *Cell*,

86(4), 589–598. https://doi.org/10.1016/s0092-8674(00)80132-4

Pla, P., & Monsoro-burq, A. H. (2018). The neural border : Induction , speci fi cation and maturation of the territory that generates neural crest cells. *Developmental Biology*, *444*(May), S36–S46. https://doi.org/10.1016/j.ydbio.2018.05.018

Prager, A., Hagenlocher, C., Ott, T., Schambony, A., & Feistel, K. (2017). hmmr mediates anterior neural tube closure and morphogenesis in the frog Xenopus. *Developmental Biology*, *430*(1), 188–201. https://doi.org/10.1016/j.ydbio.2017.07.020

Quinlan, R. A., Schwarz, N., Windoffer, R., Richardson, C., Hawkins, T., Broussard, J. A., Leube, R. E. (2017). A rim-and-spoke hypothesis to explain the biomechanical roles for cytoplasmic intermediate filament networks. *Journal of Cell Science*, *130*(20), 3437–3445. https://doi.org/10.1242/jcs.202168

Rozenblum, G. T., & Gimona, M. (2008). Calponins: Adaptable modular regulators of the actin cytoskeleton. *International Journal of Biochemistry and Cell Biology*, *40*(10), 1990–1995. https://doi.org/10.1016/j.biocel.2007.07.010

Ryan, A. K., Blumberg, B., Rodriguez-Esteban, C., Yonei-Tamura, S., Tamura, K., Tsukui, T., … Belmonte, J. C. I. (1998). Pitx2 determines left-right asymmetry of internal organs in vertebrates. *Nature*, *394*(6693), 545–551. https://doi.org/10.1038/29004

Sadaghiani, B., & Thiébaud, C. H. (1987). Neural crest development in the Xenopus laevis embryo, studied by interspecific transplantation and scanning electron microscopy. *Developmental Biology*, *124*(1), 91–110. https://doi.org/10.1016/0012-1606(87)90463-5

Saka, Y., & Smith, J. C. (2001). Spatial and temporal patterns of cell division during early Xenopus embryogenesis. *Developmental Biology*, *229*(2), 307–318. https://doi.org/10.1006/dbio.2000.0101

Salbreux, G., Charras, G., & Paluch, E. (2012). Actin cortex mechanics and cellular morphogenesis. *Trends in Cell Biology*, *22*(10), 536–545. https://doi.org/10.1016/j.tcb.2012.07.001

Samaha, F. F., Ip, H. S., Morrisey, E. E., Seltzer, J., Tang, Z., Solway, J., & Parmacek, M. S. (1996). Developmental pattern of expression and genomic organization of the calponin-h1 gene: A contractile smooth muscle cell marker. *Journal of Biological Chemistry*, *271*(1), 395–403. https://doi.org/10.1074/jbc.271.1.395

Sauka-Spengler, T., & Bronner-Fraser, M. (2008). A gene regulatory network orchestrates neural crest formation. *Nature Reviews Molecular Cell Biology*, *9*(7), 557–568. https://doi.org/10.1038/nrm2428

Sawyer, J. M., Harrell, J. R., Shemer, G., & Sullivan-Brown, Jessica Roh-Johnson, Minna Goldstein, B. (2010). Apical Constriction: A Cell Shape Change that Can Drive Morphogenesis Jacob. *Development Biology*, *341*(1), 5–19. https://doi.org/doi:10.1016/j.ydbio.2009.09.009.

Schmalholz, S. (2008). Deskriptive und funktionelle Analyse der Mitglieder der Calponin-Genfamilie Xclp1, Xclp2 und Xclp3 während der Embryonalentwicklung von Xenopus laevis. *Dissertation Zur Erlangung Des Doktorgrades Der Naturwissenschaften (Dr. Rer. Nat.)*.

Schneider, S., Steinbeisser, H., Warga, R. M., & Hausen, P. (1996). B-Catenin Translocation Into Nuclei Demarcates the Dorsalizing Centers in Frog and Fish Embryos. *Mechanisms of Development*, *57*(2), 191–198. https://doi.org/10.1016/0925-4773(96)00546-1

Schroeder, T. (1970). Neurulation in Xenopus laevis. An analysis and model based upon light and electron microscopy. *J Embryol Exp Morphol.*, *23*(2), 427–462.

Schroeder, T. E. (1971). Mechanisms of morphogenesis: The embryonic neural tube. *International Journal of Neuroscience*, *2*(4–5), 183–197. https://doi.org/10.3109/00207457109147001

Schweickert, A., Weber, T., Beyer, T., Vick, P., Bogusch, S., Feistel, K., & Blum, M. (2007). Cilia-Driven Leftward Flow Determines Laterality in Xenopus. *Current Biology*, *17*(1), 60–66. https://doi.org/10.1016/j.cub.2006.10.067

Sena, E., Feistel, K., & Durand, B. C. (2016). An evolutionarily conserved network mediates development of the zona limitans intrathalamica, a Sonic Hedgehog-secreting caudal forebrain signaling center. *Journal of Developmental Biology*, *4*(4). https://doi.org/10.3390/jdb4040031

Session, A. M., Uno, Y., Kwon, T., Chapman, J. A., Toyoda, A., Takahashi, S., … Veenstra, G. J. C. (2016). Genome evolution in the allotetraploid frog Xenopus laevis. *Nature*, *538*(7625), 1–15. https://doi.org/10.1038/nature19840

Shibukawa, Y., Yamazaki, N., Daimon, E., & Wada, Y. (2013). Rock-dependent calponin 3 phosphorylation regulates myoblast fusion. *Experimental Cell Research*, *319*(5), 633–648. https://doi.org/10.1016/j.yexcr.2012.12.022

Shibukawa, Y., Yamazaki, N., Kumasawa, K., Daimon, E., Tajiri, M., Okada, Y., … Wada, Y. (2010). Calponin 3 regulates actin cytoskeleton rearrangement in trophoblastic cell fusion. *Molecular Biology of the Cell*, *21*(22), 3973–3984. https://doi.org/10.1091/mbc.E10-03-0261

Shih, J., & Keller, R. (1992). Cell motility driving mediolateral intercalation in explants of Xenopus laevis. *Development*, *116*(4), 901–914.

Small, J. V., & Resch, G. P. (2005). The comings and goings of actin: Coupling protrusion and retraction in cell motility. *Current Opinion in Cell Biology*, *17*(5 SPEC. ISS.), 517–523. https://doi.org/10.1016/j.ceb.2005.08.004

Sokol, S. Y. (2016). *Mechanotransduction During Vertebrate Neurulation*. *Current Topics in Developmental Biology* (1st ed., Vol. 117). Elsevier Inc. https://doi.org/10.1016/bs.ctdb.2015.11.036

Steventon, B., Carmona-Fontaine, C., & Mayor, R. (2005). Genetic network during neural crest induction: From cell specification to cell survival. *Seminars in Cell and Developmental Biology*, *16*(6), 647–654. https://doi.org/10.1016/j.semcdb.2005.06.001

Suzuki, A., Ueno, N., & Hemmati-brivanlou, A. (1997). Xenopus msx1 mediates epidermal induction and neural inhibition by BMP4 Xenopus msx1 mediates epidermal induction and neural inhibition by BMP4. *Development*, *124*, 3037–3044.

https://doi.org/10.1242/dev.124.16.3037

Szymanski, P. T. (2004). Calponin (CaP) as a latch-bridge protein - A new concept in regulation of contractility in smooth muscles. *Journal of Muscle Research and Cell Motility*, *25*(1), 7–19. https://doi.org/10.1023/B:JURE.0000021349.47697.bf

Takahashi, K., Hiwada, K., & Kokubu, T. (1986). Isolation and characterization of a 34,000-dalton calmodulin- and F-actin-binding protein from chicken gizzard smooth muscle, *141*(1), 20–26.

Tang, J., Hu, G., Hanai, J. I., Yadlapalli, G., Lin, Y., Zhang, B., … Sukhatme, V. P. (2006). A critical role for calponin 2 in vascular development. *Journal of Biological Chemistry*, *281*(10), 6664–6672. https://doi.org/10.1074/jbc.M506991200

Tao, Q., Yokota, C., Puck, H., Kofron, M., Birsoy, B., Yan, D., … Heasman, J. (2005). Maternal Wnt11 activates the canonical Wnt signaling pathway required for axis formation in Xenopus embryos. *Cell*, *120*(6), 857–871. https://doi.org/10.1016/j.cell.2005.01.013

Theveneau, E., & Mayor, R. (2010). Collective cell migration of the cephalic neural crest: The art of integrating information. *Genesis*, *49*(4), 164–176. https://doi.org/10.1002/dvg.20700

Theveneau, E., & Mayor, R. (2012). Neural crest delamination and migration: From epithelium-to-mesenchyme transition to collective cell migration. *Developmental Biology*, *366*(1), 34–54. https://doi.org/10.1016/j.ydbio.2011.12.041

Trainor, P. A. (2014). *Neural Crest Cells Evolution, Development, Disease*. (P. A. Trainor, Ed.), *Academic Press*. Elsevier Inc.

Tsunekawa, S., Takahashi, K., Abe, M., Hiwada, K., Ozawa, K., & Murachi, T. (1989). Calpain proteolysis of free and bound forms of calponin, a troponin T-like protein in smooth muscle. *FEBS Letters*, *250*(2), 493–496. https://doi.org/10.1016/0014-5793(89)80783-5

Ulmer, B., Hagenlocher, C., Schmalholz, S., Kurz, S., Schweickert, A., Kohl, A., … Blum, M. (2013). Calponin 2 Acts As an Effector of Noncanonical Wnt-Mediated Cell Polarization during Neural Crest Cell Migration. *Cell Reports*, *3*(3), 615–621. https://doi.org/10.1016/j.celrep.2013.02.015

Ulmer, B. M. (2012). Goosecoid und Calponin : Zwei neue Regulatoren des PCP-Signalwegs. *Dissertation Zur Erlangung Des Doktorgrades Der Naturwissenschaften (Dr. Rer. Nat.)*.

Valles, J. M., Wasserman, S. R. R. M., Schweidenback, C., Edwardson, J., Denegre, J. M., & Mowry, K. L. (2002). Processes that occur before second cleavage determine third cleavage orientation in Xenopus. *Experimental Cell Research*, *274*(1), 112–118. https://doi.org/10.1006/excr.2001.5456

Wallingford, J. B. (2012). Planar Cell Polarity and the Developmental Control of Cell Behavior in Vertebrate Embryos. *Annual Review of Cell and Developmental Biology*, *28*(1), 627–653. https://doi.org/10.1146/annurev-cellbio-092910-154208

Wallingford, J. B., & Harland, R. M. (2002). Neural tube closure requires Dishevelled-

dependent convergent extension of the midline. *Development*, *129*(24), 5815–5825. https://doi.org/10.1242/dev.00123

Wallingford, J., Niswander, L., Shaw, G., & Finnell, R. (2013). The continuing challenge of understanding and preventing neural tube defects. *Science*, *339*(6123), 1–14. https://doi.org/10.1126/science.1222002.The

Weaver, C., & Kimelman, D. (2004). Move it or lose it: Axis specification in Xenopus. *Development*, *131*(15), 3491–3499. https://doi.org/10.1242/dev.01284

Wilson, S. I., & Edlund, T. (2001). Neural induction: Toward a unifying mechanism. *Nature Neuroscience*, *4*(11s), 1161–1168. https://doi.org/10.1038/nn747

Winder, S. J., & Walsh, M. P. (1990). Smooth muscle calponin. Inhibition of actomysosin MgATPase and regulation by phosphorylation. *Journal of Biological Chemistry*, *265*(17), 10148–10155. https://doi.org/10.1016/s0021-9258(19)38792-7

Winder, Steven J, & Ayscough, K. R. (2005). Actin-binding proteins. *Journal of Cell Science*, *118*, 651–654. https://doi.org/10.1242/jcs.01670

Winder, Steven J, & Walsh, M. P. (1993). CALPONIN: THIN FILAMENT-LINKED REGULATION OF SMOOTH MUSCLE CONTRACTION. *Cellular Signalling*, *5*(6).

Winklbauer, R., & Damm, E. W. (2012). Internalizing the vegetal cell mass before and during amphibian gastrulation: Vegetal rotation and related movements. *Wiley Interdisciplinary Reviews: Developmental Biology*, *1*(2), 301–306. https://doi.org/10.1002/wdev.26

Yang, J., Tan, C., Darken, R. S., Wilson, P. A., & Klein, P. S. (2002). β-catenin/Tcf-regulated transcription prior to the midblastula transition. *Development*, *129*(24), 5743–5752. https://doi.org/10.1242/dev.00150

Yang, Y., & Mlodzik, M. (2015). Wnt-Frizzled/Planar Cell Polarity Signaling: Cellular Orientation by Facing the Wind (Wnt). *Annual Review of Cell and Developmental Biology*, *31*, 623–646. https://doi.org/10.1146/annurev-cellbio-100814-125315

Acknowledgements

I would like to dedicate this work to my husband Timm Mantino, who supported me over the last years and helped me in every possible way to keep on going!

First of all, I would like to thank Prof. Dr. Martin Blum for giving me the opportunity to complete my studies with a PhD thesis.
I also thank PD. Dr. Kerstin Feistel and Prof. Dr. Dalit Sela-Donenfeld for their supervision and for stimulating thesis advisory committee meetings.
A big thank goes to Dr. Tim Ott, who taught me how to clone deletion constructs and successfully use CRSPR/Cas. In addition to that, I would like to thank Elly Schuster for her precious help in the lab and Fee Wielath as well as Valentina Trivigno, who donated their time for proofreading of my thesis.
And I thank Dr. Silke Schmalholz and all lab technicians as well as the animal keepers for their work and friendly collegiality at the Department of Zoology.

I am very grateful and thank the “Studienstiftung des deutschen Volkes“ for their incredible funding and great support during my entire studies. Without my fellowships, I wouldn´t have been able to study or to complete my PhD.

Last but not least I would like to thank my loving family as well as my dear friends, for always cheering me up and believing in my talents.
And I thank Don, the greatest office buddy I have ever had.

CURRICULUM VITAE

Personal Profile

Name Sabrina Mantino

Address

Phone

E-Mail

Education

02/2017 – today **PhD student - Biology**

Institute of Zoology, University of Hohenheim
Project title: „The role of the actin binding protein Calponin2 during embryonic development of Xenopus laevis"
Thesis submission: 07/2021
Discipline: Molecular embryology
Model organism: African clawed frog, mouse

10/2014 – 01/2017 **Master of Science - Biology**

University of Hohenheim
Total grade: 1.1
Title master thesis: „Funktionelle Analyse von Gastrulations-Defekten nach Dynein-Knockdown in *Xenopus laevis*"
Discipline: Molecular embryology
Model organism: African clawed frog

10/2011 – 09/2014 **Bachelor of Science - Biology**

University of Hohenheim
Total grade: 1.7
Title bachelor thesis: „Symmetriebruch in *Paracentrotus lividus*: Klonierung und Analyse der Markergene Nodal und Bicaudal-C"
Discipline: Molecular embryology
Model organism: Sea urchin

10/2009 – 09/2011 **Bachelor of Science - „Verfahrens- und Umwelttechnik"**

Hochschule Heilbronn
Terminated after passed intermediate examination

09/2000 – 06/2009 **Allgemeinbildendes Gymnasium**

Elly-Heuss-Knapp Gymnasium Heilbronn
Degree: Allgemeine Hochschulreife
Total grade: 2.2

Research Internships

09/2017 – 10/2017 **8th Developmental Biology Course**
UPMC - Sorbonne Université, Institut Curie
Course: „From Stem Cell to Morphogenesis"

09/2015 – 03/2016 **University of Oxford**
Research Group of Dr. Sebastian Shimeld, Department of Zoology
Project: „Patterning for complexity –The evolution of complex CNS within the vertebrate lineage due to mechanisms mediated by Gli genes" (Model organism: Brook lamprey)

Teaching Experience

03/2017 – 03/2020 **Supervision of practical courses**
of bachelor and master students,
plus, support and supervision of thesis writing

04/2017 – 02/2018 **Supervision of tutors**
for „Humboldt Reloaded"
(pilot project to integrate practical research into teaching)

09/2012 – 03/2017 **Assistant**
at the Institute of Zoology, University of Hohenheim
dissection classes and courses of species identification,
field excursions visiting the Mediterranean Sea

09/2012 – 03/2014 **Tutor**
for „organismic biology und ecology"

Awards

03/2018 – 06/2021 **PhD Fellowship** of „Studienstiftung des Deutschen Volkes"

06/2014 – 12/2016 **Student Fellowship** of „Studienstiftung des Deutschen Volkes"

Publication

Tisler, M., Wetzel, F., Mantino, S., Kremnyov, S., Thumberger, T., Schweickert, A., … Vick, P. (2016). Cilia are required for asymmetric nodal induction in the sea urchin embryo. BMC Developmental Biology, 16(1), 28. doi:10.1186/s12861-016-0128-7

Stuttgart, 26.07.2021